UNIVERSITY OF CALIFORNIA, SAN DIEGO

Modeling of hydrogen isotopes retention in plasma-facing components for fusion applications

A dissertation submitted in partial satisfaction of the
requirements for the degree
Doctor of Philosophy

in

Engineering Sciences (Engineering Physics)

by

Jérôme Guterl

Committee in charge:

Professor S.I. Krashenninikov, Chair
Professor Gaurav Arya
Professor Farhat Beg
Professor Renkun Chen
Professor Vitali F. Nesterenko

2015

The dissertation of Jérôme Guterl is approved, and it is acceptable in quality and form for publication on microfilm and electronically:

_____

_____

_____

_____

_____

Chair

University of California, San Diego

2015

DEDICATION

To climate change . . .

EPIGRAPH

When a mystery is too overpowering, one dare not disobey.

— Antoine de Saint-Exupéry, *Le Petit Prince*

TABLE OF CONTENTS

LIST OF FIGURES

LIST OF TABLES

ACKNOWLEDGEMENTS

I would like to thank Sergei Krasheninnikov and Roman Smirnov for their scientific and academic guidances, as well as Art Voter, Blas Uberuaga and Danny Perez for their scientific collaborations. I would also like to thank Heline Mirzakhanian for her support during my PhD.

Chapter 2, in full, is a reprint of the material as it appears in J. Guterl, R.D. Smirnov, S.I. Krasheninnikov, Revisited reaction-diffusion model of thermal desorption spectroscopy experiments on hydrogen retention in material, accepted in *Journal of Applied Physics*, 2015. The dissertation author was the primary investigator and author of this paper.

Chapter 3, in full, is a reprint of the material as it appears in J. Guterl, R.D. Smirnov, S.I. Krasheninnikov, M. Zibrov and A. Pisarev, Theoretical analysis of deuterium retention in tungsten plasma-facing components induced by various traps via thermal desorption spectroscopy, accepted in *Nuclear Fusion*, 2015. The dissertation author was the primary investigator and author of this paper.

Chapter 4, in full, is a reprint of the material as it appears in J. Guterl, R.D. Smirnov, S.I. Krasheninnikov, Long-Term Hydrogen Outgassing from Plasma Facing Components in *Contributions to Plasma Physics* 54 (4-6), 415-420 (2013). The dissertation author was the primary investigator and author of this paper.

Chapter 5, in part, is a reprint of the material as it appears in J. Guterl, R.D. Smirnov, S.I. Krasheninnikov, B. Uberuaga, A.F. Voter, D. Perez, Modeling of hydrogen desorption from tungsten surface in *Journal of Nuclear Materials*, 2014. The dissertation author was the primary investigator and author of this paper.

VITA

2005-2009	M.S. Engineering Physics - SUPAERO, Toulouse, France
2007-2009	M.S. Physics - École Polytechnique Fédérale de Lausanne, Switzerland "Investigation of sheath effects on interchange modes in TORPEX plasmas"
2010-2015	Ph. D. in Engineering Sciences - University of California, San Diego, USA "Modeling of hydrogen isotopes retention in plasma-facing components for fusion applications"

PUBLICATIONS

J. Guterl, R.D. Smirnov, S.I. Krasheninnikov, Revisited reaction-diffusion model of thermal desorption spectroscopy experiments on hydrogen retention in material, *Journal of Applied Physics* (2015)

J. Guterl, R.D. Smirnov, S.I. Krasheninnikov, A. Pisarev, M. Zibrov, Theoretical analysis of deuterium retention in tungsten plasma-facing components induced by various traps via thermal desorption spectroscopy, *Nuclear Fusion* (2015)

J. Guterl, R.D. Smirnov, S.I. Krasheninnikov, B. Uberuaga, A. Voter, D. Perez, Modeling of hydrogen desorption from tungsten surface, *Journal of Nuclear Materials* (2014)

J. Guterl, R.D. Smirnov, S.I. Krasheninnikov, Long-Term Hydrogen Outgassing from Plasma Facing Components, *Contributions to Plasma Physics* 54 (4-6), 415-420 (2013)

ABSTRACT OF THE DISSERTATION

Modeling of hydrogen isotopes retention in plasma-facing components for fusion applications

by

Jérôme Guterl

Doctor of Philosophy in Engineering Sciences (Engineering Physics)

University of California, San Diego, 2015

Professor S.I. Krashenninikov, Chair

Plasma-material interactions might strongly affect plasma performances and life-time of future magnetic fusion devices. For example, retention and recycling of hydrogen isotopes in plasma-facing components (PFC) may lead to dynamics plasma-material interactions and significant accumulation of tritium in material. Understanding the multifaceted physics of hydrogen retention in PFC is thus crucial, but remains challenging due to the wide spectrum of retention processes on PFC surface (erosion, co-deposition, etc.) and in PFC bulk (trap sites, bubbles, etc.) induced by long-time exposure of PFC to high flux of energy and particles.

In this context, we revisit in this work some aspects of the reaction-diffusion models used to describe retention of hydrogen implanted in material in fusion relevant. We first focus on the analysis of thermal desorption spectroscopy (TDS) experiments, showing that the evolution of hydrogen concentration

in material during TDS experiments is usually quasi-static. An analytic description of thermal desorption spectra (TDSP) is then obtained in quasi-static regime and is used to highlight dependencies of TDSP on hydrogen retention parameters. The interpretation of Arrhenius plots to characterize hydrogen retention processes is then revisited. Moreover, it is shown that retention processes can be characterized using the shape of desorption peaks in TDSP, and that long desorption tails in TDSP can be used to estimate activation energy of diffusion of hydrogen in PFC.

Hydrogen retention induced by a large number of different types of traps is examined next. A reaction-diffusion model of TDSP with a large number of types of traps is presented for the first time. The application of this model is illustrated on several experimental TDSP available in literature, which are consistently reproduced using several types of traps with a unique broad spectrum of detrapping energies. The values of these detrapping energies are shown to be in agreement with values predicted by density functional theory simulations when several hydrogen atoms are trapped in one material vacancy.

Effects of surface processes on hydrogen retention and recycling are investigated in the second part. First, long-term outgassing of hydrogen from PFC during off-plasma events is considered. The super-diffusive power-law decay in time of the hydrogen outgassing flux is modeled with a revisited single trap reaction-diffusion model, showing that hydrogen outgassing is either surface-limited or diffusion-limited. The outgassing regime is shown to be governed either by processes in the bulk or on the surface of material. The influence of hydrogen concentration profiles in material on the power-law exponents is analyzed as well. Finally, the different models proposed in the literature to describe power-law decays of hydrogen outgassing flux experimentally observed during off-plasma events are reconciled.

Hydrogen recombination and desorption on tungsten surface is investigated next using molecular dynamics (MD) and accelerated molecular dynamics simulations. Adsorption states, diffusion, hydrogen recombination into molecules, and clustering of hydrogen on tungsten surfaces are analyzed. It is shown that tungsten hydrogen interatomic potential, available in literature and used in MD simulations, cannot reproduce main features of hydrogen molecular recombination on tungsten surface. Hydrogen clustering on tungsten surface is nevertheless observed during MD simulations. Effects of hydrogen clustering on hydrogen desorption are thus analyzed by introducing a kinetic model describing the competition between surface diffusion, clustering and recombination. Different desorption regimes are identified, which reproduce some aspects of desorption regimes experimentally observed when tungsten surface is saturated with hydrogen.

Chapter 1

Introduction

1.1 Controlled thermonuclear fusion: a path toward clean and unlimited energy

The 1985 Geneva Summit between Gorbachev and Reagan marked the end of the Cold war era and the subsequent race for nuclear weapons, and announced the beginning of a new era for the controlled nuclear fusion research. Both Western and Soviet powers recognized "the potential importance of the work aimed at utilizing controlled thermonuclear fusion for peaceful purposes" and advocated "the widest practicable development of international cooperation in obtaining this source of energy, which is essentially inexhaustible, for the benefit for all mankind" [1]. The International Thermonuclear Experimental Reactor (ITER) project was born, equally supported by the United States, the Soviet Union and The European Union, joined later by Japan, China, South Korea and India [2].

Controlled thermonuclear fusion is more than ever of prime interest in today's world where demand for energy continues to increase while pollution and climate changes, as well as depletion of fossil fuel reserves, are raising strong concerns about the long-term sustainability of the human habitat [3]. In this context, controlled thermonuclear fusion may offer a renewable and abundant source of energy with limited environmental impacts. In contrast, the controlled nuclear fission industry can sustain a large and reliable production of electricity but at high environmental costs, considering difficulties posed by the storage of nuclear waste and environmental risks illustrated by the catastrophes of Chernobyl in 1986 and of Fukushima in 2011. Controlled thermonuclear fusion projects like ITER are therefore conceived today

to pave the way toward large powerful power plants. As such, the development of a sustainable source of thermonuclear energy is complementary with the development of other renewable sources of energy, such as solar, photovoltaic, wind or marine energies, which are expected to form a network of local distributed intermittent sources of energy.

Thermonuclear energy is naturally produced in the sun through a chain reaction initiated by a proton-proton fusion reaction [4]. In civilian fusion programs, the fusion reaction (1.1) between a nucleus of deuterium D and a nucleus of tritium T was identified in the early 50's as the most promising fusion reaction because of its large cross section $\sigma_{\text{D-T}}$ at relatively low energy $\sim 10-1000\,\text{keV}$ (fig. 1.1) [5].

$$\underbrace{{}^{2}_{1}\text{H}}_{\text{D}} + \underbrace{{}^{3}_{1}\text{H}}_{\text{T}} \rightarrow \underbrace{{}^{4}_{2}\text{He}}_{3.5\,\text{MeV}} + \underbrace{\text{n}_{\text{e}}}_{14.1\,\text{MeV}} \tag{1.1}$$

The mass-energy balance of the D-T reaction results in a gain of kinetic energy $\text{E}_{\text{D-T}} = 17.59\,\text{MeV}$ carried by a neutron ($\text{E}_{\text{n}_\text{e}} = 14.1\,\text{MeV}$) and by an α-particle ($\text{E}_{\alpha} = 3.5\,\text{MeV}$).

The mixture of deuterium and tritium in the energy range $\sim 10-1000\,\text{keV}$ forms a D-T plasma where deuterium and tritium atoms are fully ionized and thermalized. The volumetric rate $\text{R}_{\text{D-T}}$ of the fusion reaction (1.1) in hot D-T plasma is thus obtained by averaging the reaction rate over the Maxwellian velocity distribution of D and T particles at density n_{D} and n_{T} contained in the plasma.

$$\text{R}_{\text{D-T}} = \text{n}_{\text{T}}\text{n}_{\text{D}} \left\langle \sigma_{\text{D-T}} \text{v} \right\rangle \tag{1.2}$$

D-T plasma are produced with an 50:50 mixture of deuterium and tritium ($\text{n}_{\text{D}} = \text{n}_{\text{T}} = \frac{\text{n}}{2}$) to maximize the reaction rate $\text{R}_{\text{D-T}}$. D-T fusion reactions predominantly occur in the tail of the Maxwellian velocity distribution of plasma particles in the temperature[1] range $10\,\text{keV} < \text{T} < 100\,\text{keV}$, where the magnitude of $\left\langle \sigma_{\text{D-T}} \text{v} \right\rangle$ is maximum (fig. 1.2). D-T fusion reactions which occur in thermalized plasma are then designated by the term thermonuclear fusion, where "thermo" refers to thermalized particles.

The power produced by fusion reactions in D-T plasma per volume unit is

$$\text{P}_{\text{fusion}} = \frac{1}{4}\text{n}^2 \left\langle \sigma_{\text{D-T}} \text{v} \right\rangle \text{E}_{\text{D-T}} \tag{1.3}$$

A external power $\text{P}_{\text{heating}}$ must be supplied to plasma to balance energy loss. The rate of energy loss from plasma P_{loss} can be defined by introducing the characteristic confinement time τ_{E} of the energy contained in

[1] The Boltzmann constant k_b is omitted in this manuscript, and the temperatures are expressed indifferently in Kelvin or electronvolt.

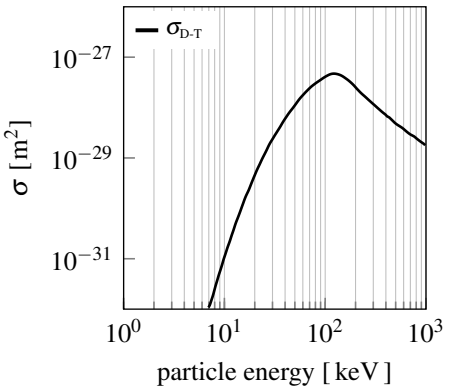

Figure 1.1: Cross-section of the D-T fusion reaction (1.1) [5].

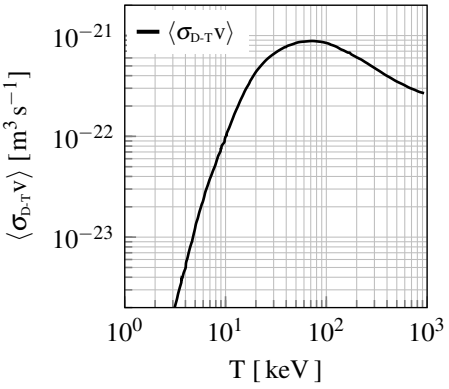

Figure 1.2: Average cross-section of the D-T fusion reaction (1.1) in thermalized plasma at temperature T [5].

plasma $W \approx \frac{3}{2} nT \left(P_{loss} = \frac{W}{\tau_E} \right)$. The power per volume unit $P_\alpha = \frac{1}{4} n^2 \langle \sigma_{D\text{-}T} v \rangle E_\alpha$ carried by the α particles is transferred by collisions to the plasma. The heating power required to balance the energy loss is thus

$$P_{heating} = P_{loss} - P_\alpha = \frac{\frac{3}{2} nT}{\tau_E} - \frac{1}{4} n^2 \langle \sigma_{D\text{-}T} v \rangle E_\alpha \tag{1.4}$$

The quality of a fusion reactor can be evaluated with the factor $Q = \frac{P_{fusion}}{P_{heating}}$. In the vicinity of $T \sim 20\,keV$ where $\langle \sigma_{D\text{-}T} v \rangle$ is maximum, the approximation $\langle \sigma_{D\text{-}T} v \rangle \approx 1.1 \times 10^{24}\, T^2\, m^{-3}\, s^{-1}$ holds and the factor Q can be recast considering expressions (1.3) and (1.4) into

$$Q = \frac{6}{\frac{3 \times 10^{30}}{nT\tau_E} - 1} \tag{1.5}$$

The ignition of plasma, for which plasma burning is self-sustained ($Q = \infty$), can be reached when $nT\tau_E > 5 \times 10^{21}\, m^{-3}\, eV\, s^{-1}$. This latter condition, known as the Lawson criterion, may however not be required in industrial fusion reactors where large values of Q are sufficient to achieve electricity production.

Fusion reactors should be thus designed to operate plasma at high density, high temperature and with long confinement time in order to maximize the triple product $nT\tau_E$ and thus achieve high Q (exp. 1.5).

1.2 ITER: a project to demonstrate the feasibility of the thermonuclear fusion energy

Several concepts of plasma confinement have been investigated since the early 50's to achieve large values of Q. These concepts can be divided into two main categories:

- **Inertial Confinement Fusion (ICF)**, which consists in heating and compressing a mixture of deuterium and tritium using high-intensity lasers. Such concepts are investigated today in projects like the NIF in the US or the MegaJoule Laser in France.
- **Magnetic Confinement Fusion (MCF)** where fusion conditions are met by confining plasma with magnetic fields. Different magnetic configurations have been proposed and tested, such as linear devices, magnetic bottles, stellerators or Tokamaks.

Tokamaks are the most promising concept of MCF devices to achieve large values of Q [3]. For this reason, the ITER project is a large Tokamak designed to demonstrate the feasibility of the production of

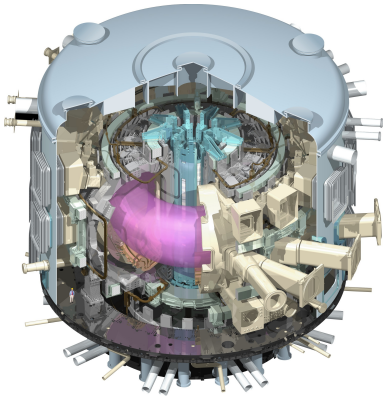

Figure 1.3: View of ITER [6].

energy with controlled thermonuclear fusion. In Tokamaks like ITER, plasma confinement is provided by a toroidal magnetic field created by large magnetic coils and a poloidal magnetic field created by a toroidal current generated by induction in the plasma. Plasma in Tokamaks are then contained inside a doughnut-shaped vacuum chamber surrounded by a series of magnetic coils (fig. 1.3).

Plasma in Tokamaks must be separated from the vacuum chamber to avoid polluting the plasma with impurities, which may strongly degrade the energy confinement due to radiative energy losses induced by these impurities. The separation between the plasma and the vacuum chamber in Tokamaks can be obtained with two different configurations:

- **a limiter configuration** where plasma boundaries are imposed by a piece of material introduced near inner walls of the vacuum chamber.

- **a divertor configuration** where plasma boundaries are imposed by close magnetic surfaces forming a X-point configuration, which maintains the plasma core isolated from the vacuum chamber (fig. 1.4). In this configuration, plasma particles escaping the core plasma flow along open magnetic field lines toward material plates located at the bottom of the vacuum chamber, which form the divertor. Plasma particles escaping the core plasma also flow across these open magnetic field lines in the scrape-off layer toward inner walls of the vacuum chamber.

Values of $Q > 1$ are not achievable in current and past Tokamaks as summarized in the figure 1.5. To reach larger values of Q, the triple product $nT\tau_E$ must be increased and plasma in Tokamak must be operated at higher temperature, higher density and with a better energy confinement. However, the plasma temperature is imposed by the D-T reaction rate which is maximum around $T \sim 20\,\text{keV}$ and strongly diminishes when plasma temperature is above $20\,\text{keV}$ (fig. 1.2). Moreover, the plasma density must remain lower than

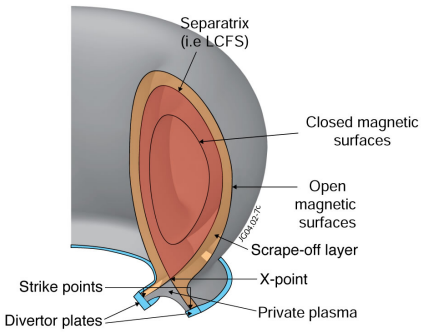

Figure 1.4: Divertor configuration in Tokamak [6].

the Greenwald density limit $n_G \approx 10^{21}\,m^{-3}$ to avoid plasma disruptions [7]. The plasma density and the plasma temperature being imposed, only the energy confinement can be significantly improved to operate Tokamaks at $Q > 1$.

Improvements of the energy confinement have been experimentally observed in divertor configuration above a certain power threshold in a confinement scenario called 'H-mode', in which strong pressure and temperature gradients are visible in edge plasma. Because of this enhanced confinement, the divertor configuration has been privileged in ITER to achieve better plasma confinement. Several scaling laws of the confinement time τ_E were obtained in H-mode by analyzing data collected from different Tokamaks operating around the world [3]. These empirical scaling laws show that τ_E depends on the Tokamak minor and major radius a and R and on the magnitude of the magnetic field B through the Larmor radius $\rho_{Larmor} \sim B^{-1}$, in close agreement with theoretical expressions similar to the relationship (1.6) predicted in [8].

$$\tau_E \sim \frac{a R^2}{\rho_{Larmor}^3} \frac{1}{B} \tag{1.6}$$

This scaling law (1.6) indicates that the energy confinement can be improved by increasing the magnitude of the magnetic field and the radius of the Tokamak. Generating high intensity magnetic fields is however very costly. Increasing magnetic fields to improve energy confinement is thus excluded due to economical considerations. A significant enhancement of the energy confinement thus requires to operate big Tokamaks. In this context, ITER is designed to be the largest Tokamak ever built with a major radius about 6 m and a volume of plasma about $860\,m^3$ (tab. 1.1). The main goal of ITER is to demonstrate the feasibility of thermonuclear fusion reactors by operating D-T plasma to reach $Q = 10$ during $t_{plasma} \sim 400 - 500\,s$ [9] (fig. 1.5). ITER is however not expected to produce usable energy and the development of industrial fusion power plants is planned on long term via the DEMO project, which

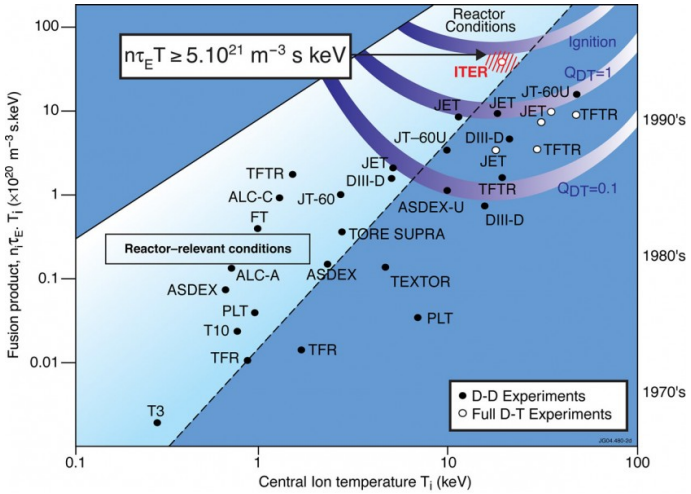

Figure 1.5: Values of Q experimentally achieved in current and past Tokamaks. Reproduced from [6].

Table 1.1: ITER specifications in baseline scenario to reach Q = 10 [9].

Major radius	R = 6 m	Plasma density	$n \sim 10^{20}\,m^{-3}$
Minor radius	a = 2 m	Core Plasma Temperature	$T \sim 20$ keV
Plasma volume	$840\,m^3$	Confinement time	$\tau_E \sim 4$ s
Magnetic field	$B = 6$ T	Plasma Lifetime	$t_{plasma} \sim 400 - 500$ s
Fusion power	$P_{fusion} = 400$ MW	Input Power	$P_{heating} = 40$ MW

should follow ITER [10].

1.3 How to put the sun in a box: plasma-material interactions in ITER and future fusion reactors

The energy confinement in ITER is expected to be increased by a factor 4 ($\tau_E \sim 4$ s) compared to the energy confinement in current Tokamaks ($\tau_E \sim 1$ s). Power and particles exhaustions during plasma operations in ITER will also significantly increase because of the large amount of energy and particles carried in ITER plasma. In a divertor configuration, the majority of hydrogen [2] and helium particles mainly flows along open magnetic field lines toward divertor plates. A small portion of particles however flows radially across the open magnetic field lines toward inner walls of the vacuum chamber. Divertor plates and inner walls of the vacuum chamber, usually referred to as Plasma-Facing Components (PFC), will be also exposed to large heat flux, principally carried by plasma electrons. In addition, PFC will also face

[2] hydrogen designates indifferently hydrogen, deuterium or tritium species in this work

significant flux of energetic neutrons, which can activate and damage PFC material.

Divertor plates in ITER will be exposed to large flux of hydrogen particle $\left(\Gamma \sim 10^{24}\,\mathrm{m}^{-2}\cdot\mathrm{s}^{-1}\right)$ during steady-state plasma operations. Hydrogen plasma will flow toward PFC surface at plasma temperature around $T_{\mathrm{plasma}} \sim 10\,\mathrm{eV}$. In contrast, inner walls will face lower flux of hydrogen particles $\left(\Gamma \sim 10^{20}\,\mathrm{m}^{-2}\cdot\mathrm{s}^{-1}\right)$ at lower plasma temperature $T_{\mathrm{plasma}} \sim 1\,\mathrm{eV}$. Both divertor and inner walls will also face similar flux of α-particles during plasma operations. Besides, the temperature of PFC material will depend on the heat flux deposited on PFC surfaces during plasma operations. The temperature of divertor plates will be thus close to $T \sim 500-1300\,\mathrm{K}$ during plasma operations, whereas the temperature of inner walls will be lower $T \sim 500-700\,\mathrm{K}$ [11]. In addition to these steady-state heat and particles flux summarized in the table 1.2, PFC will be also exposed to various intermittent plasma phenomenon such as Edge-Localized Mode (ELM), disruption events or runaway electrons. Such transient events may lead to significant depositions of heat and particles on PFC material in very short times [12].

Extreme conditions which will be encountered by PFC in ITER and in future fusion reactors will likely lead to new regimes of plasma-material interactions, susceptible of revealing some new aspects of material behavior in extreme environment (e.g. fuzz growth on tungsten surface exposed to large helium flux [13]). The term Plasma-Material Interactions (PMI) designates here physical processes taking place at the interface between "hot" plasma and "cold" material, either in plasma or in PFC material. PMI include a broad range of physical phenomena, which combine atomic and molecular physics, collisional and non-collisional plasma physics and materials science. As such, PMI are complex and multi-faceted and giving an exhaustive review of PMI is difficult. Detailed discussions on the different aspects of PMI can be however found in literature [14, 15, 16].

PMI have not been a major limiting factor for plasma operations in current and past Tokamaks, in particular because heat and particles flux faced by PFC in plasma regimes operated in these machines are low compared to conditions expected in ITER. However, PMI are expected to become stronger as fusion reactors get bigger in order to reach larger values of Q. PMI will then become an inevitable issue not only in ITER but also for any future fusion reactor, which raises concerns about the sustainability and the lifetime of PFC material in fusion reactors [17]. These concerns could be summarized by the eloquent statement of Sebastien Balibar in its public critics of the ITER project [18]

> *We say that we will put the sun into a box. The idea is pretty. The problem is, we don't know how to make the box.*

Among critical consequences of PMI in ITER, the erosion and the melting of PFC material during steady-state operations or intermittent events may strongly affect the lifetime of divertor and walls and produce

Table 1.2: Conditions encountered by plasma-facing components in ITER [11] and properties of beryllium and tungsten material, which will respectively constitute inner walls of the vacuum chamber and divertor plates in ITER [19].

Steady-state plasma	Wall	Divertor
Heat flux	$0.2-0.5\,\mathrm{MW.m^{-2}}$	$20\,\mathrm{MW.m^{-2}}$
Particle flux	$10^{20}\,\mathrm{m^{-2}\cdot s^{-1}}$	$10^{24}\,\mathrm{m^{-2}\cdot s^{-1}}$
Plasma Temperature	$\sim 1\,\mathrm{eV}$	$\sim 10\,\mathrm{eV}$
PFC Temperature	$500\,\mathrm{K}-700\,\mathrm{K}$	$500\,\mathrm{K}-1300\,\mathrm{K}$
PFC Material	Beryllium (Be)	Tungsten (W)
Atomic Number	$Z=4$	$Z=74$
Melting Temperature	$1560\,\mathrm{K}$	$3695\,\mathrm{K}$
Cohesion Energy	$3.32\,\mathrm{eV/atom}$	$8.90\,\mathrm{eV/atom}$

large quantities of impurities into the vacuum chamber. To limit these deleterious effects, divertor plates will be built in tungsten (W), which is a hard metal with very high melting temperature (tab. 1.2). In contrast, inner walls of ITER vacuum chamber will be made of beryllium (Be). Significant erosion and sputtering of inner walls are expected (beryllium is a low Z element with $Z=4$), although heat and particles flux faced by inner walls will be much lower than flux faced by divertor plates. Effects of Be impurities on plasma performances should be however limited since the intensity of radiations induced by impurities in plasma scale as Z^2.

1.3.1 Plasma-material interactions in plasma-facing components material

Investigating and understanding "how to make the box" to confine hot plasma, in which nuclear fusion reactions take place, is extremely complex because of the microscopic, mesoscopic and macroscopic physical processes constituting PMI in both plasma and PFC material. In view of the complexity of the PMI, the scope of this work is thus limited to PMI taking place in bulk and on surface of PFC material exposed to fusion relevant conditions such as described in table 1.2.

When PFC are exposed to high flux of hydrogen and helium characteristic of fusion relevant conditions, a portion of the incoming particles is reflected or interact with material surface (physical or chemical sputtering). Meanwhile, the other particles penetrate into the bulk of PFC material and become implanted inside a narrow region near the material surface exposed to plasma. This region, called the implantation layer, usually extends from some nanometers up to tens of nanometers depending on PFC material and on the energy of incoming particles. For instance, hydrogen and helium particles at

$E_k \sim 1 - 100\,\mathrm{eV}$ are usually implanted in tungsten in the first ten nanometers below tungsten surface exposed to particle flux. Hydrogen and helium implanted in material either diffuse back toward material surface and desorp into vacuum (fuel recycling), or diffuse further into material bulk where they can be trapped in various material defects (fuel retention).

Various processes in material may result from the exposure of PFC to plasma in fusion related conditions (fig. 1.6) [14, 20, 21]:

- **on PFC material surface:**
  - desorption of adsorbed hydrogen or helium in atomic or molecular form into vacuum and absorption into material bulk
  - surface saturation with hydrogen or helium atoms
  - impurities,e.g oxygen, which may for instance affect desorption process of other species
  - redeposition of eroded PFC material and formation of porous codeposited layers
  - erosion caused by physical or chemical sputtering and release of impurities and dusts
- **in PFC material bulk:**
  - vacancies, dislocations, damages created by neutrons, grain boundaries, self-interstitial atoms, impurities , . . . which may constitute traps for hydrogen and helium particles in the material
  - formation of cavities which can contain hydrogen and helium atoms
  - formation of helium bubbles and helium clusters which may trap hydrogen
  - stress and plastic deformation of material caused by the saturation of sub-surface regions with hydrogen and helium

In addition to these various processes, properties and structure of PFC material can be also altered due to the large heat flux, in particular during intermittent events such ELM [22]. These complex effects are however out of the scope of this work and are ignored. Damages created by neutrons in material are also ignored since significant fuel retention arise in PFC material whether material is exposed to neutrons or not [23]. Besides, damaging of material by neutrons results anyhow in the creation of additional material defects which are not different in their nature from other material defects naturally present in material or induced by the exposure of material to plasma.

Fuel retention in PFC material can be also affected by interactions between helium and hydrogen in material bulk, as illustrated in [24]. Helium retention in PFC material is however itself complex and

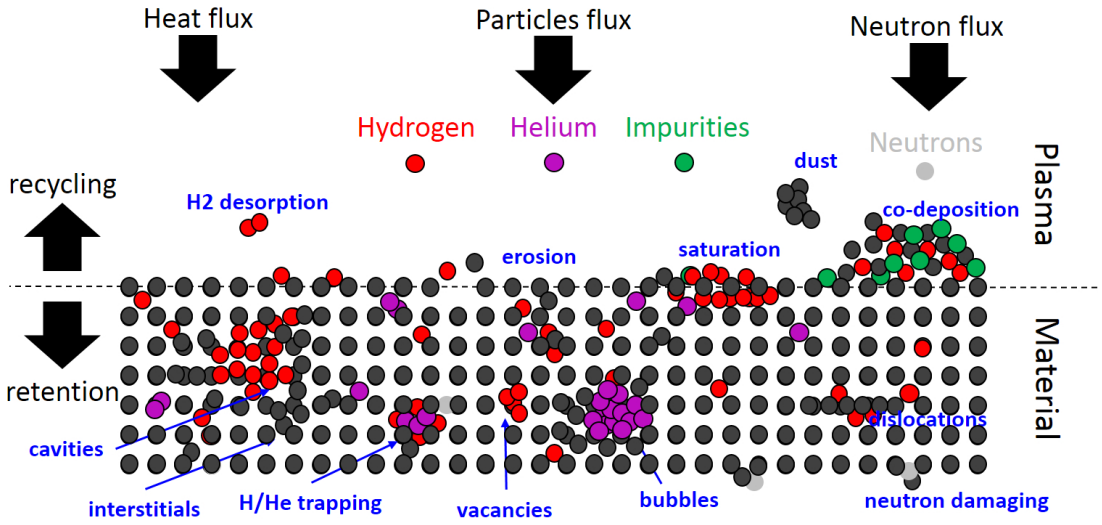

Figure 1.6: Processes inducing plasma-material interactions in bulk and on surface of plasma-facing components.

subject to numerous investigations [25], and as such is ignored here. This work therefore addresses only hydrogen retention in plasma facing-components, which is itself a crucial issue for ITER and future fusion reactors as described hereafter.

1.3.2 Hydrogen retention in plasma-facing components: a critical issue for ITER

Hydrogen retention in plasma-facing components is considered as one of the key issues in ITER and future fusion reactors for both safety and operational reasons. First, tritium is a radioactive hydrogen isotope of half-time about 12.3 years. For this reason, tritium inventory in the vacuum vessel of ITER is limited to 700 g, which is the administrative limit imposed by the French Nuclear Safety agency to operate ITER. ITER divertor will be exposed to a fluence around $\phi \sim 10^{26}$particles.m^{-2} of deuterium and tritium during one plasma discharge. The divertor surface directly exposed to plasma in ITER will be around $6\,\mathrm{m}^2$ and will be thus hit by a cumulated quantity of $2-3$ g of tritium during an entire single plasma discharge. Fortunately, most of deuterium and tritium implanted in divertor are recycled back into the vacuum chamber, and only a tiny portion is retained in material.

The accumulation of little quantities of tritium in PFC material during each plasma discharge may nevertheless conduct to a long-term accumulation of tritium in PFC, and thus limit the duration of plasma operations in ITER. This issue was encountered for example in experiments performed with carbon

PFC in several Tokamaks. The erosion rate of carbon material (graphite) in fusion relevant conditions is large, leading to large redeposition of carbon-tritium codeposited layers on PFC surface. Because of the considerable retention of tritium in these codeposited layers, the inventory of tritium in an ITER design with carbon PFC would largely exceed the administrative limit of 700 g after only tens of plasma discharges [26]. Carbon was thus discarded as PFC material and replaced by tungsten and beryllium in the current ITER design.

Tritium retention in ITER is predicted to be mostly induced by the redeposition of beryllium-tritium layers on PFC surface. In contrast, tritium retention is expected to be limited in tungsten divertor, based on experimental results from current experimental Tokamaks operating with tungsten divertor such as JET in ITER-like wall configuration [27] or Asdex-U [28]. These machines however operate in plasma regimes where heat and particles flux hitting PFC are much lower than expected in ITER and where plasma discharges are usually much shorter than ITER discharges in operational scenario ($t_{plasma} \sim 400 - 500$ s). In this context, further investigations on long-term tritium retention in tungsten PFC are required.

Long-term exposure of PFC material to plasma may also affect plasma operations. For example, systematic density-limit disruptions were encountered in plasma produced in the carbon-based Tokamak ToreSupra after only 20 long plasma discharges, which corresponded to a total time of plasma operation about ~ 200 s [29]. In the machine JT-60, also operated with carbon PFC, lower values of pressure in plasma edge were observed during plasma discharges following several long plasma discharges of ~ 30 s, and were attributed to the uncontrollable recycling of hydrogen from wall [30].

The retention of deuterium and tritium in plasma-facing components may be thus a crucial issue in ITER and in future fusion reactors due to both safety and operational issues. In this context, this work is centered on hydrogen retention in PFC with a particular focus on tungsten plasma-facing components. As such, this work may be also of interest for DEMO, which is planned to be an industrial fusion reactor with both wall and divertor in tungsten [10].

1.4 Understanding and predicting hydrogen retention in plasma facing components: a challenging problem

1.4.1 The complex multiscale nature of hydrogen retention in plasma facing components

Operating a Tokamak in fusion conditions requires to understand and predict effects of dynamical plasma-material interactions and long-term hydrogen retention in PFC on very different time and space scales. For example, the typical time scale of intermittent edge plasma events like ELM is about $t_{meso} \gtrsim 10^{-3}$ s whereas effects of fuel retention occur on longer time scales $t_{macro} \gtrsim t_{plasma} \approx 400 - 500$ s. Besides, hydrogen retention may take place in PFC on a a space scale as large as the PFC material thickness $L_{macro} \sim 1$ mm when $t \sim t_{macro}$.

In contrast, elementary processes responsible for hydrogen retention and recycling in PFC are atomic processes characterized by very short time scales ($t_{micro} \sim 1$ ps) and very short space scales of the order of several material lattices or less ($L_{micro} \lesssim 10$ nm). These atomic processes are various and numerous, even when effects of heat flux, of neutron irradiation, and of helium retention are ignored (fig. 1.7). Understanding and predicting hydrogen retention and recycling in PFC thus require to reconcile microscopic time and space scales, characteristic of atomic processes , with mesoscopic and macroscopic time and space scales, characteristic of dynamical PMI and long-term plasma operations in fusion reactors (fig. 1.8).

Physical processes governing hydrogen retention and recycling in carbon PFC have been largely investigated in plenty of theoretical and experimental works, partially motivated by the various industrial and scientific applications of carbon in other domains. By comparison, mechanisms governing hydrogen retention and recycling in beryllium and tungsten have become intensively investigated only in the last decade. Mechanisms governing hydrogen retention and recycling in tungsten remain however not well understood as pointed out in several recent reviews [20, 21, 31, 32]. The comprehension of these mechanisms is complex for at least three reasons:

- the versatility of the processes inducing hydrogen retention, which strongly depend on plasma and material conditions (hydrogen flux, hydrogen fluence, material temperature and crystalline structure, ...).

- the variety and the number of retention processes, which can also dynamically evolve and interact

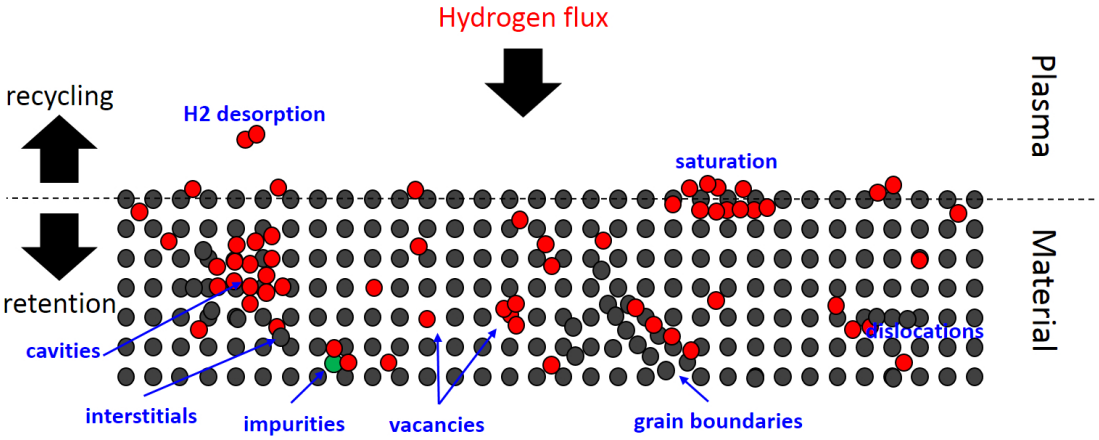

Figure 1.7: Elementary atomic processes responsible for hydrogen retention and recycling in tungsten plasma-facing components.

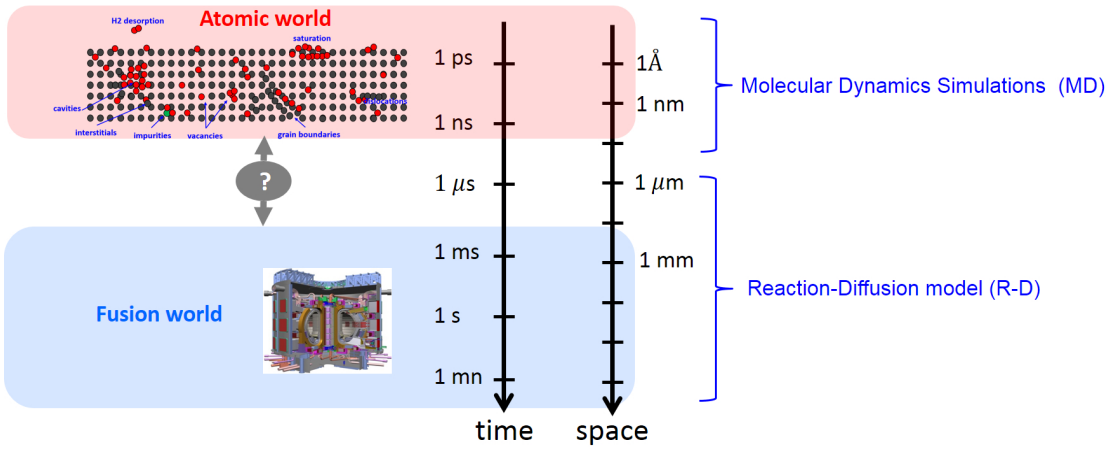

Figure 1.8: Comparison between time and space scales of atomic processes responsible for hydrogen retention and recycling in PFC (red) and during operational plasma conditions in fusion reactors (blue).

when the material is exposed to heat and particle flux.

- the difficulty to observe these processes in material due to their microscopic nature. In general, only mesoscopic or macroscopic effects of retention mechanisms are experimentally observable.

Hindrances in experimental analysis and characterization of hydrogen retention processes in PFC are due to limitations in experimental methods available to examine retention processes. These experimental methods mainly consist in:

- producing images: optical, x-ray or electron microscopy imaging which can picture material surface morphology with a precision up to some nanometers (fig. 1.9a).

- in-situ hydrogen concentration measurements: the concentration of hydrogen isotopes in material can be evaluated using MeV ion beams. The most common method is the Nuclear Reaction Analysis (NRA), which consists in bombarding material containing hydrogen with highly energetic particles (e.g. protons) and counting the number of nuclear reactions between energetic ions and hydrogen [33]. NRA is a non destructive method which does not significantly affect material properties and hydrogen concentration in material. The resolution of NRA is usually limited to material depths below $10\,\mu$m and to hydrogen concentrations above $\sim 10^{-5}$ at.% (fig. 1.9b).

- Thermal Desorption Spectroscopy(TDS): TDS, also called temperature programmed desorption, consists in the measurement of the hydrogen outgassing flux while heating up a material sample previously exposed to hydrogen flux. The resulting plot of the outgassing flux as a function of the sample temperature forms a thermal desorption spectra (TDSP), which exhibits desorption peaks similar to the one plotted in figure 1.9c.

  TDSP are used to determine the activation energy E of retention processes based on the assumption that the release of retained hydrogen in material is an activated process, which thus occurs at a rate ν described by an Arrhenius law [34]. In that case, the evolution of the concentration of hydrogen c in the material while the material temperature is increasing can be described by

$$\frac{\partial c}{\partial T} \propto \underbrace{\nu_0 e^{-\frac{E}{T}}}_{\nu} c \tag{1.7}$$

  Variations of the hydrogen concentration in the material are also proportional to the hydrogen outgassing flux Γ_{out}

$$\frac{\partial c}{\partial T} \propto -\Gamma_{\text{out}} \tag{1.8}$$

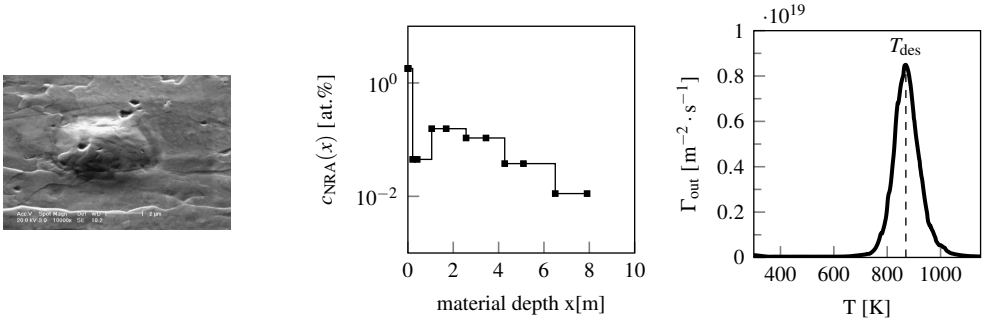

(a) W surface irradiated with D (b) D concentration profile in W (c) Thermal Desorption Spectra

Figure 1.9: Example of experimental results obtained with tungsten samples implanted with deuterium using scanning electron micrograph (a), nuclear reaction analysis (b) and thermal desorption spectroscopy (c). Data reproduced from [35], [36] and [37], respectively.

When the outgassing flux is maximum at T_{des} $\left(\left.\frac{\partial \Gamma_{\text{out}}}{\partial T}\right|_{T=T_{\text{des}}} = 0 \right)$, the relationship $\nu(T_{\text{des}}) = \frac{E}{T_{\text{des}}^2}$ holds and the activation energy E can be determined. The total quantity of retained hydrogen in PFC can be also estimated from TDSP by integrating the outgassing flux over the duration of the TDS experiment.

The analysis and the characterization of retention mechanisms with the experimental methods showcased above may be delicate regarding the variety and the complexity of material processes inducing hydrogen retention. For instance, determining the activation energy of a retention process may be difficult when a TDSP contains multiple desorption peaks induced by different material defects retaining hydrogen. Moreover, the basic model previously introduced, which describes the evolution of hydrogen concentration in material during TDS experiments, usually fails to capture main features of hydrogen retention in material when surface processes or hydrogen diffusion in material affect hydrogen outgassing. Analyzing retention mechanisms with TDS experiments may be thus not straightforward and NRA are then usually performed in parallel to evaluate the concentration of retained hydrogen in the depth of the material. NRA however does not provide indications on the nature and the number of defects inducing hydrogen retention. Similarly, imaging methods only offer pictures of some visible aspects of retention processes, such as morphological modifications of material surfaces or formation of bubbles in material bulk.

Although experimental methods can provide only partial and limited pictures of hydrogen retention processes in tungsten, the numerous experimental results published in the literature form a large database which portrays the effects of different experimental and material conditions on hydrogen retention. The establishment of such a database is today supported by the International Atomic Energy Agency to identify main processes governing hydrogen retention in fusion related conditions and to orientate technological

developments of PFC material in ITER and DEMO [38]. However, no model of hydrogen retention in tungsten PFC in fusion relevant conditions has emerged yet to consistently and accurately reproduce experimental data. The development of such models is necessary to predict long-term hydrogen retention and dynamics of PMI in tungsten PFC, but also to analyze experimental data available in literature.

1.4.2 Modeling microscopic and macroscopic aspects of hydrogen retention in plasma facing components

Both microscopic and macroscopic aspects of hydrogen retention in PFC material must be taken into account to model hydrogen retention in fusion relevant environment (fig. 1.8). Microscopic processes inducing hydrogen retention are usually modeled using:

- Density Functional Theory (DFT): DFT is a quantum mechanical simulation method to model quantum electronic structure of atomic system by solving Schrödinger equations using Hohenberg-Kohn theorems [39]. DFT simulations are mainly used to determine properties of material defects, such as the activation energy of detrapping of hydrogen isotopes from defects. DFT results can also be used to build interatomic potentials used in molecular dynamics simulations (see below). DFT simulations are usually limited to hundreds atoms and are not suitable to resolve dynamics beyond atomic time scales.

- Molecular Dynamics (MD): MD simulations consist in solving Newton equations for each atom, defining interactions between atoms by an interatomic potential which must be provided for each type of atomic interactions in simulations. The quality of MD simulations principally relies on the quality of the interatomic potentials used in simulations. The definition of these potentials can be difficult when the electronic structure of the material is complex, e.g. tungsten. MD simulations are usually performed to investigate dynamics and properties of atomic processes in relevant conditions (temperature, stress, geometry, ...) in atomic systems with 1000 to millions of atoms, on time scales which usually do not exceed $t_{MD} \sim 10\,ns$. The recent development of Accelerated Molecular Dynamics (AMD) methods allows to extend the time scale of MD simulations of one or several orders of magnitude in certain circumstances [40].

Mesoscopic and macroscopic evolutions of hydrogen retention in PFC can be modeled using Kinetic Monte Carlo (KMC) simulations [41] or reaction-diffusion (R-D) equations. These both methods require to provide rates characterizing each process involved in hydrogen retention. As such, these methods

capture similar features of retention processes at mesoscopic and macroscopic scales. Unlike R-D models, KMC methods do not furnish a convenient analytical background to analyze hydrogen retention and is thus of little interest to model and predict long-term hydrogen retention and dynamics of PMI in PFC material, which are therefore model in this work with R-D equations .

Reaction and diffusion rates characterizing retention processes in material are usually described by an Arrhenius law (e.g the relationship 1.7), relying on the assumption that retention processes are activated processes. As such, rates characterizing retention and diffusion processes can be generically expressed as $\nu \sim \nu_0 e^{-\frac{E}{T}}$. As previously mentioned, the activation energy E and the pre-exponential factor ν_0, also called attempt frequency, can be experimentally estimated via TDS experiments and theoretically determined in DFT or MD simulations.

Reaction-diffusion models have been widely used in literature to describe hydrogen retention and outgassing in metallic or carbon PFC [42, 43, 44] and to analyze TDSP resulting from TDS experiments [45, 35, 46]. The area of PFC surface $\sim \lambda_{\text{PFC}}^2$ exposed to plasma in fusion related experiments or in fusion reactors is usually large in the sense that the characteristic depth of retention $\lambda_{\text{retention}}$ is small compared to λ_{PFC} ($\lambda_{\text{retention}} \ll \lambda_{\text{PFC}}$). Consequently, the evolution of hydrogen concentration in PFC material can be described in an 1D framework using the following R-D equations (1.9).

$$\frac{\partial c_{\text{f}}(x,t)}{\partial t} = D\frac{\partial^2 c_{\text{f}}(x,t)}{\partial x^2} - K_{\text{tr}}\left[c_{\text{trap}}(x) - c_{\text{t}}(x,t)\right] c_{\text{f}}(x,t) + \nu_{\text{dt}}\, c_{\text{t}}(x,t) \tag{1.9a}$$

$$\frac{\partial c_{\text{t}}(x,t)}{\partial t} = K_{\text{tr}}\left[c_{\text{trap}}(x) - c_{\text{t}}(x,t)\right] c_{\text{f}}(x,t) - \nu_{\text{dt}}\, c_{\text{t}}(x,t) \tag{1.9b}$$

c_{f} is the concentration of free (solute) hydrogen which can freely diffuse in material and c_{t} is the concentration of hydrogen trapped in material defects at the concentration c_{trap}. Material defects causing hydrogen retention in the material are usually called "traps". The equations (1.9a) and (1.9b) include only on type of traps, in which free hydrogen particles in the material are trapped at the trapping rate K_{tr} and are detrapped at the detrapping rate ν_{dt}. Traps are here assumed to be immobile in the material, whether they are occupied by hydrogen or not, and only free hydrogen can diffuse in the material, hence the diffusion term in equation (1.9a) with D the diffusion coefficient of hydrogen in material. The creation and the evolution in time of traps are not modeled by equations (1.9). The R-D model formed by these equations can thus only picture some aspects of hydrogen retention, e.g. hydrogen outgassing during TDS experiments.

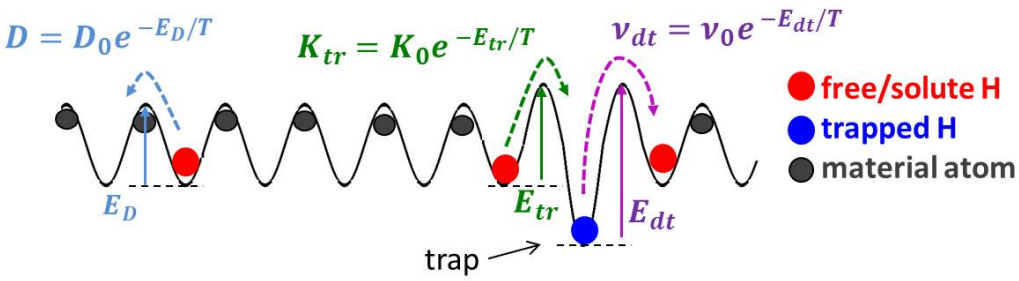

Figure 1.10: Hydrogen trapping, detrapping and diffusion in material, modeled as activated processes corresponding to transitions between microscopic states of hydrogen in material.

As mentioned earlier, trapping, detrapping and diffusion of hydrogen in material are usually considered as activated processes and are thus described by Arrhenius laws with $K_{\mathrm{tr}} = K_{\mathrm{tr},0} e^{-\frac{E_{\mathrm{tr}}}{T}}$, $\nu_{\mathrm{tr}} = \nu_{\mathrm{tr},0} e^{-\frac{E_{\mathrm{dt}}}{T}}$ and $D = D_0 e^{-\frac{E_{\mathrm{D}}}{T}}$, respectively. In the framework of the transition state theory [41], the activation energy of trapping E_{tr}, of detrapping E_{dt} and of diffusion E_{D} can be seen as energy barriers separating two micro states of hydrogen in material as illustrated in figure 1.10. The pre-exponential factors $K_{\mathrm{tr},0}$, $\nu_{\mathrm{tr},0}$ and D_0 include the frequency ν_0, which can be interpreted as the attempt frequency of hydrogen particle to transit from one state to another one. The exponential term $e^{-\frac{E}{T}}$ can be then seen as the probability that such a transition occurs in material at the temperature T.

Boundary conditions of equations (1.9) are modeled by equations (1.10), which describe the evolution of the hydrogen concentration c_{s} on material surface (eq. 1.10a) and the conservation of hydrogen particles between material surface and material bulk (eq. 1.10b).

$$\frac{\partial c_{\mathrm{s}}}{\partial t} = -\underbrace{K_{\mathrm{r}} c_{\mathrm{s}}^2}_{\Gamma_{\mathrm{out}}} + \underbrace{K_{\mathrm{b}} c_{\mathrm{f}}(x_{\mathrm{s}},t)}_{\Gamma_{\mathrm{b}}} - \underbrace{K_{\mathrm{a}} c_{\mathrm{s}}}_{\Gamma_{\mathrm{a}}} \tag{1.10a}$$

$$D \frac{\partial c_{\mathrm{f}}(x,t)}{\partial x}\bigg|_{x=x_{\mathrm{s}}} = \pm \left(\underbrace{K_{\mathrm{b}} c_{\mathrm{f}}(x_{\mathrm{s}},t)}_{\Gamma_{\mathrm{b}}} - \underbrace{K_{\mathrm{a}} c_{\mathrm{s}}}_{\Gamma_{\mathrm{a}}} \right) \tag{1.10b}$$

$x_s = 0$ and $x_s = L$ are the position of the front and rear material surfaces, considering PFC material of thickness L. This surface model relies on the energy diagram in figure 1.11 proposed in [47]. $K_{\mathrm{b}} = K_{\mathrm{b},0} e^{\frac{-E_{\mathrm{b}}}{T}}$ is the rate of readsorption of hydrogen from the first sub-surface atomic layer onto surface, $K_{\mathrm{a}} = K_{\mathrm{a},0} e^{\frac{-E_{\mathrm{a}}}{T}}$ is the rate of absorption of hydrogen on surface into material bulk and $K_{\mathrm{r}} = K_{\mathrm{r},0} e^{\frac{-E_{\mathrm{r}}}{T}}$ is the rate of molecular recombination and desorption of hydrogen on tungsten surface. The flux Γ_{out} of hydrogen outgassed from

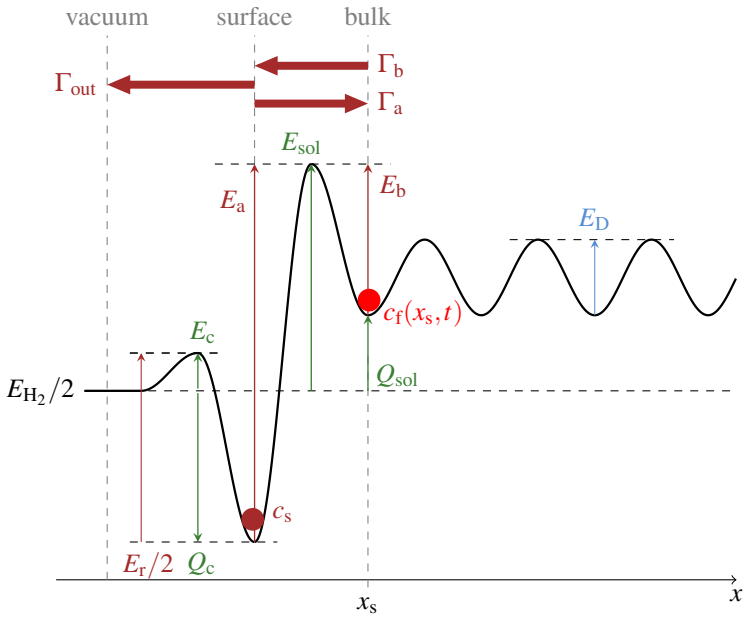

Figure 1.11: Energy diagram of material surface [47] where $E_b = E_{sol} - Q_{sol}$, $E_r/2 = E_c - Q_c$ and $E_a = E_{sol} - Q_c$.

material is then $\Gamma_{out} = K_r c_s^2$.

Hydrogen-tungsten systems have been investigated in the scientific community for long time [48] and are used for various industrial applications, such as ionization of hydrogen gas exposed to hot tungsten surface [49, 50, 51, 52, 53]. Consequently, thorough investigations on hydrogen-tungsten systems have been abundantly reported since the early 40's in a variety of papers until the late eighties [54, 55, 56, 57, 58, 59, 60, 61, 62, 63, 64]. However, most of works available in literature mainly focus on exposure of tungsten material to hydrogen gas or to hydrogen ions at very low energy and temperature where hydrogen retention and recycling in tungsten are governed by surface processes.

Results and models developed in surface-dominated regimes are however not fully applicable for exposure of tungsten to plasma in fusion relevant conditions, id est exposure of tungsten to high flux of energetic particles, where retention and recycling of hydrogen is also governed by bulk processes. In this context, a large number of TDS experiments have been performed since 2000's, as outlined previously, to investigate effects of plasma exposure and material state on hydrogen retention in tungsten. For instance, thermal desorption spectra (TDSP) were obtained with different hydrogen flux [65, 66, 67, 68, 69], hydrogen energies [70, 71, 72], hydrogen fluences [73, 74, 75, 76, 77] and using tungsten samples implanted at different temperatures [46, 78, 79, 80, 81], previously damaged with ions beams [82, 83, 84, 85, 86, 87, 88, 89, 90, 91], pre-annealed [92, 35, 93], recrystallized [94, 71, 36, 95], single

crystal and polycrystalline [96, 97, 98, 99, 100, 101, 102] or containing impurities [103, 104, 105, 106]. Effects of the storage period and the air exposure of implanted samples between the plasma exposure and the measurement of the outgassing flux have been also investigated [107, 108], as well as surface effects [109, 110].

Experimental TDSP were then analyzed and interpreted in literature with R-D models similar to the one formed by equations (1.9) and (1.10) [45], using modeling softwares like TMAP [111]. Desorption peaks in experimental TDSP were found to correspond to various traps characterized by activation energies of detrapping varying from 0.5 eV to 2.1 eV [32, 20]. The nature of these traps remains however unclear, partly because of limitations of R-D models. For instance, the number of different types of traps used in R-D models to fit TDSP is thus usually limited to two or three, which does not allow a consistent and accurate reproduction of experimental TDSP. Besides, no clear analytical description of retention processes affecting hydrogen outgassing during TDS experiments is available. Large discrepancies also exist in activation energies and pre-exponential factors characterizing surface processes which define boundary conditions of R-D models [20, 32].

Analyzing and predicting hydrogen retention in tungsten PFC thus require further investigations on R-D models describing hydrogen retention on macroscopic scales, in particular during TDS experiments or when surface effects govern hydrogen outgassing. Such investigations are the main topic of this work and are reported in this manuscript following the outline presented below.

1.5 Roadmap

In summary, plasma facing components (PFC) in future fusion devices will be exposed to various plasma conditions, which can alter PFC material and strongly affect retention and recycling of hydrogen isotopes during long-term plasma exposure. Understanding mechanisms involved in the long-term retention of hydrogen isotopes in tungsten, which will be used as PFC material in future fusion devices (divertor in ITER, divertor and walls in DEMO), is thus crucial. Mechanisms responsible of hydrogen retention take place both on material surface (erosion, co-deposition, blistering, ...) and in material bulk (vacancies, dislocations, voids, ...) and are the results of various atomic processes. Atomic processes inducing hydrogen retention are difficult to observe and quantify in experiments and only macroscopic effects of retention mechanisms can be measured. Both microscopic and macroscopic modeling of retention processes are thus required to determine and describe processes governing hydrogen retention and recycling.

Hydrogen outgassing and retention in tungsten are macroscopically described with reaction-

diffusion (R-D) models, which are also used to analyze and interpret thermal desorption spectra (TDSP) resulting from thermal desorption spectroscopy (TDS) experiments performed on tungsten samples implanted with hydrogen. Various types of traps have been characterized in TDSP but their nature remains unclear because of limitations in R-D models. Moreover, experimental characterizations of surface processes forming boundary conditions in R-D models exhibit large discrepancies. In this context, this work focuses on the analysis of R-D models describing hydrogen retention in tungsten bulk and on tungsten surface in fusion related conditions. The first part of this manuscript formed by the chapters 2 and 3 is devoted to the modeling and the interpretation of TDSP characteristic of hydrogen retention in tungsten. The second part of this work, constituted by the chapters 4 and 5, is dedicated to the modeling of surface processes affecting hydrogen outgassing from tungsten.

The desorption phase in TDS experiments performed on tungsten PFC exposed to hydrogen isotopes in fusion relevant conditions is analyzed in the chapter 2 with a R-D model describing hydrogen retention in PFC bulk. Two regimes of hydrogen outgassing are identified depending on whether hydrogen trapping rate is larger than hydrogen diffusion rate in material during TDS experiments. In both regimes, a majority of hydrogen released from material defects is immediately outgassed instead of diffusing deeply in PFC when the evolution of hydrogen concentration in PFC is quasi-static, which is the case during TDS experiments performed with tungsten samples exposed to a flux of hydrogen isotopes in fusion related conditions. In this context, analytical expressions of the hydrogen outgassing flux as a function of the material temperature are obtained with sufficient accuracy to describe main features of thermal desorption spectra. These expressions are then used to highlight how characteristic temperatures of TDSP depend on hydrogen retention parameters, such as trap concentration or activation energy of detrapping processes. The use of Arrhenius plots to characterize detrapping processes is then revisited when hydrogen trapping plays a role during TDS experiments. Retention processes are also characterized using the shape of desorption peaks in TDSP and it is shown that diffusion of hydrogen in PFC material during TDS experiments can induce long desorption tails visible aside desorption peaks at high temperature in TDSP. These desorption tails can be used to estimate activation energy of diffusion of hydrogen in PFC.

TDSP reported in literature resulting from thermal desorption experiments performed on tungsten samples exposed to deuterium at several fluences are analyzed in the chapter 3 using a reaction-diffusion model including a large number of different types of traps. The use of a large number of types of traps allows accurate fits of TDSP at all fluences. Fits are obtained using a unique broad spectrum of detrapping energy. Detrapping energies found in this work are in good agreement with detrapping energies predicted

by density functional theory when several hydrogen atoms are trapped in a single tungsten vacancy. The comparison between distributions of deuterium concentrations in material and distributions of trapped deuterium concentrations in TDSP suggests that traps characterized by a broad spectrum of detrapping energy, which may correspond to tungsten vacancies, are predominantly located near material surface.

The time evolution of hydrogen outgassing flux from PFC at room temperature in Tokamaks is investigated in the chapter 4 using R-D model with a single trap in the bulk of PFC material. The release of hydrogen is surface-limited or diffusion-limited depending on properties of material and surface processes. In both surface and diffusion-limited regimes, the long-term decay of the hydrogen outgassing flux follows a power-law in time $\sim t^{-\kappa}$, for which κ depends on the concentration of hydrogen in the material and on the kinetic order of surface desorption processes. In surface-limited regime, reaction-diffusion models of hydrogen outgassing from material bulk are shown to be equivalent to models of hydrogen outgassing from material surfaces only. Experimental results showing power-law decays of hydrogen outgassing flux from PFC during long off-plasma events ($\kappa = 0.7$ for graphite and $\kappa = 0.8$ for ITER-like JET configuration) can be then reproduced using a diffusion-reaction model in surface-limited regime.

Hydrogen recombination and desorption on tungsten surface is investigated in the chapter 5, using molecular dynamics (MD) and accelerated molecular dynamics simulations. Adsorption states, diffusion, hydrogen recombination into molecules, and clustering of hydrogen on tungsten surfaces are then analyzed. The quality of the tungsten hydrogen interatomic potential used in MD simulations is discussed regarding results of MD simulations. It is shown that that three body interactions, as parametrized in interatomic potentials available in literature, do not allow the reproduction of main experimental features of hydrogen molecular recombination and desorption. Hydrogen clustering on tungsten surface is also observed during MD simulations. Effects of hydrogen clustering on hydrogen desorption are analyzed by introducing a kinetic model describing the competition between surface diffusion, clustering and recombination. Different desorption regimes are identified, which reproduce some aspects of desorption regimes experimentally observed when tungsten surface is saturated with hydrogen.

Chapter 2

Revisited model of hydrogen outgassing from tungsten plasma-facing components during thermal desorption spectroscopy experiments

2.1 Motivation and outline

Hydrogen-tungsten systems have been investigated in the scientific community for long time [48] and are used for various industrial applications, such as dissociation of hydrogen under gaseous form exposed to hot tungsten filament surfaces[51]. Consequently, thorough investigations on hydrogen-tungsten systems have been abundantly reported since the early 40's in a variety of papers. However, most of works on hydrogen-tungsten reported in literature mainly focus on exposure of tungsten material to hydrogen gas or to hydrogen ions at very low energy [112, 52]. In this context, hydrogen retention and outgassing from tungsten material are mostly governed by surface processes. TDS experiments have been therefore modeled focusing mainly on surface processes [113, 114].

Models developed to investigate hydrogen retention and desorption induced by surface processes may be not suitable to analyze experiments performed in fusion relevant conditions where tungsten material

is usually exposed to energetic hydrogen at very large fluence. In those conditions, hydrogen retention mainly occurs in the material bulk where hydrogen can be retrapped by empty traps and can also diffuse further into material bulk during hydrogen desorption. When these bulk processes take place during TDS experiments, thermal desorption spectra may strongly differ from spectra obtained when hydrogen desorption is dominated by surface processes.

TDSP obtained in TDS experiments performed on tungsten samples implanted in fusion relevant conditions (high flux and fluence of energetic hydrogen particles) are consequently modeled in this work taking into account diffusion and retrapping of hydrogen in material bulk. It is shown that TDSP not only depend on detrapping processes but also on these bulk processes. In this context, dependencies of TDSP on trapping and detrapping activation energies, on initial filling of traps with hydrogen and on shape of trap concentration profiles are examined. Hydrogen desorption regime is shown to depend on the ratio of the detrapping rate over the trapping rate, leading to revisited interpretations of TDSP and Arrhenius plots for TDS experiments where hydrogen desorption is governed by bulk processes. We also demonstrate how the skewness of desorption peaks in TDSP can be used to evaluate whether hydrogen desorption is governed by bulk processes. Moreover, we describe how hydrogen activation energy of diffusion can be evaluated using desorption tails in TDSP.

Hydrogen desorption from tungsten samples during TDS experiments is described in this chapter with a reaction-diffusion (R-D) model, which is widely used in literature to describe hydrogen retention in metallic or carbon material [45, 35, 46, 42, 43, 44]. This work being focused on hydrogen retention and desorption induced by processes in material bulk, effects of surface processes on hydrogen desorption are ignored. Moreover, only a single type of traps is taken into account and issues related to the existence of several type of traps and their interactions are addressed in the chapter 3. The model and results outlined in this chapter can be nevertheless extended to include several types of traps as long as traps do not interact with each other (e.g. clustering of vacancies). Presented results can be naturally applied to TDS experiments performed with material and retained species other than tungsten and hydrogen. The modeling of the implantation of hydrogen into tungsten tungsten is not covered in this work.

The R-D model describing hydrogen desorption during TDS experiments, which was shortly sketched in the introduction, is detailed in the first section along with assumptions and retention and desorption parameters for hydrogen in tungsten. With these parameters, two regimes of desorption are identified depending on whether hydrogen trapping rate is larger than hydrogen diffusion rate in the retention region. In both regimes, we show in the third section that most of hydrogen detrapped during

TDS experiments diffuse toward the material front surface and desorb instead of diffusing beyond the retention region when free (solute) hydrogen concentration is in equilibrium (quasi-static desorption).

In this framework, analytical expressions of the outgassing flux as a function of the material temperature are obtained in the next section. This analytical description of TDSP is then used to analyze main features of TDSP, such as dependencies of desorption temperatures (characterizing desorption peaks in TDSP) on retention and desorption parameters. In the light of these results, the use of Arrhenius plots, generated from TDSP obtained at different heating rates, to estimate activation energy and pre-exponential factor of detrapping rates is revisited.

In addition, desorption regimes and traps can be also characterized using the skewness and the shape of desorption peaks in TDSP. The nature and the origin of long desorption tails observed sometimes in TDSP are discussed as well, and we show that activation energy of hydrogen diffusion in material can be evaluated using these desorption tails.

2.2 Reaction-diffusion model of thermal desorption spectroscopy experiments

2.2.1 Reaction-diffusion equations

We examine in this chapter the R-D model formed by the equations (1.9a) and (1.9b), briefly portrayed in the introduction, which describes hydrogen retention and desorption from metallic PFC during TDS experiments and which includes only one type of traps. This R-D model relies on the following standard assumptions:

- *Traps in material are immobile, whether they are occupied by hydrogen or not*. This assumption is valid for defects with high activation energy of diffusion like vacancies(e.g. activation energy of diffusion of tungsten vacancies is about 1.6 eV [115]).
- *Trap concentrations in material are constant* Effects of recombination and mutation of defects during TDS experiments are ignored.
- *Only one hydrogen atom can be trapped in each trap*. Although DFT simulations have shown that a single tungsten vacancy could trap several hydrogen atoms [116, 117, 118], this assumption is however reasonable considering that trapping of several hydrogen atoms in one defect can be modeled with several distinct traps [119]. This specific issue is addressed in the chapter 3.

- The temperature of the material T is uniform in material and increases at the constant heating rate α ($T = T_0 + \alpha t$) from room temperature T_0 up to $T_{\max}$ usually about 1200 K.

With these assumptions, the 1D evolution of hydrogen concentration profiles as a function of the temperature T in a material sample of thickness L in presence of one type of traps and without any source of incoming hydrogen is described by the following reaction-diffusion equations :

$$\frac{\partial \hat{c}_{\mathrm{f}}(x,T)}{\partial T} = D(T)\frac{\partial^2 \hat{c}_{\mathrm{f}}(x,T)}{\partial x^2} - \nu_{\mathrm{tr}}(T)\left[\hat{c}_{\mathrm{trap}}(x) - \hat{c}_{\mathrm{t}}(x,T)\right]\hat{c}_{\mathrm{f}}(x,T) + \nu_{\mathrm{dt}}(T)\,\hat{c}_{\mathrm{t}}(x,T) \tag{2.1a}$$

$$\frac{\partial \hat{c}_{\mathrm{t}}(x,T)}{\partial T} = \nu_{\mathrm{tr}}(T)\left[\hat{c}_{\mathrm{trap}}(x) - \hat{c}_{\mathrm{t}}(x,T)\right]\hat{c}_{\mathrm{f}}(x,T) - \nu_{\mathrm{dt}}(T)\,\hat{c}_{\mathrm{t}}(x,T) \tag{2.1b}$$

where we have introduced the following notations sketched in fig. 2.1 :

- x is the depth of the material
- $\hat{c}_{\mathrm{trap}}(x) = \frac{c_{\mathrm{trap}}(x)}{\langle c_{\mathrm{trap}} \rangle}$ is the dimensionless concentration of traps, which occupy the retention region of depth Δ, and $\langle c_{\mathrm{trap}} \rangle = \int_0^{\Delta} c_{\mathrm{trap}}(x)\mathrm{d}x$.
- $\hat{c}_{\mathrm{f}}(x,T) = \frac{c_{\mathrm{f}}(x,T)}{\langle c_{\mathrm{trap}} \rangle}$ and $\hat{c}_{\mathrm{t}}(x,T) = \frac{c_{\mathrm{t}}(x,T)}{\langle c_{\mathrm{trap}} \rangle}$ are the dimensionless concentrations of free (solute) hydrogen and trapped hydrogen
- D is the diffusion coefficient of free hydrogen assumed to be uniform in material and described by the Arrhenius law $D = \alpha^{-1} D_0\, e^{-E_{\mathrm{D}}/T}$. E_{D} is the activation energy of diffusion and $D_0 \approx \nu_0 \lambda_0^2$ where ν_0 is the lattice vibration frequency approximated by the Debye frequency ($\nu_0 \approx 10^{13}\,\mathrm{s}^{-1}$). λ_0 is the characteristic lattice cell size.
- ν_{tr} and ν_{dt} are the trapping rate and detrapping rate given by $\nu_{\mathrm{tr}} = \alpha^{-1}\nu_{tr,0}\, e^{-E_{\mathrm{tr}}/T}$ and $\nu_{dt} = \alpha^{-1}\nu_{dt,0}\, e^{-E_{\mathrm{dt}}/T}$, where E_{tr} and E_{dt} are the trapping and detrapping energies. $\nu_{\mathrm{tr},0}$ can be expressed in general as $\nu_{\mathrm{tr},0} \approx \nu_0 \rho_{\mathrm{trap}}$ where $\rho_{\mathrm{trap}} = \lambda_0^3 \langle c_{\mathrm{trap}} \rangle$ is the average dimensionless concentration of traps in material usually expressed in atomic percent (at.%). $\nu_{dt,0}$ is approximated by $\nu_{dt,0} \approx \nu_0$.

As mentioned in the first chapter, the Boltzmann constant k_b is omitted in the paper. Effects of surface retention processes on hydrogen outgassing are neglected as mentioned in the introduction, and thus boundary conditions of equations (2.1) are

$$\hat{c}_{\mathrm{f}}(0,T) = 0 \;\text{ and }\; \hat{c}_{\mathrm{f}}(L,T) = 0 \tag{2.2}$$

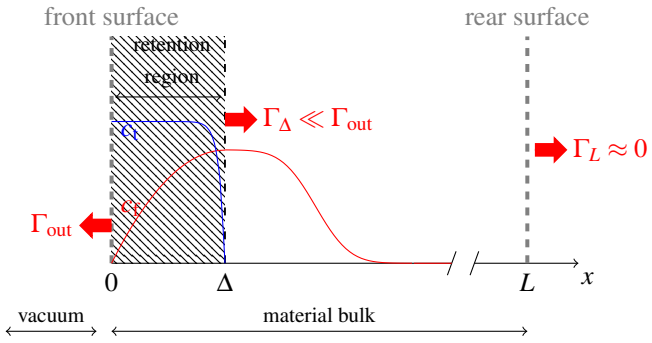

Figure 2.1: Hydrogen outgasssing from material during TDS experiments.

where $x = 0$ is the position of the material front surface, which was exposed to incoming hydrogen flux, and $x = L$ is the position of the material rear surface.

Trapped hydrogen is usually concentrated in the first micrometers near the material front surface ($\Delta \sim 0.1 - 10\,\mu$m) after implantation of material with hydrogen, whereas the material thickness is usually around some millimeters ($L \sim 1$ mm). Consequently, it can be reasonably assumed that hydrogen does not diffuse up to the material rear surface during TDS experiments $\left(\Delta + \sqrt{\int_{T_0}^{T_{max}} D(T)\mathrm{d}T} \sim 10^{-4}\,\mathrm{m} < L\right)$. Hydrogen desorption flux from rear material surface is thus neglected and the outgassing flux of hydrogen Γ_{out} from material is

$$\Gamma_{out} = D \left.\frac{\partial c_f}{\partial x}\right|_{x=0} \tag{2.3}$$

Material samples implanted with hydrogen are usually stored for long periods at room temperature after implantation and before being analyzed with TDS. It is assumed here that the storage periods are long enough such that the majority of free hydrogen remaining in material after material implantation are outgassed from material before TDS experiments are performed.

$$\hat{c}_f(x, T_0) \approx 0 \tag{2.4}$$

2.2.2 Parameters of reaction-diffusion equations relevant to thermal desorption spectroscopy experiments

TDS experiments are examined here considering hydrogen desorption and retention in tungsten samples implanted with hydrogen in fusion relevant conditions (high flux and fluence of energetic hydrogen particles). Typical retention and desorption parameters corresponding to this framework are outlined in

table 2.1. In literature, hydrogen trapping in tungsten defects is usually supposed to be limited only by diffusion without additional trapping energy barrier ($E_{\mathrm{tr}} = E_{\mathrm{D}}$ [120]).

Many DFT simulations [116, 117, 118] have suggested that activation energy of detrapping of hydrogen in tungsten vacancies decreases from $1.4\,\mathrm{eV}$ to $0.80\,\mathrm{eV}$ when several hydrogen atoms are trapped in a single vacancy. However, no indication is given about corresponding values of the trapping energy E_{tr}. One thus cannot exclude that $E_{\mathrm{tr}} \neq E_{\mathrm{D}}$ when several hydrogen atoms occupy one tungsten vacancy. Nevertheless, we assume in general in this work that $E_{\mathrm{tr}} = E_{\mathrm{D}}$, unless otherwise mentioned.

Traps are supposed to be initially uniformly filled with hydrogen

$$\frac{\hat{c}_0(x)}{\hat{c}_{\mathrm{trap}}(x)} = \tilde{c}_0 \tag{2.5}$$

where $\hat{c}_0(x) = \hat{c}_{\mathrm{t}}(x, T_0)$. Trapped hydrogen concentration is usually close to saturation at the end of the implantation phase ($\tilde{c}_0 \approx 1$) when tungsten samples are exposed to large flux and fluence of hydrogen typical of fusion relevant conditions. However, $\tilde{c}_0$ also depends on the storage time and conditions, and may thus remain unknown. We therefore consider in this work a large range of initial trap filling $(0 < \tilde{c}_0 < 1)$.

The concentration of traps $\hat{c}_{\mathrm{trap}}$ is taken uniform in the retention region when performing numerical simulations in this work:

$$\hat{c}_{\mathrm{trap}}(x) = \begin{cases} 1 \text{ if } x < \Delta \\ 0 \text{ otherwise} \end{cases} \tag{2.6}$$

This assumption is motivated by the weak dependency of TDSP on the shape of trap concentration profiles, which is detailed in section 2.5.3.

The heating rate $\alpha = 1\,\mathrm{K\,s^{-1}}$ is used to perform calculations in this work , unless otherwise stated.

2.3 Quasi-static hydrogen thermal desorption

Retention processes are analyzed in TDS experiments based on the variations of the outgassing flux as a function of the material temperature. In this part, we examine the R-D model to provide suitable analytical descriptions of outgassing flux during TDS experiments with conditions and parameters specified in tab. 2.1.

The evolution of the trapped hydrogen concentration $\hat{c}_{\mathrm{t}}$ as a function of T strongly depends on the magnitude of the trapping process. The characteristic rate of trapping ν_{tr} can be compared to the

Table 2.1: Parameters of retention and TDS experiments for tungsten samples implanted with hydrogen.

W Lattice	$\lambda_0 = 3.16$, $\nu_0 = 10^{13}\,\mathrm{s}^{-1}$	
Material thickness	$L = 0.1 - 1$ mm	
Diffusion H	$D_0 = 10^7\,\mathrm{m}^2\mathrm{s}^{-1}$, $E_\mathrm{D} = 0.40\,\mathrm{eV}$	[59]
Trapping H	$\nu_{\mathrm{tr},0} = 0$, $E_\mathrm{tr} = E_\mathrm{D}$	[36]
	$\rho_\mathrm{trap} \approx 10^{-8} - 10$ at.%	
Detrapping of H	$\nu_{\mathrm{dt},0} = \nu_0$, $E_\mathrm{dt} = 1.00 - 1.60\,\mathrm{eV}$	[20]
Initial trap filling	$0 < \tilde{c}_0 < 1$	
Retention depth	$\Delta = 0.1 - 10\,\mu\mathrm{m}$	[36]
$T_0 - T_\mathrm{max}$	$300\,\mathrm{K} - 1200\,\mathrm{K}$	
α	$1\,\mathrm{K\,s}^{-1}$	

characteristic rate of diffusion in the retention region $\frac{D}{\Delta^2}$ using the dimensionless parameter

$$\xi_\mathrm{trapping} = \frac{\nu_\mathrm{tr}}{D/\Delta^2} \tag{2.7}$$

and two regimes of hydrogen thermal desorption can be distinguished:

- **the detrapping-limited regime** characterized by $\xi_\mathrm{trapping} \ll 1$, for which hydrogen is not trapped in the retention region while diffusing toward material surface. Hydrogen desorption is thus limited by hydrogen detrapping, hence the term *detrapping-limited regime*.
- **the retrapping-limited regime** characterized by $\xi_\mathrm{trapping} \gg 1$ and for which hydrogen is retrapped in the retention region while diffusing toward material surface. Hydrogen desorption is thus limited by hydrogen retrapping in the retention region, hence the term *retrapping-limited regime*.

We demonstrate in the following sections that the evolution of the free hydrogen concentration in material during TDS experiments is quasi-static under certain conditions in both retrapping-limited and detrapping-limited regimes. The term quasi-static stands here to indicate that variations of free hydrogen concentrations are negligible compared to variations of trapped hydrogen concentrations with the material temperature, which translates as $\left|\frac{\partial \hat{c}_\mathrm{f}}{\partial T}\right| \approx 0$ in equation (2.1a). When hydrogen outgassing is quasi-static, R-D equations (2.1) can be approximated and analytical expressions of the outgassing flux can be obtained in both regimes.

2.3.1 Hydrogen desorption in detrapping-limited regime

In detrapping-limited regime, hydrogen trapping is slow compared to diffusion of hydrogen in the retention region toward material surface, and the trapping term in R-D equations (2.1) can be ignored. These R-D equations can be thus recast into a single standard diffusion equation with a temperature-dependent non-uniform source. The characteristic depth of hydrogen diffusion in the material is then $\delta(T) = \sqrt{\int_{T_0}^{T} D(\tilde{T})\mathrm{d}\tilde{T}}$.

When the material temperature is large enough such that hydrogen deeply diffuses beyond the retention region (condition 2.8) and when the variations of the detrapping rate with temperature are slow compared to the hydrogen diffusion rate in the retention region (condition 2.9), variations of free hydrogen concentration are quasi-static $\left(\left|\frac{\partial \ln \hat{c}_\mathrm{f}}{\partial T}\right| \ll \left|\frac{\partial \ln \hat{c}_\mathrm{t}}{\partial T}\right| \text{in eq. 2.1a}\right)$ as depicted in figure 2.2c.

$$\delta(T) \gg 1 \tag{2.8}$$

$$\left|\frac{\partial \ln \hat{c}_\mathrm{t}}{\partial T}\right| \approx \nu_\mathrm{dt} \ll \frac{D}{\Delta^2}, \tag{2.9}$$

During quasi-static hydrogen desorption, the diffusion flux of hydrogen beyond the retention region $\Gamma_\Delta = -D\left.\frac{\partial \hat{c}_\mathrm{f}}{\partial x}\right|_{x=\Delta}$ is negligible compared to the outgassing flux ($\Gamma_\Delta \ll \Gamma_\mathrm{out}$, fig. 2.2a). Γ_Δ is actually low because of the fast diffusion of hydrogen in the retention region and beyond the retention region (fig. 2.2b), which allows slow variations of the free hydrogen concentration in the retention region and thus flat profiles of free hydrogen concentration

The conditions (2.8) and (2.9) correspond to the temperature range $T_\mathrm{D} < T < T_\mathrm{dt}$ where T_D and T_dt are defined by $\delta(T_\mathrm{D}) = \Delta$ and $\nu_\mathrm{dt}(T_\mathrm{dt}) = \frac{D(T_\mathrm{dt})}{\Delta^2}$. In this temperature range, majority of hydrogen detrapped in the retention region diffuses toward the front surface of material and desorbs. Therefore, the outgassing flux does not depend on the spatial distribution of the trapped hydrogen concentration $\hat{c}_0(\hat{x}) \sim \hat{c}_\mathrm{trap}(\hat{x})$ in the material but only on the quantity of total hydrogen retained in the material $\int_0^\Delta \hat{c}_0(x')\mathrm{d}x'$.

Consequently, the concentration of traps can be conveniently assumed to be uniform in the retention region and the initial concentration of trapped hydrogen $\hat{c}_0(x)$ can be replaced by the average concentration $\langle \hat{c}_0 \rangle = \int_0^\Delta \hat{c}_0(x)\mathrm{d}x$. Profiles of the free hydrogen concentration in the retention region thus follow

$$\hat{c}_\mathrm{f}(x,T) \sim \langle \hat{c}_0 \rangle \left(\frac{x}{\Delta} - \frac{x^2}{2\Delta^2}\right) \tag{2.10}$$

The diffusion operator and the outgassing flux can be then explicitly formulated as a function of

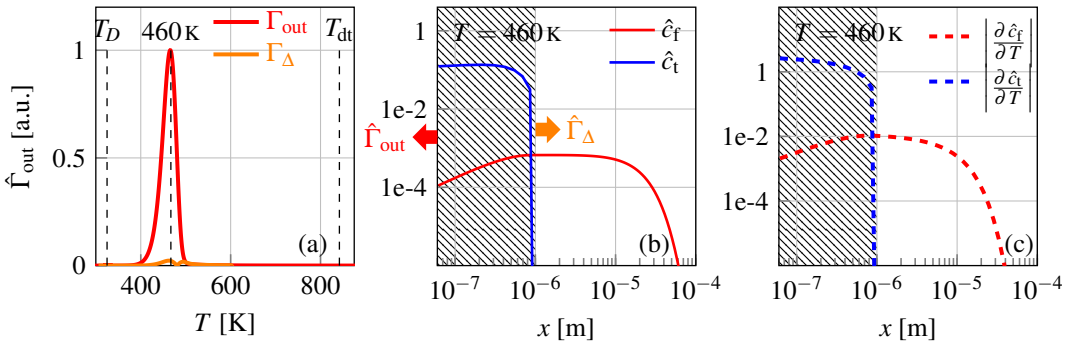

Figure 2.2: Hydrogen desorption in detrapping-limited regime simulated with R-D equations (2.1) using $E_{dt} = 1.40\,\text{eV}$, $\Delta = 1\,\mu\text{m}$, $\tilde{c}_0 = 1$ and $\rho_{trap} = 10^{-6}$ at.%.

the free hydrogen concentration at the boundary of the retention region $\hat{c}_f(\Delta, T)$ (exp. 2.11 and 2.12).

$$\hat{D}(T)\frac{\partial^2 \hat{c}_f(x,T)}{\partial \hat{x}^2} \approx 2D(T)\frac{\hat{c}_f(\Delta,T)}{\Delta^2} \tag{2.11}$$

$$\hat{\Gamma}_{out}(T) \approx 2D(T)\frac{\hat{c}_f(\Delta,T)}{\Delta} \tag{2.12}$$

In the temperature range $T_D < T < T_{dt}$, it is thus legitimate to replace the R-D equations (2.1) by the first-order differential equations (2.13), where $\bar{c}_f = \hat{c}_f(1,T)$, $\bar{c}_t = \hat{c}_t(1,T)$ and $\nu_D = 2\frac{D}{\Delta^2}$.

$$\frac{d\bar{c}_f}{dT} = -\nu_D \bar{c}_f - \nu_{tr}\bar{c}_f(1-\hat{c}_t) + \nu_{dt}\bar{c}_t \tag{2.13a}$$

$$\frac{d\bar{c}_t}{dT} = \nu_{tr}\bar{c}_f(1-\bar{c}_t) - \nu_{dt}\bar{c}_t \tag{2.13b}$$

The outgassing flux as a function of $\bar{c}_f$ then reads

$$\hat{\Gamma}_{out} = \nu_D \bar{c}_f \tag{2.14}$$

The terms $\frac{d\bar{c}_f}{dT}$ and $\nu_{tr}\bar{c}_f(1-\bar{c}_t)$ can be ignored in equations (2.13) but are kept for the sake of generality. An analytical expression of the outgassing flux can be obtained by solving the equations (2.13) in the temperature range $T_D < T < T_{dt}$ (see sec. 2.4).

2.3.2 Hydrogen desorption in retrapping-limited regime

In retrapping-limited regime, the trapped hydrogen concentration can be in equilibrium, *id est* $\frac{\partial \hat{c}_t}{\partial T} \approx 0$ in eq. (2.1b), only when the trapping rate is larger than the detrapping rate (condition 2.15).

$$\xi_{dt} = \frac{\nu_{dt}}{\nu_{tr}} \ll 1 \tag{2.15}$$

The condition (2.15) is valid when $T < T_{tr}$, where T_{tr} is defined by $\xi_{dt}(T_{tr}) = 1$. In this temperature range, the equation (2.1b) reads

$$\hat{c}_t(x,T) = \hat{c}_{trap}(x)\frac{\nu_{tr}(T)\hat{c}_f(x,T)}{\nu_{dt}(T) + \nu_{tr}(T)\hat{c}_f(x,T)} \tag{2.16}$$

In this work, we consider uniform trap concentration profiles in the retention region, i.e. $\hat{c}_{trap} = 1$ if $x < \Delta$ and $\hat{c}_{trap} = 0$ otherwise, and effects of non-uniform trap concentrations are thus ignored. It can be shown that these effects are however limited, and results derived below remain valid also for non-uniform trap concentrations.

When the relationship (2.16) holds, the free hydrogen concentration $\hat{c}_f$ can be expressed as a function of the total hydrogen concentration $\hat{c}_H = \hat{c}_t + \hat{c}_f$ (eq. 2.17).

$$\hat{c}_f \approx \xi_{dt}\frac{\hat{c}_H}{1-\hat{c}_H} \tag{2.17}$$

The reaction-diffusion equations (2.1a) can be then recast into a single non-linear diffusion equation for $\hat{c}_H$ (eq. 2.18), where $D_{eff} = D\frac{\nu_{dt}}{\nu_{tr}}$ is the effective diffusion coefficient.

$$\frac{\partial \hat{c}_H}{\partial T} = \frac{\partial}{\partial x}\left(\frac{D_{eff}}{(1-\hat{c}_H)^2}\frac{\partial \hat{c}_H}{\partial x}\right) \tag{2.18}$$

The characteristic depth of diffusion of hydrogen in the material is thus approximated by $\delta_{eff}(T) = \sqrt{\int_{T_0}^{T} D_{eff}(T')\mathrm{d}T'}$.

In this context, the outgassing flux reads

$$\hat{\Gamma}_{out} = D_{eff}\left.\frac{\partial \hat{c}_H/(1-\hat{c}_H)}{\partial x}\right|_{x=0} \tag{2.19}$$

In the temperature range $T_{eq} < T < T_{tr}$, the condition (2.15) imposes $\hat{c}_f \ll \hat{c}_t$ and thus $\left|\frac{\partial \hat{c}_f}{\partial T}\right| \ll \left|\frac{\partial \hat{c}_t}{\partial T}\right|$, which guarantees that the evolution of $\hat{c}_f$ is quasi-static ($\frac{\partial \hat{c}_f}{\partial T} \approx 0$ in eq. 2.1a). We might therefore expect that most of hydrogen desorb through the front surface of material rather than diffuse beyond the

retention region like in detrapping-limited regime.

The inequality $\hat{\Gamma}_{\text{out}} \gg \hat{\Gamma}_{\Delta}$ cannot be analytically established in retrapping-limited regime because of the non-linearities in equation (2.18). We however show hereafter that this inequality qualitatively holds in the temperature range $T_D < T < T_{\text{tr}}$ where T_D is again defined by $\delta(T_D) = \Delta$.

The characteristic temperature of desorption T_{des} can be defined by $\int_{T_0}^{T_{\text{des}}} \hat{\Gamma}_{\text{out}}(T')\mathrm{d}T' \approx \Delta$. When the characteristic depth of effective diffusion is shorter than the retention depth ($\delta_{\text{eff}}(T) < \Delta$), $\hat{\Gamma}_{\text{min}} = \frac{D_{\text{eff}}}{\Delta}$ is a low bound for estimations of outgassing flux, and T_{des} can be evaluated by

$$D_{\text{eff}} \frac{T_{\text{des}}^2}{E_{\text{eff}}} \approx \Delta^2 \tag{2.20}$$

where $E_{\text{eff}} = E_{\text{dt}} - E_{\text{tr}} + E_{\text{D}}$. The relationship (2.20) can be recast into $\delta_{\text{eff}}(T_{\text{des}}) \approx \Delta$, which indicates that most of hydrogen are outgassed when hydrogen atoms can effectively diffuse from the retention region toward the front surface of material. The characteristic width δT_{des} of the desorption peak can be estimated from the relationship (2.20) to be $\delta T_{\text{des}} \sim \frac{T_{\text{des}}^2}{E_{\text{eff}}}$.

Let now compare the characteristic concentration of free hydrogen in the retention region $\langle \hat{c}_{\text{f}}(T_{\text{des}}) \rangle \sim \xi_{\text{dt}}(T_{\text{des}})$ to the characteristic concentration of free hydrogen beyond the retention region $\bar{c}_{\text{f}}(T_{\text{des}}) \sim \frac{1}{\sqrt{D(T_{\text{des}})}} \int_{T_0}^{T_{\text{des}}} \frac{\hat{\Gamma}_D(T')}{\sqrt{T-T'}} \mathrm{d}T'$ during hydrogen outgassing.

If $\hat{\Gamma}_{\Delta} \sim \hat{\Gamma}_{\text{out}} \gtrsim \frac{D_{\text{eff}}}{\Delta}$, the free hydrogen concentration at $x = \Delta$ obeys $\bar{c}_{\text{f}}(T_{\text{des}}) \gtrsim \frac{D_{\text{eff}}(T_{\text{des}})}{\Delta^2} \sqrt{\frac{\delta T_{\text{des}} \Delta^2}{D(T_{\text{des}})}}$. Since $D_{\text{eff}} = D \frac{\nu_{\text{dt}}}{\nu_{\text{tr}}}$, we have

$$\frac{\bar{c}_{\text{f}}(T_{\text{des}})}{\langle \hat{c}_{\text{f}}(T_{\text{des}}) \rangle} \gtrsim \frac{\delta(T_{\text{des}})}{\Delta} \sqrt{\frac{E_{\text{D}}}{E_{\text{eff}}}} \tag{2.21}$$

Free hydrogen diffuses way beyond the retention region when $T_{\text{des}} > T_{\text{D}}$ ($\delta(T_{\text{des}}) \gg \Delta$). According to the relationship (2.21), the free hydrogen concentration would be much larger beyond the retention region than in the retention region itself in the temperature range $T_{\text{D}} < T < T_{\text{tr}}$ if $\hat{\Gamma}_{\Delta} \sim \hat{\Gamma}_{\text{out}}$. Such accumulation of free hydrogen beyond the retention region contradicts the fact that a majority of hydrogen is supposed to have desorbed when $T \sim T_{\text{des}}$.

Therefore, the majority of hydrogen diffuses from the retention region toward the front surface of material instead of diffusing beyond the retention region $\left(\hat{\Gamma}_{\Delta} \ll \hat{\Gamma}_{\text{out}}\right)$ in the temperature range $T_{\text{D}} < T < T_{\text{tr}}$. These qualitative results are confirmed when numerically solving equations (2.1) as illustrated in figure 2.3a and 2.3b. We might thus expect that R-D equations can be also well approximated by equations (2.13) in retrapping-limited regime. The outgassing flux is however underestimated when approximating $\frac{\partial \hat{c}_{\text{H}}}{\partial x}$ by $\frac{\hat{c}_{\text{H}}}{\Delta}$

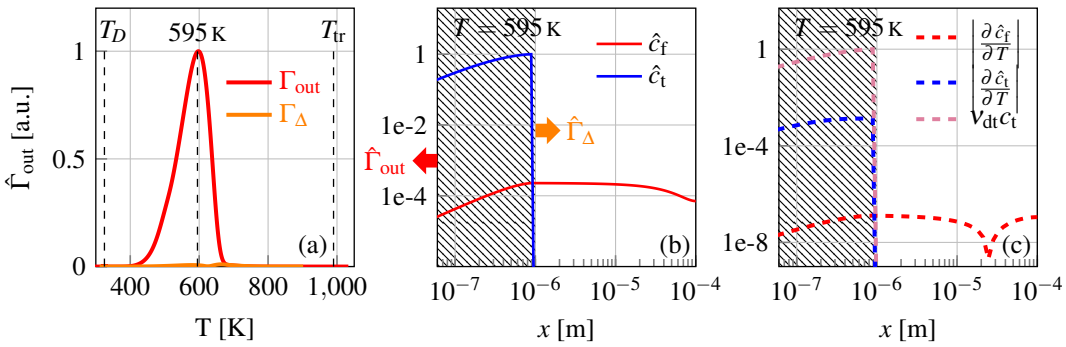

Figure 2.3: Hydrogen desorption in retrapping-limited regime simulated with R-D equations (2.1) using $E_{dt} = 1.40\,\text{eV}$, $\Delta = 1\,\mu\text{m}$, $\tilde{c}_0 = 1$ and $\rho_{trap} = 10^{-3}$ at.%.

when $T < T_{des}$ because of the slow effective diffusion of hydrogen ($\delta_{eff}(T) < \Delta$). This approximation may nevertheless holds when $T > T_{des}$.

Consequently, the first order differential equations (2.13) cannot provide a very accurate approximation of the R-D equations (2.1) but can provide reasonable upper bounded estimations of the outgassing flux as a function of the temperature in the temperature range $T_D < T < T_{tr}$, as illustrated in figure 2.7. In particular, temperatures of desorption peaks estimated with the first order differential equations (2.13) are close to T_{des} obtained with equations (2.1) (sec. 2.5.1).

Hydrogen trapped concentration have been assumed to be in equilibrium when $T < T_{tr}$ (eq. 2.16). However, equilibrium of $\hat{c}_t$ is formally reached when $T > T_{eq}$ where the equilibrium temperature T_{eq} is defined by $\int_{T_0}^{T_{eq}} \nu_{tr}(T')\hat{c}_f(\Delta,T') + \nu_{dt}(T')\mathrm{d}T' = 1$. Noticing that $\int_{T_0}^{T} \nu_{tr}(T')\hat{c}_f(\Delta,T') + \nu_{dt}(T')\mathrm{d}T' \sim \int_{T_0}^{T} \nu_{dt}(T')\mathrm{d}T'$ and that $\delta_{eff}(T < T_{des}) < \Delta$, one can deduce that $T_{eq} < T_{des}$ in retrapping-limited regime where $\xi_{trapping} = \frac{\nu_{tr}}{D/\Delta^2} \gg 1$. Hydrogen trapped concentration is thus in equilibrium $\left(\left|\frac{\partial \hat{c}_t}{\partial T}\right| \ll \nu_{dt}\hat{c}_t\right)$ during main part of hydrogen desorption (fig. 2.3c).

It is therefore legitimate to neglect effects of initial trap filling when qualitatively analyzing hydrogen outgassing in the temperature range $T_D < T < T_{tr}$. A quantitative description of these effects is nevertheless provided in section 2.5.2.

In the region $x < \Delta/\xi_{trapping}$, hydrogen cannot be retrapped and immediately desorbs from material. Hydrogen concentration in this narrow region is close to zero when $\delta_{eff}(T) > \Delta/\xi_{trapping}$. In parallel, hydrogen desorption takes place as if the retention region was semi-infinite while $\delta_{eff}(T) < \Delta$. This invites us to seek solutions of the diffusion equation (2.18) under a self-similar form $\frac{\hat{c}_H}{1-\hat{c}_H} = f(\chi = \frac{x}{\delta_{eff}})$ in the temperature range $\Delta/\xi_{trapping} < \delta_{eff}(T) < \Delta$ with $f(0) \approx 0$ and $f'(+\infty) \to 0$. This latter asymptotic condition results from the limited diffusion of hydrogen beyond the retention region highlighted earlier in

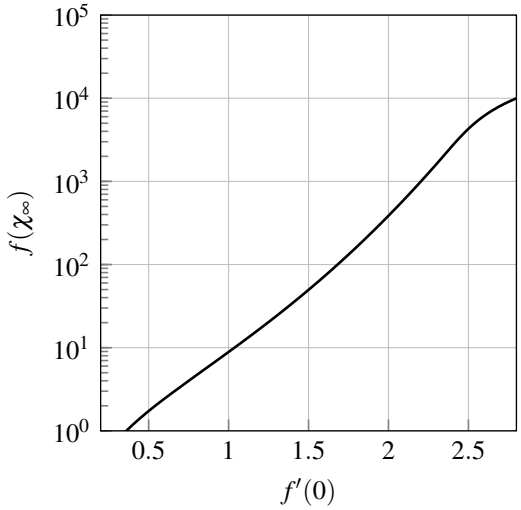

Figure 2.4: $f(\chi_\infty)$ as a function of $f'(0)$ for self-similar solutions of equation (2.18) obtained by shooting method for $0 \leq \chi \leq \chi_\infty = 10^5$ with f(0)=0.

this section. The outgassing flux can be then expressed as a function of $f'(0)$.

$$\hat{\Gamma}_{\text{out}} = \frac{D_{\text{eff}}}{\delta_{\text{eff}}} f'(0) \tag{2.22}$$

The introduction of a self-similar solution in equation (2.18) however leads to an ill-conditioned problem since the value of $\hat{c}_{\text{H}}$ at $x = \Delta$, which determine $f(+\infty)$, varies with temperature during hydrogen desorption. One can nevertheless numerically show that $f'(0)$ weakly depends on $f(+\infty)$ when $\delta_{\text{eff}}(T) < \Delta$ for which $f(+\infty) > 1$ (fig. 2.4). The expression (2.22) thus constitutes a good approximation of the outgassing flux and the following dependency

$$\hat{\Gamma}_{\text{out}} \sim \frac{D_{\text{eff}}}{\delta_{\text{eff}}} \tag{2.23}$$

holds when $\Delta/\xi_{\text{trapping}} < \delta_{\text{eff}}(T) < \Delta$ with $f(0) \approx 0$. The validity of the dependency 2.23 is numerically verified in section 2.7.3.

2.4 Retrapping-limited vs detrapping-limited thermal desorption

When hydrogen trapping is only limited by diffusion ($E_{\text{tr}} = E_{\text{D}}$), the dimensionless parameter ξ_{trapping} reads $\xi_{\text{trapping}} = \left(\frac{\Delta}{\lambda_0}\right)^2 \rho_{\text{trap}}$, where ρ_{trap} is the atomic concentration of traps. Hydrogen desorption

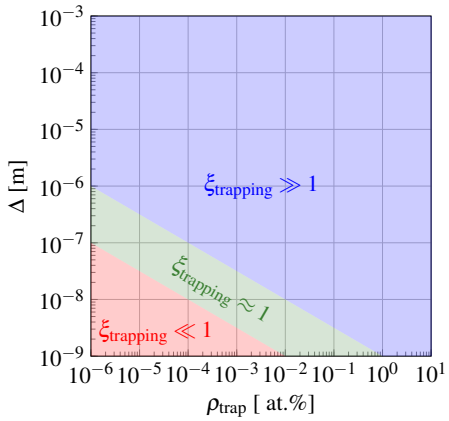

Figure 2.5: Graph of ξ_{trapping} as a function of the trap concentration ρ_{trap} and the retention depth Δ assuming $E_{\text{tr}} = E_{\text{D}}$.

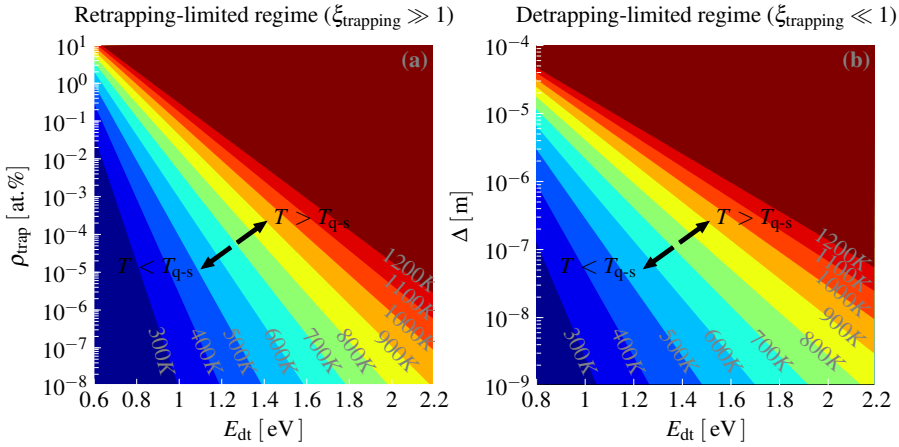

Figure 2.6: Temperature $T_{\text{q-s}}$ in retrapping-limited regime (b) and detrapping-limited regime (c) calculated assuming $E_{\text{tr}} = E_{\text{D}}$. Each color represents a range of 100K (e.g. the yellow color corresponds to $800\,\text{K} < T < 900\,\text{K}$).

is thus retrapping-limited when either the trap concentration is large $\left(\rho_{\text{trap}} \gg \left(\frac{\lambda_0}{\Delta}\right)^2\right)$ or when traps are located far in the material bulk $\left(\Delta \gg \lambda_0 \frac{1}{\sqrt{\rho_{\text{trap}}}}\right)$. On the other hand, the detrapping-limited regime corresponds to either low trap concentration or to traps concentrated in shallow regions under material surface. The detrapping-limited regime might then be reached in the first sub-surface atomic layers where hydrogen implantation usually takes place ($\Delta \sim 10\,\text{nm}$), but concentrations of traps might be very high in this region as well. In general, $\Delta \gtrsim 1\,\mu\text{m}$ and $\rho_{\text{trap}} > 10^{-5}$ at.% for material samples exposed to flux and fluence of hydrogen particles relevant to fusion conditions. Hydrogen desorption is therefore likely to be retrapping-limited during TDS experiments performed on tungsten samples implanted with hydrogen in fusion relevant conditions (fig. 2.5).

Let now examine whether outgassing of hydrogen is quasi-static during TDS experiments, *id est* whether hydrogen thermal desorption occurs in the temperature range $T_\mathrm{D} < T < T_\mathrm{dt}$ in detrapping-limited regime and $T_\mathrm{D} < T < T_\mathrm{tr}$ in retrapping-limited regime. The upper bound temperatures T_dt and T_tr are equal to the temperature $T_\mathrm{q\text{-}s}$ defined by $\xi_\mathrm{q\text{-}s}(T_\mathrm{q\text{-}s}) = 1$, where

$$\xi_\mathrm{q\text{-}s}(T) = \frac{\nu_\mathrm{dt}(T)}{\nu_\mathrm{tr}(T) + D(T)/\Delta^2} \tag{2.24}$$

Considering the activation energy of diffusion of hydrogen in tungsten $E_\mathrm{D} = 0.39\,\mathrm{eV}$ and typical retention depths $\Delta \sim 1\,\mu\mathrm{m}$ for samples implanted with hydrogen in fusion relevant conditions (tab. 2.1), the lower bound temperature T_D defined by $\delta(T_\mathrm{D}) = \Delta$ is usually close to room temperature (exp. 2.25).

$$T_\mathrm{D} \sim 300\,\mathrm{K} \tag{2.25}$$

Assuming that trapping is only limited by diffusion ($E_\mathrm{tr} = E_\mathrm{D}$), $T_\mathrm{q\text{-}s}$ depends either on the retention depth Δ and on the activation energy of detrapping E_dt in detrapping-limited regime, or on the trap concentration ρ_trap and E_dt in retrapping-limited regime. Considering standard retention and desorption parameters summarized in tab. 2.1, the temperature $T_\mathrm{q\text{-}s}$ is thus around $800 - 1000\,\mathrm{K}$ in retrapping-limited and detrapping-limited regimes (fig. 2.5b and fig. 2.5c).

Experimental values of temperature of desorption peaks in TDSP reported in literature are well above room temperature and are usually below $1000\,\mathrm{K}$. Since TDS experiments are expected to occur in retrapping-limited regime, it is thus likely that hydrogen desorption occurs in the temperature range $T_\mathrm{D} < T < T_\mathrm{q\text{-}s}$ in most of TDS experiments. These conclusions do not depend on the heating rate α used in TDS experiments.

We can therefore seek analytical descriptions of the hydrogen outgassing flux as a function of the material temperature by substituting the R-D equations (2.1) with the first order differential equations (2.13), although the accuracy of these latter equations to describe hydrogen outgassing during TDS experiments is limited (but still acceptable) in retrapping-limited regime (see below). Equations (2.13) can be analytically solved noticing that the evolution of $\bar{c}_\mathrm{f}$ is also quasi-static in the temperature range $T_\mathrm{D} < T < T_\mathrm{q\text{-}s}$ $\left(\frac{\partial \bar{c}_\mathrm{f}}{\partial T} \approx 0 \text{ in eq. 2.13a}\right)$. The outgassing flux is then determined using the relationship (2.14) (see appendix B).

- in detrapping-limited regime

$$\hat{\Gamma}_{\text{out}}(T) = \quad \Delta\hat{c}_0 \nu_{\text{dt}}(T) e^{-\Omega_{\text{dt}}(T)} \tag{2.26}$$

where $\Omega_{\text{dt}}(T) = \int_{T_0}^{T} \nu_{\text{dt}}(T')\text{d}T'$.

- in retrapping-limited regime

$$\hat{\Gamma}_{\text{out}}(T) = \quad 2\frac{D_{\text{eff}}(T)}{\Delta} \frac{\omega\left(-\hat{c}_0 e^{-\hat{c}_0} e^{-\Omega_{\text{eff}}(T)}\right)}{1+\omega\left(-\hat{c}_0 e^{-\hat{c}_0} e^{-\Omega_{\text{eff}}(T)}\right)} \tag{2.27}$$

where $\Omega_{\text{eff}}(T) = \int_{T_0}^{T} \nu_D(T') \frac{\nu_{\text{dt}}(T')}{\nu_{\text{tr}}(T')}\text{d}T'$ and ω is the Lambert function.

Estimations of the outgassing flux with the relationship (2.26) in detrapping-limited regime are very accurate (fig. 2.7a), as outlined in section 2.3.2.

Estimations of the outgassing flux with the expression (2.27) are less accurate in retrapping-limited regime because of the slow effective diffusion of hydrogen in the retention region. These estimations remain nevertheless good enough to describe main features of TDSP (fig. 2.7b-h). This point is illustrated in the next section, where dependencies of TDSP on retention and desorption parameters are investigated in retrapping-limited regime using expressions (2.27).

2.5 Properties of thermal desorption spectra

Properties of thermal desorption spectra are investigated in this section using typical retention and desorption parameters detailed in section 2.2.2. It can be easily verified that hydrogen desorption peaks in TDSP, calculated with these retention and desorption parameters, are in the temperature range $T_{\text{D}} < T < T_{\text{q-s}}$, in which the relationships (2.26) and (2.27) can be used to calculate the outgassing flux.

2.5.1 Temperature of desorption

The temperature of desorption T_{des} in TDSP is the temperature at which the outgassing flux is maximum during TDS experiment (eq. 2.28).

$$\left.\frac{\partial \hat{\Gamma}_{\text{out}}}{\partial T}\right|_{T=T_{\text{des}}} = 0 \tag{2.28}$$

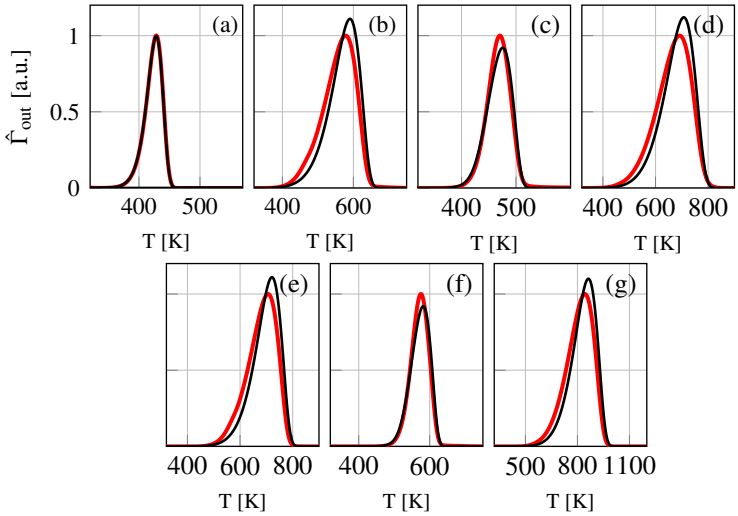

Plot		(a)	(b)	(c)	(d)	(e)	(f)	(g)
Δ	$[\mu m]$	1	1	1	10	1	1	10
ρ_{trap}	[at.%]	10^{-7}	10^{-2}	10^{-5}	10^{-2}	10^{-2}	10^{-5}	10^{-2}
E_{dt}	[eV]	1.40	1.30	1.30	1.30	1.60	1.60	1.60
$\xi_{trapping}$		10^{-2}	10^{3}	1	10^{5}	10^{2}	1	10^{5}

Figure 2.7: Comparaison between TDSP calculated with R-D equations (2.1) (red) and TDSP calculated with the expressions (2.26) and (2.27) (black) in detrapping-limited regime (a) and retrapping-limited regime (b-g).

T_{des} can be expressed as a function of retention and desorption parameters using expressions (2.26) and (2.27) (appendix C):

- in detrapping-limited regime, T_{des} is the solution of $\Omega_{dt}(T_{des}) \approx 1$ and

$$T_{des} = \frac{E_{dt}}{2} \frac{1}{\omega\left(\sqrt{\frac{\nu_{dt,0} E_{dt}}{4\alpha}}\right)} \tag{2.29}$$

- in retrapping-limited regime, T_{des} is the solution of $\Omega_{eff}(T_{des}) = \Theta(\hat{c}_0)$, where Θ is defined in appendix C and verifies $0.46 < \Theta < 1$. T_{des} then reads

$$T_{des} = \frac{E_{eff}}{2} \frac{1}{\omega\left(\sqrt{\frac{\nu_{eff,0} E_{eff}}{2\alpha\Theta(\hat{c}_0)}}\right)} \tag{2.30}$$

where ω is the Lambert function, $E_{eff} = E_{dt} + E_D - E_{tr}$ and $\nu_{eff,0} = \frac{\nu_{dt,0} D_0}{\nu_{tr,0} \Delta^2}$. We have used the exact pre-exponential factors $\nu_{dt,0}$ and $\nu_{eff,0}$ in both expressions of T_{des} for the sake of generality. $\nu_{dt,0} = \nu_0$

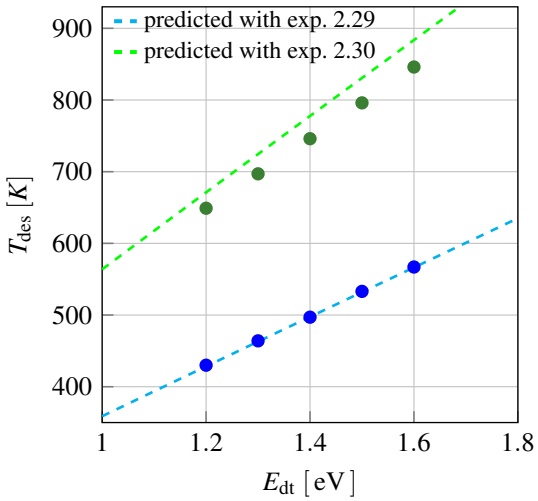

Figure 2.8: Values of T_{des} from TDSP calculated using eq. (2.1) with $E_{dt} = 1.2 - 1.6\,\text{eV}$, $\Delta = 10^{-6}\,\text{m}$ and $\hat{c}_0 = 1$ in detrapping-limited regime (blue dots, $\rho_{trap} = 10^{-6}$ at.%) and in retrapping-limited regimes (green dots, $\rho_{trap} = 10^{-3}$ at.%).

and $\nu_{eff,0} = \left(\frac{\lambda_0}{\Delta}\right)^2 \frac{\nu_0}{\rho_{trap}}$ with the notations introduced in section 2.2.1.

T_{des} is well predicted by formula (2.29) in detrapping-limited regime (fig. 2.8). In retrapping-limited regime, predictions of T_{des} with the formula (2.30) are less accurate but still reasonable considering that the linear dependency of T_{des} on E_{dt} is well reproduced and that logarithmic dependencies on ρ_{trap} and Δ can be also well reproduced. The equation $\Omega_{eff}(T_{des}) = \Theta(\hat{c}_0)$ can be indeed approximated into $\delta_{eff}(T_{des}) \sim \Delta$ since $0.46 < \Theta < 1$, and this latter estimation corresponds to the qualitative estimation of T_{des} in retrapping-limited regime obtained in section 2.3.2 (eq. 2.20).

Values of T_{des} significantly differ between detrapping-limited regime and retrapping-limited regime (fig. 2.8) because of the different pre-exponential factors in the expressions of T_{des} ($\nu_{dt,0}$ in exp. 2.29 in detrapping-limited regime and $\nu_{eff,0}$ in exp. 2.30 in retrapping-limited regime). Since $\nu_{eff,0} \ll \nu_{dt,0}$ with typical retention and desorption parameters, T_{des} is larger in retrapping-limited regime than in detrapping-limited regime. This can be seen as a consequence of the retrapping of hydrogen in the retention region, which slows down hydrogen desorption.

2.5.2 Effects of initial filling of traps with hydrogen on thermal desorption spectra

The initial concentration of trapped hydrogen $\hat{c}_0$ is generally unknown when modeling

The initial filling of traps with hydrogen $\hat{c}_0$ is generally unknown when modeling TDS experiments, although traps are often assumed to be initially close to saturation ($\hat{c}_0 \approx 1$). It might be therefore

useful to predict the dependency of desorption peaks on $\hat{c}_0$.

$\hat{\Gamma}_{\text{out}}$ depends on $\hat{c}_0$ in retrapping-limited regime but not in detrapping-limited regime according to relationships (2.26) and (2.27) (fig. 2.9a). The dependency of T_{des} on $\hat{c}_0$ is qualitatively reproduced in retrapping-limited regime(fig. 2.9b), although the expression (2.30) does not give an precise estimation of T_{des}.

The dependency of T_{des} on $\hat{c}_0$ is only significant when $\hat{c}_0 > 0.1$. For these values of $\hat{c}_0$, desorption peaks shift toward low temperature and become wider due to the quick detrapping of hydrogen from traps filled with hydrogen when hydrogen desorption starts, which leads to a quick depletion of detrapped hydrogen to maintain equilibrium of $\hat{c}_{\text{t}}$.

Shift and widening of desorption peaks in TDSP produced when $\hat{c}_0$ increases may be experimentally used to investigate traps mutations or recombination when a same tungsten sample is repeatedly exposed to different hydrogen doses between TDS experiments, or when investigating the decay of retained hydrogen during storage of samples before performing TDS experiments.

2.5.3 Effects of the shape of trap concentration profiles on thermal desorption spectra

In this work, effects of the shape of trap concentration profiles on hydrogen desorption are ignored by assuming that the trap concentration $\hat{c}_{\text{trap}}$ is uniform in the retention region. In detrapping-limited regime, the outgassing flux does not depend on the shape of trap concentration profile (sec. 2.3.1). In retrapping-limited regime, the diffusion coefficient in the equation (2.18) reads $\frac{D_{\text{eff}}}{(\hat{c}_{\text{trap}}-\hat{c}_{\text{H}})^2}$ when taking into account variations of $\hat{c}_{\text{trap}}$ along the depth of the material. Differences in desorption peaks induced by variations of trap concentration in material depth are thus small and fall in experimental error bars when $\frac{d}{dx}\hat{c}_{\text{trap}}(x) \sim 1/\Delta$ (fig. 2.10).

Effects of the non-uniformity of trap concentrations can be thus ignored when modeling and analyzing hydrogen desorption in TDS experiments. Rough experimental estimations of the shape of trap concentration profiles are then sufficient to examine main features of TDSP. Similar conclusions can be made when the initial filling of traps with hydrogen $\tilde{c}_0$ is not uniform in material, provided that $\frac{d}{dx}\tilde{c}_0(x) \sim 1/\Delta$.

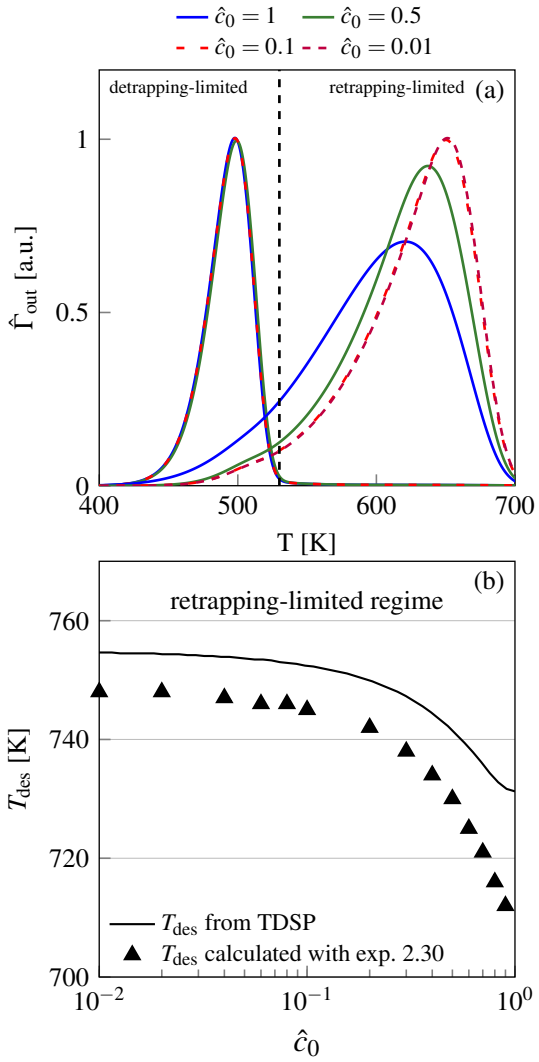

Figure 2.9: (a): TDSP calculated with $E_{dt} = 1.40\,\text{eV}$ and $\Delta = 5\,\mu\text{m}$ in detrapping-limited regime ($\rho_{trap} = 10^{-8}$ at.%) and in retrapping-limited regime ($\rho_{trap} = 10^{-4}$ at.%), and rescaled as a function of $\hat{c}_0^{-1}$.
(b): Desorption temperature T_{des} obtained from TDSP calculated in retrapping-limited regime (triangle) and T_{des} evaluated with the expression (2.30)(solid line) plotted as a function of $\hat{c}_0$.

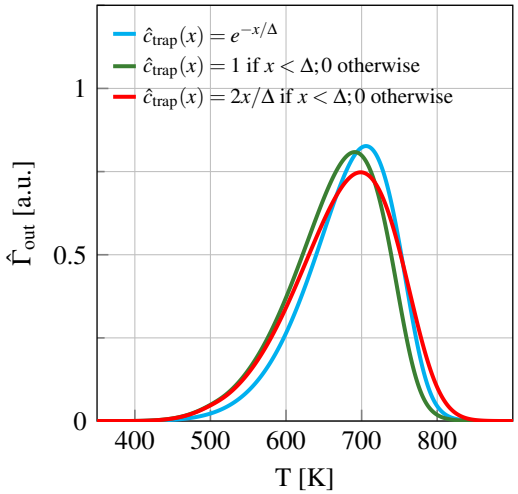

Figure 2.10: TDSP in retrapping-limited regime calculated for different shapes of trap concentration profiles assuming $\hat{c}_0(x) = \hat{c}_{trap}(x)$ with $E_{dt} = 1.40\,\text{eV}$, $\Delta = 5\,\mu\text{m}$ and $\rho_{trap} = 10^{-4}$ at.%. The total quantity of traps in material is constant.

2.5.4 Similarities of thermal desorption spectra

The diffusion equation (2.18) indicates that hydrogen outgassing in retrapping-limited regime is only characterized by the effective diffusion coefficient $D_{eff} = D\frac{\nu_{dt}}{\nu_{tr}}$ when temperature varies. It thus suggests that similar TDSP can be obtained in retrapping-limited regime either with different trapping and detrapping energies or with different trap concentration profiles. Both cases are examined below.

Similar thermal desorption spectra induced by different trapping and detrapping energies

The dependency of $\hat{\Gamma}_{out}$ on D_{eff} in retrapping-limited regime implies a dependency of $\hat{\Gamma}_{out}$ on the effective detrapping activation energy $E_{eff} = E_{dt} - E_{tr} + E_D$. Desorption peaks in this regime can be thus induced with different values of E_{tr} and E_{dt}, provided that the difference $E_{dt} - E_{tr}$ is constant. Consequently, a given desorption peak may not correspond unequivocally to one type of traps, as portrayed in figure 2.11c where TDSP in retrapping-limited regime are similar when both E_{dt} and E_{tr} are increased of $0.3\,\text{eV}$, but differ when only E_{dt} is increased of $0.3\,\text{eV}$.

The outgassing flux does not explicitly depend on hydrogen trapping and diffusion in detrapping-limited regime (eq. 2.26), and therefore similar TDSP can be obtained in this regime with different values of E_{tr}, provided that $\xi_{trapping} \ll 1$ (fig. 2.11a). In mixed regime when $\xi_{trapping} \approx 1$, TDSP depend on both $E_{dt} - E_{tr}$ and E_{dt} (fig. 2.11b).

In general, only the difference $E_{dt} - E_{tr}$ can be estimated in retrapping-limited regime, and

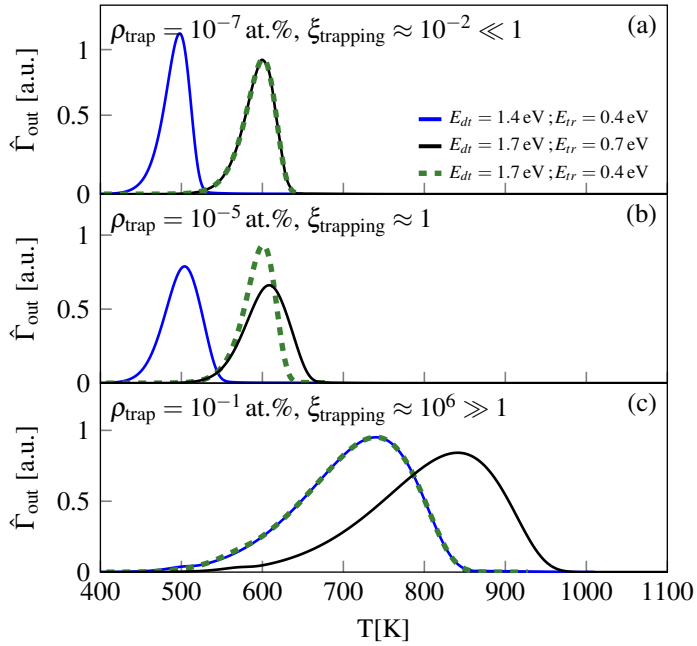

Figure 2.11: TDSP calculated with different set of trapping and detrapping activation energies in detrapping-limited regime (a), mixed regime (b) and retrapping-limited regime (c) with $\Delta = 10^{-6}$ m and $\hat{c}_0 = 1$.

thus E_{dt} can be only estimated in this regime when trapping is only limited by diffusion ($E_{tr} = E_D$). Estimations of E_{tr} could be obtained if TDS experiments can be performed in both retrapping-limited and detrapping-limited regimes.

Similar thermal desorption spectra induced by different trap concentration profiles

In retrapping-limited regime, desorption peaks with similar shape and position can be also generated with different trap concentration profiles provided that $\rho_{trap}\Delta^2$ is constant since $D_{eff} \propto \frac{1}{\Delta^2 \rho_{trap}}$ (fig. 2.12). The total amount of hydrogen $\hat{c}_0 \rho_{trap} \Delta$ may be not constant and therefore only the shape and the position of TDSP are comparable.

These similarities in TDSP could be advantageously exploited in TDS experiments performed with samples pre-irradiated with energetic ion beams creating displacement damages, for which trap concentration profiles in material can be controlled [121, 122]. Such similarities are not expected in detrapping-limited regime since the outgassing flux does not explicitly depend on hydrogen trapping and diffusion is this regime. Therefore, TDS experiments performed with constant value of $\rho_{trap}\Delta^2$ but several values of ρ_{trap} and Δ may give indications on whether hydrogen desorption is detrapping-limited or retrapping-limited.

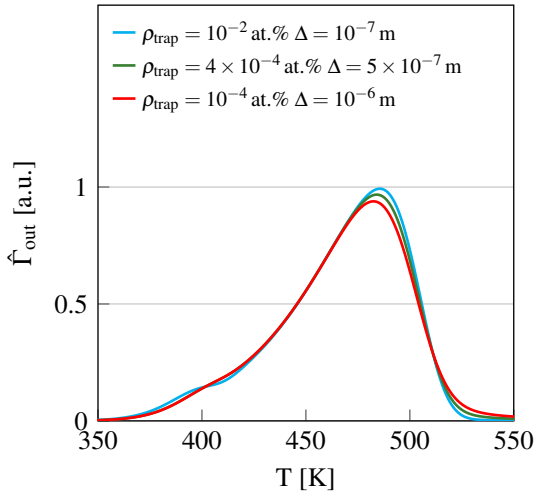

Figure 2.12: Similar TDSP induced by different trap concentration profiles calculated using $E_{dt} = 1.40\,\text{eV}$, $\hat{c}_0 = 1$ and $\rho_{trap}\Delta^2/\lambda_0^2 = 10$. TDSP are rescaled since the total quantity of hydrogen $\hat{c}_0\rho_{trap}\Delta$ is not constant.

2.6 Revisited interpretation of Arrhenius plots for thermal desorption spectra generated with several heating ramps

Activation energies and pre-exponential factors of detrapping rates are usually evaluated either by fitting experimental TDSP solving equations (2.1) or by generating an Arrhenius plot for several TDSP obtained at different heating rates α. This latter method is advantageous by its simplicity and its better accuracy due to a larger number of experimental data. However, the interpretation of Arrhenius plots strongly depends on whether hydrogen desorption is retrapping-limited or detrapping-limited.

Activation energies are deduced in Arrhenius plots from the slope of the graph $-\ln(\alpha)+2\ln(T_{des})$ as a function of $1/T_{des}$. The logarithm of the inverse expression of the equation (2.29) and (2.30) indeed reads

- in detrapping-limited regime

$$-\ln(\alpha)+2\ln(T_{des}) = E_{dt}\left(\frac{1}{T_{des}}\right) - \ln\left(\frac{\nu_{dt,0}}{E_{dt}}\right) \tag{2.31}$$

- in retrapping-limited regime

$$-\ln(\alpha)+2\ln(T_{des}) = E_{eff}\left(\frac{1}{T_{des}}\right) - \ln\left(\frac{\nu_{eff,0}}{E_{eff}}\right) \tag{2.32}$$

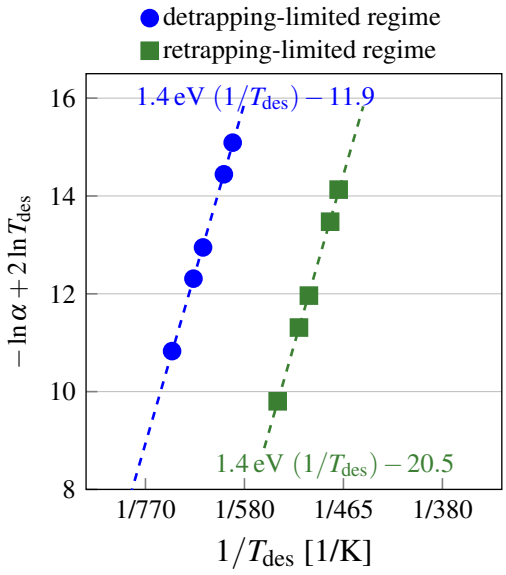

Figure 2.13: Arrhenius plots for TDSP calculated with several (five) heating ramps ($0.1\,\mathrm{K\,s^{-1}} < \alpha < 10\,\mathrm{K\,s^{-1}}$) in retrapping-limited regime ($\rho_{trap} = 10^{-4}$ at.%) and detrapping-limited regime ($\rho_{trap} = 10^{-8}$ at.%). Other parameters are $E_{dt} = 1.40\,\mathrm{eV}$, $\Delta = 5\,\mu\mathrm{m}$ and $\hat{c}_0 = 0.5$.

The equation (2.32) has been derived assuming that $\Theta(\hat{c}_0) \approx 1$ since $0.46 < \Theta(\hat{c}_0) < 1$.

Slopes of Arrhenius plots are equal to $E_{eff} = E_{dt} - E_{tr} + E_D$ in retrapping-limited regime and to E_{dt} in detrapping-limited regime (fig. 2.13). This difference in measured activation energies is only of interest when trapping is not limited by diffusion only ($E_{tr} \neq E_D$).

The pre-exponential factor of the detrapping rate is also often evaluated with offsets of curves in Arrhenius plots [36]. This method is only valid in detrapping-limited regime where the pre-exponential factor in expression (2.31) is indeed $\nu_{dt,0}$. In retrapping-limited regime, the pre-exponential factor in expression (2.32) is $\nu_{eff,0} = \frac{\nu_{dt,0} D_0}{\nu_{tr,0} \Delta^2}$. Consequently, offsets measured in Arrhenius plots may vary from several orders of magnitude depending on the desorption regime since $\nu_{eff,0} \ll \nu_{dt,0}$. For example, the measurement of the offset in retrapping-limited regime in figure 2.13 gives a pre-exponential factor $\nu_{dt,0}$ about $2.6 \times 10^9\,\mathrm{s^{-1}}$ ($\nu_{eff,0} = 1.7 \times 10^9\,\mathrm{s^{-1}}$ in simulations). In contrast, the measurement of the offset in detrapping-limited regime gives a pre-exponential factor $\nu_{eff,0}$ about $6.22 \times 10^{12}\,\mathrm{s^{-1}}$ ($\nu_{dt,0} = 10^{13}\,\mathrm{s^{-1}}$ in simulations).

Knowing the desorption regime is thus crucial to correctly estimate the pre-exponential factors from the curve offsets in Arrhenius plots. Moreover, values of pre-exponential factors $\nu_{tr,0}$ and $\nu_{dt,0}$ of trapping and detrapping rates cannot be explicitly inferred from Arrhenius plots in retrapping-limited regime. Only the value of $\nu_{eff,0}$ can be directly estimated in this regime.

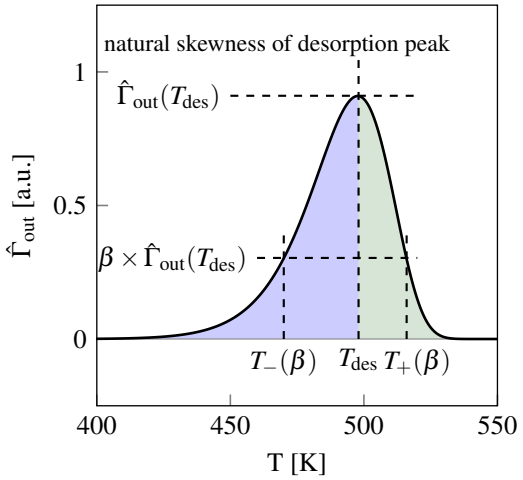

Figure 2.14: Natural skewness of desorption peak.

2.7 Skewness, tails and slopes of desorption peaks in thermal desorption spectra

Besides Arrhenius plots or direct fitting of TDSP with R-D models, the shape and slopes of desorption peaks and broad desorption tails in TDSP can also be used to characterize desorption regimes and traps.

Desorption peaks in TDSP can be usually described in an approximated form by

$$\hat{\Gamma}_{out}(T) \sim \nu(T) e^{-\int_{T_0}^{T} \nu(T')\mathrm{d}T'} \tag{2.33}$$

where $\nu(T) \sim e^{-E/T}$, as suggested by expressions (2.26) and (2.27). Variations of $\hat{\Gamma}_{out}$ with temperature therefore depend on whether $\int_{T_0}^{T} \nu(\tilde{T})\mathrm{d}\tilde{T} < 1$ or $\int_{T_0}^{T} \nu(\tilde{T})\mathrm{d}\tilde{T} > 1$. The natural skewness of desorption peaks is therefore non-zero and desorption peaks are naturally asymmetric (fig. 2.14). In addition, the expression (2.33) also suggests that the slope of $\hat{\Gamma}_{out}$ in TDSP can be directly used to obtain estimations of the activation energy of detrapping when $\int_{T_0}^{T} \nu(\tilde{T})\mathrm{d}\tilde{T} < 1$.

Another type of asymmetry can be observed in TDSP when broad desorption tails appear at high temperature as sketched in figure 2.15. These long desorption tails are induced by the outgassing of hydrogen which has diffused beyond the retention region during TDS experiments.

The interest of skewness, slopes and tails of desorption peaks when analyzing TDSP is discussed and illustrated in this section with some experimental TDSP reported in literature [36].

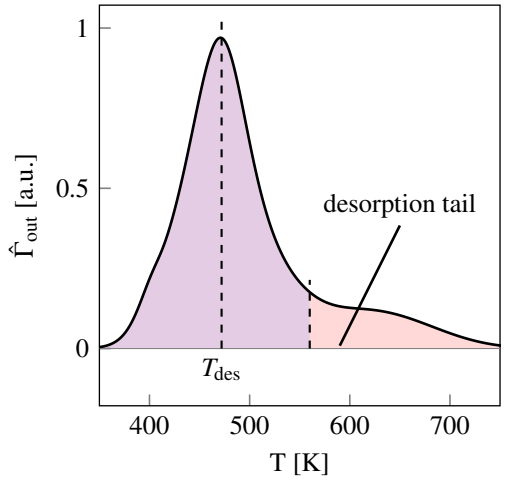

Figure 2.15: Tails in thermal desorption spectra.

2.7.1 Skewness of desorption peaks

The skewness of desorption peaks can be quantified by

$$\hat{S}(\beta) = \frac{1}{T_{\text{des}}} \left(\frac{T_+(\beta) + T_-(\beta)}{2} - T_{\text{des}} \right) \tag{2.34}$$

where the temperatures $T_+ > T_{\text{des}}$ and $T_- < T_{\text{des}}$ are formally defined by $\frac{\Gamma_{out}(T_\pm)}{\Gamma_{out}(T_{\text{des}})} = \beta$ with $0 < \beta \leq 1$ (fig. 2.14).

The skewness estimator $\hat{S}$ was used for example to analyze TDSP induced by surface processes [123]. A negative skewness $\hat{S} < 0$ indicates that the left shoulder of desorption peak, which stands at low temperature $(T < T_{\text{des}})$ is wider than the shoulder at high temperature $(T > T_{\text{des}})$. A desorption peak with negative skewness is then asymmetric toward low temperature as portrayed in figure 2.14.

$\hat{S}(\beta)$ can be estimated using the analytical expressions of the outgassing flux (2.26) and (2.27) in detrapping-limited and retrapping-limited regimes (appendix D). In retrapping-limited regime, the accuracy of the expression (2.27) is limited when $T < T_{\text{des}}$ because of the slow effective hydrogen diffusion in the retention region, as pictured in section 2.4. Desorption peaks predicted with the expression (2.27) then stand at higher temperature than real desorption peaks (sec. 2.5.1), and slopes of desorption peaks calculated with the expression (2.27) are more pronounced than real slopes when $T < T_{\text{des}}$ (fig. 2.7). Consequently, only lower bounds for the estimation of skewness can be obtained in retrapping-limited regime with the expression (2.27).

The width of desorption peak $|T_+ + T_-|$ grows as β decreases, *id est* $\frac{\partial|\hat{S}|}{\partial\beta} < 0$. The sign of $\hat{S}$ is

thus equal to the sign of the skewness $\hat{S}_{\text{des}}$ in the vicinity of T_{des} $\left(\hat{S}_{\text{des}} = T_{\text{des}}^3 \left.\frac{\partial^3 \ln(\hat{\Gamma}_{\text{out}})}{\partial T^3}\right|_{T=T_{\text{des}}}\right)$. It can be analytically shown using expressions (2.26) and (2.27) that $\hat{S}_{\text{des}} < 0$ in both detrapping-limited and retrapping-limited regimes. The skewness of desorption peaks is thus always negative

$$\hat{S}(\beta) < 0 \tag{2.35}$$

Desorption peaks induced by processes which can be described with the R-D equations (2.1) thus always exhibit negative skewness and are asymmetric toward low temperature.

As detailed in appendix D, it can be shown after some algebra that $\hat{S} \propto \ln\beta$ (fig. 2.16a) and that the value of $\hat{A} = \frac{\partial \hat{S}}{\partial \ln\beta}$ strongly depends on whether hydrogen desorption is detrapping-limited or retrapping-limited. $\hat{A} < 0.01$ in detrapping-limited regime and $\hat{A} > 0.01$ in retrapping-limited regime for typical retention and desorption parameters (fig. 2.16b). Since $\frac{\partial|\hat{S}|}{\partial\beta} < 0$ and $\hat{S} < 0$, desorption regimes and properties of experimental desorption peaks can be conveniently determined using $\hat{A}$:

- if $\hat{A} > 0.01$, hydrogen desorption is retrapping-limited, and the skewness of desorption peak is negative.
- if $0.01 > \hat{A} > 0$, hydrogen desorption is detrapping-limited, and the skewness of desorption peak is negative.
- if $\hat{A} < 0$, the skewness of the desorption peak is positive, *id est* desorption peak is asymmetric toward high temperature, suggesting that hydrogen desorption may be governed by retention and desorption processes which are not described in R-D equations (2.1), such as surface effects, mutating traps, interactions between traps, ...

The threshold value $\hat{A} = 0.01$ separating detrapping-limited and retrapping-limited regimes weakly depends on the heating rate and can be used to analyze desorption regime with any heating rate.

The practical use of $\hat{A}$ to analyze experimental TDSP may be not straightforward when TDSP are complex, like for instance experimental TDSP reproduced from literature [36] in figure 2.17a, where at least two desorption peaks are visible. This issue can be overcome by estimating $\hat{A}$ with the average value of $\frac{\partial \hat{S}}{\partial \ln\beta}$ in the range $\beta_{\min} < \beta < 0.90$

$$\hat{A}(\beta_{\min}) = \left\langle \frac{\partial \hat{S}}{\partial \ln\beta} \right\rangle_{\beta_{\min}<\beta<0.90} \tag{2.36}$$

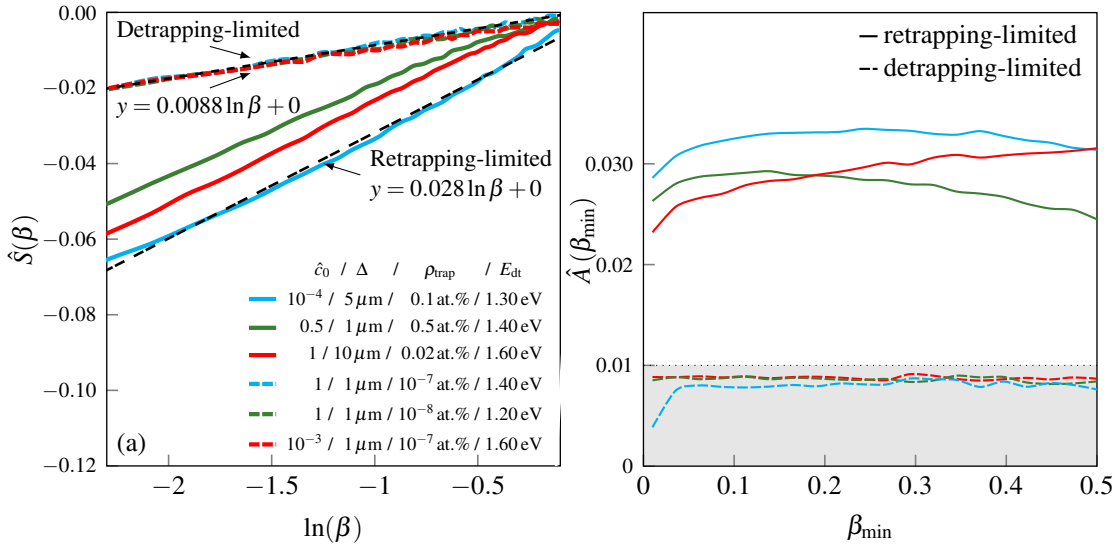

Figure 2.16: (a): Skewness $\hat{S}$ as a function of $\ln(\beta)$ for desorption peaks calculated using R-D equations (2.1) with different set of parameters. (b): Values of skewness estimator $\hat{A}$ obtained by linear interpolation of $\hat{S}$ in the range $\beta_{min} < \beta < 0.9$ as a function of β_{min}.

Practically, $\hat{A}(\beta_{min})$ is for instance the slope of the linear interpolation of $\hat{S}$ as a function of $\ln(\beta)$ in the range $\beta_{min} < \beta < 0.90$. The desorption regime can be then handily determined in the plot of $\hat{A}(\beta_{min})$ as a function of β_{min} (fig. 2.16b).

The plot of $\hat{A}(\beta_{min})$ as a function of β_{min} for experimental TDSP displayed in figure 2.17a provides a clear indication of the desorption regime when $\beta_{min} > 0.4$, *id est* when desorption peaks are distinguishable in TDSP. Values of $\hat{A}$ larger than 0.01 at high fluences indicate that skewness desorption peak is negative and hydrogen desorption might be retrapping-limited. On the other hand, the negative value of $\hat{A}$ at the lowest fluence indicates that the skewness of desorption peaks is positive, which suggests that hydrogen desorption is governed by processes not described by the R-D model (2.1).

2.7.2 Desorption tails in thermal desorption spectra

Long desorption tails observable at $T > 700\,\mathrm{K}$ in experimental TDSP (fig. 2.17a) stand at high temperature aside desorption peaks, which suggests that these tails correspond to desorption of hydrogen located out of the retention region. To characterize these tails, we use the normalized estimator $\hat{A}_+(\beta) = \frac{T_+(\beta)}{T_{des}}$. Large variations of $\hat{A}_+$ with β indicate a long desorption tail, as illustrated in figure 2.18 where $\hat{A}_+$ suddenly increases when $\beta < 0.1$.

The fraction of free hydrogen which diffuses beyond the retention region during TDS experiments

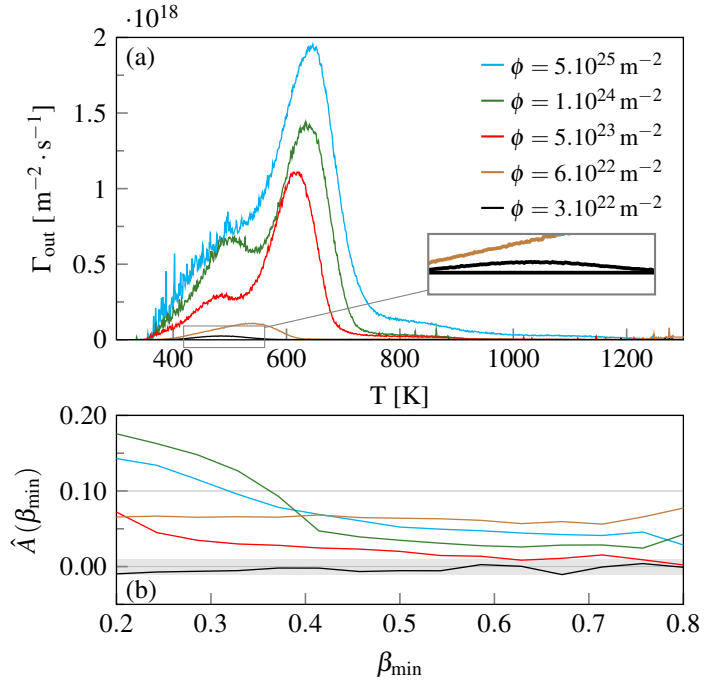

Figure 2.17: (a): Experimental TDSP reported in literature [36] for tungsten samples exposed to deuterium at different fluences. (b): Corresponding values of the skewness estimator $\hat{A}$ as a function of $\beta_{\min}$. The gray zone is the interval $[-0.01;0.01]$. The color chart is identical on plots (a) and (b).

has been ignored until now since the majority of hydrogen is assumed to be released through front surface of material when hydrogen desorption is quasi-static. This fraction may be however non negligible compared to the total quantity of retained hydrogen.

In retrapping-limited regime, free hydrogen concentration in the retention region varies as $\hat{c}_{\mathrm{f}} \approx \frac{\nu_{\mathrm{dt}}}{\nu_{\mathrm{tr}}} \frac{\hat{c}_{\mathrm{t}}}{1-\hat{c}_{\mathrm{t}}}$. Hydrogen located beyond the retention region ($x > \Delta$) can diffuse toward front material surface when $\hat{c}_{\mathrm{f}}(\Delta, T) < \hat{c}_{\mathrm{f}}(x > \Delta, T)$, which occurs when $T \gtrsim T_{\mathrm{des}}$. The fraction f_{H} of free hydrogen located beyond the retention region can be then roughly approximated by

$$f_{\mathrm{H}} = \frac{\int_{\Delta}^{\infty} \hat{c}_{\mathrm{f}}(x, T_{\mathrm{des}})\mathrm{d}x}{\int_{0}^{\Delta} \hat{c}_{\mathrm{t}}(x, T_{\mathrm{des}})\mathrm{d}x} \sim \frac{\nu_{\mathrm{dt}}(T_{\mathrm{des}})}{\nu_{\mathrm{tr}}(T_{\mathrm{des}})} \frac{\delta(T_{\mathrm{des}})}{\Delta} \tag{2.37}$$

where $\delta(T)$ is the characteristic depth of free diffusion of hydrogen in the material $\left(\delta(T) = \sqrt{\int_{T_0}^{T} D(T')\mathrm{d}T'}\right)$. Since $\Omega_{\mathrm{eff}}(T_{\mathrm{des}}) \approx \frac{\nu_{\mathrm{dt}}(T_{\mathrm{des}})}{\nu_{\mathrm{tr}}(T_{\mathrm{des}})} \frac{D}{\Delta^2} \frac{T_{\mathrm{des}}^2}{E_{\mathrm{eff}}} \approx 1$, f_{H} can be approximated by

$$f_{\mathrm{H}} \sim \frac{\Delta}{\delta(T_{\mathrm{des}})} \tag{2.38}$$

T_{des} increases with ρ_{trap} and Δ following logarithmic dependencies (exp. 2.30) and δ is thus a growing

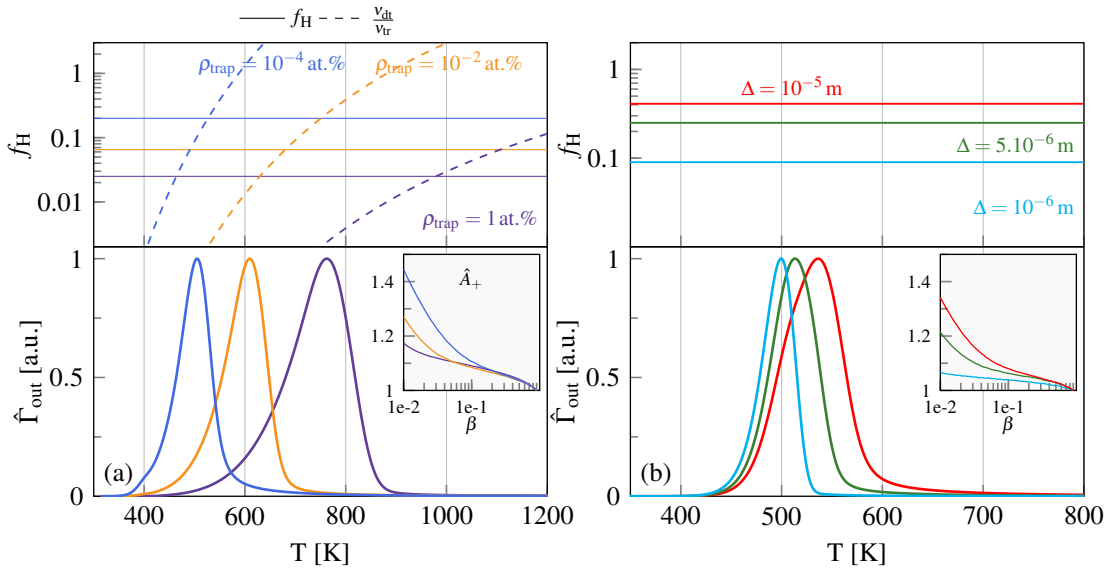

Figure 2.18: TDSP and corresponding values of f_H in retrapping-limited regime calculated with $E_{dt} = 1.10\,eV$, $\Delta = 10\,\mu m$ and $\rho_{trap} = 0.0001$ at.% $- 1$ at.% (a) and $E_{dt} = 1.40\,eV$, $\rho_{trap} = 10^{-5}$ at.% and $\Delta = 1 - 10\,\mu m$ (b).

function of T_{des}. Therefore, larger values of f_H and bigger tails are expected at lower trap concentrations (fig. 2.18a) and with deeper retention regions (fig. 2.18b) since $f_H \propto \Delta$.

Large visible desorption tails stand in TDSP at high temperature where $\frac{\nu_{dt}(T)}{\nu_{tr}(T)} \gtrsim 1$ (fig. 2.18a). When this condition is satisfied, hydrogen desorption in the retention region is no more limited by hydrogen trapping and hydrogen mainly diffuses freely toward front material surface. $\hat{\Gamma}_{out}$ can thus be estimated by $\hat{\Gamma}_{out}(T) \approx D(T)\frac{\hat{c}_{max}(T)}{\delta(T)}$ where $\hat{c}_{max}$ is the maximum of free hydrogen concentration beyond the retention region. The total quantity of free hydrogen $\hat{N}_{tot}$ retained in the material can be then estimated by $\hat{N}_{tot} \approx \frac{1}{2}\hat{c}_{max}\delta$. The outgassing flux is thus governed by the equation $\frac{\partial \hat{N}_{tot}}{\partial T} \approx -\hat{\Gamma}_{out}$, which can be recast into $\frac{\partial \ln \hat{N}_{tot}}{\partial T} \approx -\frac{E_D}{T^2}$. The outgassing flux then varies as a function of the temperature following $\hat{\Gamma}_{out} \propto e^{\frac{E_D}{T}}\frac{E_D}{T^2}$. The following relationship

$$\ln\left(\hat{\Gamma}_{out}\right) + 2\ln(T) = \frac{E_D}{T} + cst \tag{2.39}$$

thus holds for desorption tails in TDSP when $\frac{\nu_{dt}(T)}{\nu_{tr}(T)} \gtrsim 1$.

Consequently, the activation energy of diffusion E_D can be estimated from slopes of long desorption tails when $\frac{\nu_{dt}(T)}{\nu_{tr}(T)} \gtrsim 1$ in Arrhenius plots of TDSP (fig.2.19a).

For instance, the value of E_D estimated by fitting the slope of desorption tail in Arrhenius plot of

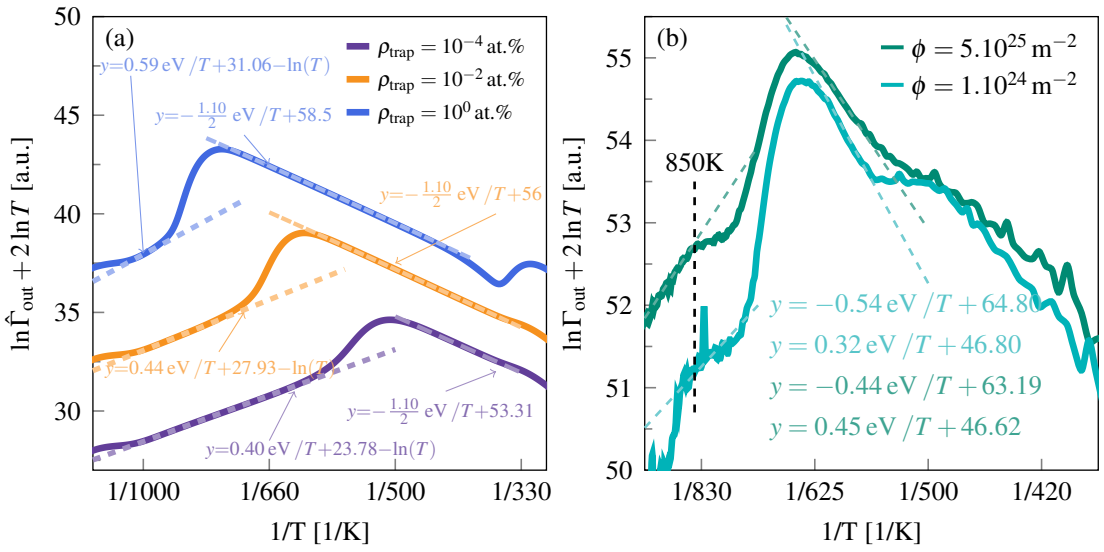

Figure 2.19: Arrhenius plots of TDSP plotted in figure 2.18a (a) and of experimental TDSP plotted in figure 2.17a (b).

experimental TDSP at the largest fluence is about 0.45 eV (fig. 2.19b), which is in agreement with values of E_D previously measured in Frauenfelder's experiments [59] ($E_D \approx 0.39$ eV). One notice that E_D can be consistently measured only at the highest fluence, where the magnitude of desorption tails is large enough at temperature where $\frac{\nu_{dt}(T)}{\nu_{tr}(T)} > 1$ holds (here $T \gtrsim 850$ K).

When long desorption tails are visible in TDSP, it is unlikely that hydrogen will be released during TDS experiments through fast diffusion paths (such as grain boundaries) toward front surface of material, since desorption tails suggest that hydrogen diffuses well beyond the retention region.

2.7.3 Estimation of activation energies in Arrhenius plots of outgassing flux

The outgassing flux in retrapping-limited regime depends on the effective diffusion $D_{eff} = D\frac{\nu_{dt}}{\nu_{tr}}$ and on the characteristic diffusion length $\delta_{eff} = \sqrt{\int_{T_0}^{T} D_{eff}(T')\mathrm{d}T'}$ according to the relationship (2.23). The logarithmic form of this relationship reads

$$\ln(\hat{\Gamma}_{out}) + \ln(T) = -\frac{E_{eff}}{2T} + \text{cst} \tag{2.40}$$

The effective detrapping energy $E_{eff} = E_{dt} - E_{tr} + E_D$ can be then directly estimated in retrapping-limited regime from slopes at $T < T_{des}$ in Arrhenius plots of $\hat{\Gamma}_{out}$ (fig. 2.19a).

Similarly, $\hat{\Gamma}_{out} \sim \nu_{dt}$ in detrapping-limited regime when $T < T_{des}$, and thus E_{dt} can be estimated

from slopes in Arrhenius plots in this regime.

Slopes at $T < T_{\text{des}}$ in Arrhenius plots can be used for example to examine whether a desorption peak is induced by a single type of trap by comparing the value of E_{dt} estimated from slopes in Arrhenius plots to values of E_{dt} estimated from the desorption temperature. If these two values of E_{dt} differ, desorption is likely induced by more than one trap. This is the case for example with experimental TDSP plotted in figure 2.17b and 2.19b where activation energy estimated from the slopes of $\hat{\Gamma}_{\text{out}}$ at $T < T_{\text{des}}$ is about $0.90 - 1.10\,\text{eV}$ whereas estimated E_{dt} of traps forming desorption peaks is about $1.35\,\text{eV}$ (see chapter 3). This discrepancy is due the widening of the desorption peak caused by the presence of another desorption peak at low temperature (fig. 2.17a).

2.8 Summary

Hydrogen desorption during TDS experiments can occur in two different regimes characterized by $\xi_{\text{trapping}} = \frac{\nu_{\text{tr}}}{D/\Delta^2}$:

- the detrapping-limited regime when $\xi_{\text{trapping}} \ll 1$ in which hydrogen trapping can be ignored.
- the retrapping-limited regime when $\xi_{\text{trapping}} \gg 1$ in which hydrogen trapping cannot be ignored.

With retention and desorption parameters relevant to TDS experiments performed on tungsten samples implanted in fusion relevant conditions (tab. 2.1), hydrogen desorption is retrapping-limited during TDS experiments.

The evolution of free hydrogen concentration in the retention region is quasi-static in the temperature range $T_{\text{D}} < T < T_{\text{q-s}}$ when hydrogen retention and desorption processes can be described with parameters given in tab. 2.1. When hydrogen desorption is quasi-static, the majority of free hydrogen in the retention region diffuses to the front surface of material and does not diffuse deeper beyond the retention region. Outgassing flux in TDS experiments can be thus analytically evaluated using the relationships (2.26) and (2.27).

These analytical estimations of outgassing flux are accurate in detrapping-limited regime, but are less precise in retrapping-limited regime because of the slow effective diffusion of hydrogen due to the retrapping of hydrogen in the retention region. Predictions of the outgassing flux in retrapping-limited regime with expression (2.27) are however accurate enough to describe main features of TDSP:

- the temperature of desorption T_{des} strongly depends on whether hydrogen desorption regime is

retrapping-limited or detrapping-limited. T_{des} linearly depends on activation energies and has logarithmic dependencies on other retention and desorption parameters.

- The shape and the position of desorption peaks depend on the initial filling of traps $\hat{c}_0$ in retrapping-limited regime when $\hat{c}_0$ exceeds 10%. Desorption peaks are wider and shifted toward low temperature as traps become saturated with hydrogen.

- Effects of the shape of trap concentration profiles in TDSP can be ignored in both retrapping-limited and detrapping-limited regimes.

- Similar desorption peaks can be produced by different traps in retrapping-limited regime when:

  - detrapping and trapping energies E_{tr} and E_{dt} are different but the values of the effective detrapping energy $E_{\mathrm{eff}} = E_{\mathrm{dt}} - E_{\mathrm{tr}} + E_{\mathrm{D}}$ are the same.
  - trap concentrations and depths of retention region are different but the values of $\rho_{\mathrm{trap}}\Delta^2$ are the same.

- For Arrhenius plots from several TDSP obtained at different heating rates:

  - Activation energies measured from slopes of Arrhenius plots are equal to E_{eff} in retrapping-limited regime and to E_{dt} in detrapping-limited regime.
  - Pre-exponential factors measured from offsets of Arrhenius plots may vary by several orders of magnitude depending on the desorption regime. The pre-exponential factor of the detrapping rate can be obtained only in detrapping-limited regime. Knowing the hydrogen desorption regime is thus crucial to interpret offset values.

- The skewness of desorption peaks in TDSP, which are induced by bulk retention processes and which can be described with the reaction-reaction model (2.1), is always negative.

- The derivative $\hat{A} = \frac{\partial \hat{S}}{\partial \ln \beta}$ of the skewness estimator $\hat{S}$ can be used to characterize desorption peaks:

  - if $\hat{A} > 0.01$, hydrogen desorption is retrapping-limited, and the skewness is negative.
  - if $0.01 > \hat{A} > 0$, hydrogen desorption is detrapping-limited, and the skewness is negative.
  - if $\hat{A} < 0$, the skewness is positive and hydrogen desorption may be governed by retention processes which are in the R-D model (2.1).

- Diffusion of hydrogen beyond the retention region during TDS experiments may induce long desorption tails in thermal desorption spectra.
- The activation energy of diffusion can be estimated using slopes of desorption tails in Arrhenius plots of TDSP when temperature is large enough such that the detrapping rate is larger than the trapping rate.
- The detrapping energy and the effective detrapping energy can be estimated using the slope of desorption peaks at low temperature $T < T_{\text{des}}$ in respectively detrapping-limited regime and retrapping-limited regime.

Results summarized above were obtained assuming that surface processes do not affect hydrogen desorption, and that traps are immobile and do not recombine or mutate in the material bulk. These latter assumptions may however not always hold in experiments. For example, effects of surface processes might be expected when material samples are exposed to high fluences of hydrogen, as shown in the chapter 4. Additional work is therefore required to include effects of these additional processes on hydrogen desorption during TDS experiments.

Chapter 2, in full, is a reprint of the material as it appears in J. Guterl, R.D. Smirnov, S.I. Krasheninnikov, Revisited reaction-diffusion model of thermal desorption spectroscopy experiments on hydrogen retention in material, accepted in *Journal of Applied Physics*, 2015. The dissertation author was the primary investigator and author of this paper.

Chapter 3

Analysis of deuterium retention in tungsten plasma-facing components induced by various defects via thermal desorption spectroscopy

3.1 Motivation and outline

Thermal desorption spectra (TDSP) resulting from TDS experiments are usually analyzed and interpreted using reaction-diffusion (R-D) models [45, 111]. Analyses of TDSP reported in literature mainly rely on R-D models including only two or three types of traps [35, 46, 124], motivated by the presence of two desorption peaks in experimental TDSP and by limitations of modeling softwares like TMAP [111].

Although R-D models with two or three types of traps can reproduce some aspects of TDSP such as temperature of desorption peaks, these models fail to accurately and consistently reproduce desorption peaks in most of experimental TDSP. Consequently, we introduce in this chapter a R-D model including a large number of different types of traps ($N_{\text{trap}} > 3$) to describe hydrogen desorption from material during TDS experiments and to analyze TDSP. The present work follows several previous works where effects of

continuous distributions of traps on hydrogen retention and outgassing were investigated [125, 126]. This approach has also recently attracted interest in the modeling of hydrogen retention in material damaged by neutrons [127].

Experimental TDSP considered in this work were obtained from TDS experiments performed by A.Manhard on tungsten samples exposed to deuterium flux at several fluences [36]. The use of a large number of types of traps in R-D model allows to consistently and accurately fit several experimental TDSP using the same spectrum of detrapping energy at all fluences.

The spectrum of detrapping energy obtained in the present work exhibits a broad distribution of detrapping energy, which can be related to the distribution of detrapping energy predicted in density functional theory (DFT) simulations when several hydrogen atoms are trapped in a single tungsten vacancy [116, 118]. This latter trapping mechanism was identified as a potential key process in hydrogen isotopes exchange experiments [119] but was not clearly pictured in TDS experiments yet. However, the use of a large number of different types of traps in R-D model allows us to analyze for the first time trapping mechanisms characterized by a broad spectrum of detrapping energy in TDSP. The comparison between trap concentrations measured by NRA and traps concentrations used to reproduce experimental TDSP with the R-D model indicates that traps exhibiting a broad spectrum of detrapping energy are likely located near material surface ($\lesssim 10\,\mathrm{nm}$).

This chapter is structured as follow. The R-D model used to fit experimental TDSP is briefly introduced in the first part, paying special attention to boundary conditions modeling surface processes and to the applicability of the R-D model to mutating traps, such as for instance tungsten vacancies containing several hydrogen atoms. Experimental conditions in which TDSP were obtained are then described. In the third part, the procedure used to fit experimental TDSP is presented and resulting trap distributions used to reproduce experimental TDSP are showcased. Effects of surface processes and the localization of traps in material are then discussed, as well as the nature of the traps which might induce desorption peaks observed in TDSP.

3.2 Experimental thermal desorption spectra and concentration profiles

We analyze in this chapter TDSP reported in [36], which were obtained by A.Manhard in TDS experiments performed on tungsten samples implanted with deuterium at several fluences. Tungsten

samples were pre-annealed at 1200 K before being irradiated in the PlaQ installation (IPP, Garching) [128]. Deuterium ions (mainly D3+) with a mean energy of 38 eV /D were extracted from a remote electron-cyclotron resonance plasma by applying a DC bias of 100 V to the sample. Irradiations were performed at the temperature of $T_{\text{irr}} = 370K$. The incoming ion flux was about $\Gamma_{\text{in}} \approx 10^{20}\,\text{m}^{-2}\cdot\text{s}^{-1}$ and the exposure time varied between $t_{\text{exp}} = 10^2$ s and $t_{\text{exp}} = 5\times10^5$ s, which correspond to fluence ranging from $\phi = 3\times10^{22}\,\text{m}^{-2}$ to $\phi = 5\times10^{25}\,\text{m}^{-2}$.

Deuterium retention in the samples was studied using TDS in the TESS installation (IPP, Garching) [129]. The samples were placed in a quartz tube, which was linearly heated up to a temperature $T_{\text{max}} =$ 1275 K with a heating rate of $\alpha = 0.05\,\text{K}\,\text{s}^{-1}$ at a background pressure of about 10^{-6} Pa. The sample temperature was measured in independent experiments in TESS by a thermocouple spot-welded to the sample. The release of 10 masses was monitored by a quadrupole mass spectrometer (QMS). In order to determine the total amount of retained deuterium, QMS signals for masses 3 (HD) and 4 (D2) were calibrated using the NIST-traceable calibrated leaks. Resulting thermal desorption spectra are reported in figure 3.1a.

Deuterium depth distributions in the samples were measured using nuclear reaction analysis (NRA) in the TANDEM accelerator (IPP, Garching) up to a material depth of $\Delta_{\text{NRA}} = 8\,\mu$m (fig. 3.1b). The D(3He,p)α reaction was used, and the energy of the 3He ion beam was varied in the range of 0.5-4.5 MeV to obtain data from different sample depths [130]. Both protons and α spectra were transformed into deuterium concentration profiles using the SIMNRA [131] and NRADC[132] programs.

3.3 Reaction-diffusion model

3.3.1 Reaction-diffusion equations

Experimental TDSP reported in figure 3.1a are fitted in this chapter with a R-D model which includes N types of traps to describe hydrogen outgassing from material during TDS experiments. In this R-D model, the 1D evolution of hydrogen concentration in tungsten samples during TDS experiments (i.e. without any source of incoming hydrogen) is described as a function of the material temperature T by the R-D equations (3.1), which are similar to R-D equations 1.9 but with several types of traps, where x is the

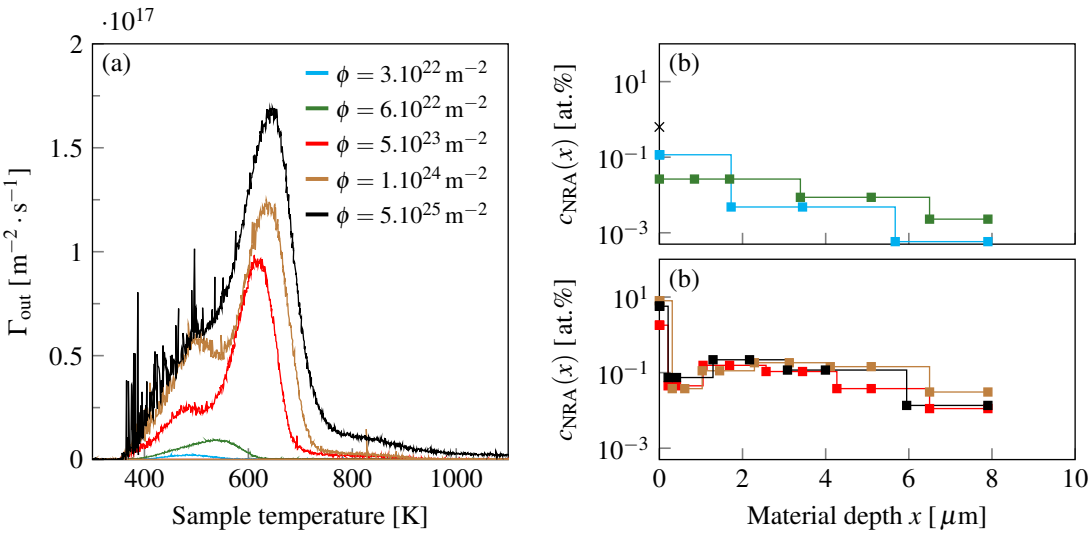

Figure 3.1: Experimental thermal desorption spectra (a) and deuterium concentration profiles measured by NRA (b) obtained by A.Manhard for tungsten samples exposed to deuterium flux at several fluences and reported in [36].

depth of the material and $\alpha = \frac{dT}{dt}$ is the heating rate.

$$\alpha \frac{\partial c_f(x,T)}{\partial T} = D(T) \frac{\partial^2 c_f(x,T)}{\partial x^2} + \sum_{k=1}^{N} \Big(- \nu_{tr}(k,T) \left[c_{trap}(k,x) - c_t(k,x,T) \right] c_f(x,T) + \nu_{dt}(k,T)\, c_t(k,x,T) \Big) \tag{3.1a}$$

$$\alpha \frac{\partial c_t(k,x,T)}{\partial T} = \nu_{tr}(k,T) \left[c_{trap}(k,x) - c_t(k,x,T) \right] c_f(x,T) - \nu_{dt}(k,T)\, c_t(k,x,T),\ k = 1 \ldots N \tag{3.1b}$$

The index k indicates the type of traps ($1 \leq k \leq N$) and $c_{trap}(k,x)$ is the concentration of traps of type k, which occupy the retention region of depth $\Delta(k)$. $c_f(x,T)$ is the concentration of free (solute) hydrogen and $c_t(k,x,T)$ is the concentration of hydrogen trapped in traps of type k.

D is the diffusion coefficient of free hydrogen, uniform in material and described by the Arrhenius law $D = D_0\, e^{-E_D/T}$. E_D is the activation energy of diffusion taken equal to 0.39 eV [59], and $D_0 \approx \nu_0 \lambda_0^2$ where ν_0 is the lattice vibration frequency approximated by the Debye frequency ($\nu_0 = 10^{13}\,s^{-1}$). The characteristic lattice cell size λ_0 is equal to $\lambda_0 = 3.16$ in tungsten.

$\nu_{tr}(k,T)$ and $\nu_{dt}(k,T)$ are the trapping and detrapping rates given by $\nu_{tr}(k,T) = \nu_{tr,0}\, e^{-E_{tr}(k)/T}$ and $\nu_{dt}(k) = \nu_{dt,0}\, e^{-E_{dt}(k)/T}$ where $E_{tr}(k)$ and $E_{dt}(k)$ are the trapping and detrapping energies. $\nu_{tr,0}$ can be expressed in general as $\nu_{tr,0} \approx \nu_0 \lambda_0^3$ and $\nu_{dt,0}$ is approximated by $\nu_{dt,0} \approx \nu_0$.

In the R-D model formed by equations (3.1), traps are assumed to be immobile in material whether they are occupied by hydrogen or not. In addition, the concentrations of traps are assumed to remain steady during TDS experiments. Interactions between traps and trap mutations are also ignored in this R-D model, and TDSP calculated with the R-D model thus approximatively correspond to the superposition of desorption peaks generated by each type of traps.

Values of E_{tr} for typical tungsten defects, such as vacancies or dislocation loops, are not available in literature. Trapping is thus usually assumed to be limited only by hydrogen diffusion without any additional activation energy and $E_{\text{tr}} = E_{\text{D}}$ [120]. We thus assume in this work that $E_{\text{tr}}(k) = E_{\text{D}}$ for all types of traps, which also conveniently reduces the number of free parameters in the R-D model when fitting experimental TDSP.

Deuterium concentration profiles obtained by NRA reported in figure 3.1b indicate that the concentrations of traps $\rho_{\text{trap}} = c_{\text{trap}}\lambda_0^3$ are larger than 10^{-4} at.% and that deuterium is retained at least up to a retention depth $\Delta \sim 8\,\mu$m. Hydrogen desorption is thus likely retrapping-limited during TDS experiments, *id est* hydrogen diffusing from the retention region toward front material surface is retrapped in the retention region (see chapter 2).

When hydrogen desorption is retrapping-limited during TDS experiments, hydrogen desorption is quasi-static in the temperature range $T_{\text{D}} < T < T_{\text{q-s}}$, where $T_{\text{D}} \approx 300\,\text{K}$ and $T_{\text{q-s}}$ is defined by $\frac{\nu_{\text{dt}}(k,T_{\text{q-s}})}{\nu_{\text{tr}}(k,T_{\text{q-s}})} = 1$ (see section 2.4 in chapter 2). Experimental desorption peaks stand between 350 K and 800 K (fig. 3.1a). Hydrogen desorption is thus quasi-static when $E_{\text{dt}}(k) < 1.5\,\text{eV}$ and $\rho_{\text{trap}} > 10^{-4}$ at.% according to the chart in figure 2.5. Most of traps used in this work to fit experimental TDSP verify these two latter conditions (sec. 3.4.1) and hydrogen desorption is thus supposed to be quasi-static during TDS experiments modeled in this chapter.

Depth profiles of trap concentration $c_{\text{trap}}(k,x)$ are assumed to be identical for each type of trap and are taken equal to profiles of deuterium concentration measured with NRA at each fluence (fig. 3.1b). Moreover, traps are assumed to be uniformly filled with deuterium at the beginning of TDS experiments (relationship 3.2), regarding the consequent time of exposure of tungsten samples to deuterium flux $\left(t_{\text{exp}} > 100\,\text{s}\right)$.

$$c_{\text{t}}(k,x,T_0) = c_{\text{trap}}(k,x) \propto c_{\text{NRA}}(x), \;\; k = 1 \ldots N \tag{3.2}$$

Tungsten samples were stored for two months after exposure to deuterium flux before being analyzed with TDS and NRA $\left(t_{\text{storage}} \sim 5 \times 10^6\,\text{s}\right)$. We therefore assume that the majority of free deuterium remaining in material after implantation of tungsten samples was outgassed from material during the

storage period.

$$c_{\mathrm{f}}(x,T_0) \ll c_{\mathrm{t}}(k,x,T_0),\ \ k = 1 \ldots N \tag{3.3}$$

The temperature of the material T is taken equal to the temperature of tungsten samples experimentally measured during TDS experiments, which increases with a heating rate $\alpha \sim 0.05\,\mathrm{K\,s^{-1}}$.

3.3.2 Surface processes and boundary conditions

To describe hydrogen transport from material bulk onto material surface and hydrogen desorption from material surface, we use the equations (1.10) outlined in the introduction

$$D\frac{\partial c_{\mathrm{f}}}{\partial x}\bigg|_{x=x_s} = \pm\left(K_{\mathrm{b}}c_{\mathrm{f}}(x_s,T) - K_{\mathrm{a}}c_s\right) \tag{3.4}$$

$$\alpha\frac{\partial c_{\mathrm{s}}}{\partial T} = -K_{\mathrm{r}}c_s^2 + K_{\mathrm{b}}c_{\mathrm{f}}(x_s,T) - K_{\mathrm{a}}c_s \tag{3.5}$$

which rely on the surface model described in [47] and sketched in figure 1.11. c_{s} is the concentration of hydrogen on material surface and x_s is the position of material surface (front surface at $x_s = 0$ and rear surface at $x_{\mathrm{s}} = L$). $K_{\mathrm{b}} = \nu_0\lambda_0 e^{\frac{-E_{\mathrm{b}}}{T}}$ is the rate of readsorption of hydrogen from the first sub-surface atomic layer onto surface, $K_{\mathrm{a}} = \nu_0 e^{\frac{-E_{\mathrm{a}}}{T}}$ is the rate of absorption of hydrogen on surface into material bulk and $K_{\mathrm{r}} = \nu_0\lambda_0^2 e^{\frac{-E_{\mathrm{r}}}{T}}$ is the molecular recombination and desorption rate of deuterium on tungsten surface. The outgassing flux Γ_{out} of hydrogen from material is then $\Gamma_{\mathrm{out}} = K_{\mathrm{r}}c_{\mathrm{s}}^2$.

The description of surface processes by equations (3.5) does not include effects of saturation of surface with hydrogen, which can drastically modify kinetic orders and rates of surface processes [64]. These saturation effects are not taken into account in this chapter because experimental outgassing flux are lower than outgassing flux expected when surface is saturated with hydrogen.

The activation energy for chemisorption is usually negligible for hydrogen interacting with tungsten surface [133] and the chemisorption heat Q_{c} is then equal to half of the activation energy of recombination and desorption ($Q_{\mathrm{c}} = \frac{E_{\mathrm{r}}}{2}$). Several experiments adressing specifically hydrogen desorption from tungsten surface have shown that $E_{\mathrm{r}} \approx 1.2 - 1.6\,\mathrm{eV}$ for low surface coverage [112] and thus $Q_{\mathrm{c}} \approx 0.6 - 0.8\,\mathrm{eV}$. Experimental measurements of the solubility heat of hydrogen in tungsten show an activation energy of hydrogen absorption from gas phase into tungsten $Q_{\mathrm{sol}} = E_{\mathrm{a}} - E_{\mathrm{r}} - Q_{\mathrm{c}}$ about $1.04\,\mathrm{eV}$ [59] such that $E_{\mathrm{a}} - E_{\mathrm{b}} = Q_{\mathrm{sol}} + Q_{\mathrm{c}} \approx 1.6 - 1.8\,\mathrm{eV}$.

Direct experimental estimations of the activation energy E_{a} of absorption of adsorbed hydrogen

in tungsten bulk are not available in literature. However, DFT simulations performed by Heinola [134] suggested that $E_a \approx 2\,\mathrm{eV}$, which thus leads to $E_b = 0.2 - 0.4\,\mathrm{eV}$. Due to this large value of E_a, hydrogen absorption can be neglected compared to hydrogen readsorption during TDS experiments (condition 3.6).

$$K_a c_s \ll K_b c_f(x_s, T) \tag{3.6}$$

The evolution of hydrogen transport from material bulk onto surface is then independent of the evolution of c_s. The absorption of hydrogen from material surface into bulk is therefore ignored in this work.

The hydrogen surface concentration is usually in equilibrium ($\frac{\partial c_s}{\partial T} \approx 0$) when modeling TDSP by numerically solving R-D equations (3.1) with boundary conditions (3.5) and values of E_r and E_b introduced above. In this context, hydrogen outgassing from material occurs as a first order kinetic process on material surface, as suggested by some previous modeling of hydrogen desorption from tungsten and other metallic surfaces [135].

In addition, the skewness of desorption peaks induced by second order hydrogen molecular desorption is positive [123] whereas desorption peaks reported in figure 3.1 exhibit a negative skewness (except at the lowest fluence), which suggests that hydrogen desorption is mainly governed by retention processes in material bulk and is not limited by surface processes (see chapter 2). Desorption peaks calculated with the R-D model are indeed too wide to reproduce main desorption peaks in experimental TDSP when hydrogen outgassing is limited by second order hydrogen molecular desorption (fig. 3.2).

We therefore assumed in this chapter that hydrogen outgassing from material is limited only by the readsorption of hydrogen from bulk onto surface and not by hydrogen recombination on tungsten surface. Boundary conditions of equations (3.1) therefore read

$$D\frac{\partial c_f}{\partial x}\bigg|_{x=x_s} = \pm K_b c_f(x_s, T) \tag{3.7}$$

Thickness of tungsten samples used in experiments was about $L \approx 0.8\mathrm{mm}$. Considering the characteristic depth $\delta(T) = \sqrt{\int_{T_0}^{T} \alpha D(T')\mathrm{d}T'}$ of diffusion of hydrogen into material, hydrogen diffuses up to the material rear surface when $T > 500\,\mathrm{K}$ ($\delta(T = 500\,\mathrm{K}) > L$). Hydrogen desorption outgassing flux is thus formally evaluated by

$$\Gamma_{out} = K_b c_f(0, T) + K_b c_f(L, T) \tag{3.8}$$

Although full descriptions of surface processes provided by equations (3.5) could have been kept when

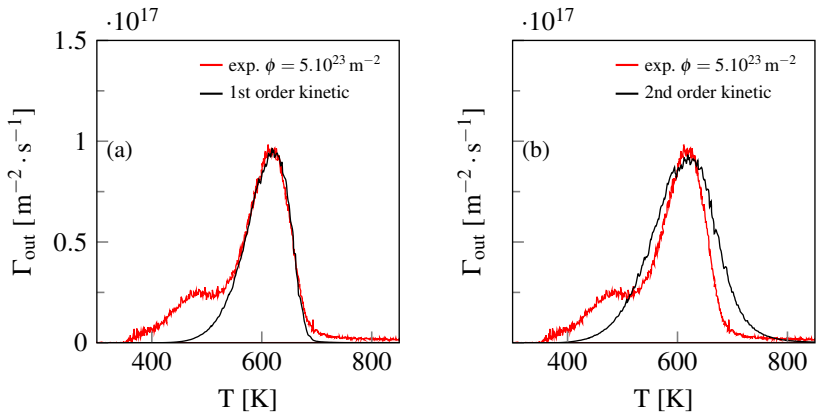

Figure 3.2: Fitting of main desorption peak in the experimental TDSP at $\phi = 5 \times 10^{23}\,\mathrm{m}^{-2}$ with first order boundary conditions $\Gamma_{\mathrm{out}} \sim c_{\mathrm{f}}$ (a) and second order boundary conditions $\Gamma_{\mathrm{out}} \sim (c_{\mathrm{f}})^2$ (b).

modeling TDS experiments, prescribing boundary conditions with the relationship (3.7) conveniently reduces the number of uncertain parameters in the R-D model and avoids some numerical hindrances induced by the second order kinetic of molecular desorption.

Although the values of the readsorption activation energy $E_{\mathrm{b}} = 0.2 - 0.4\,\mathrm{eV}$ deduced previously are in agreement with DFT predictions [134], E_{b} is kept as a free parameter in this work motivated by

- the large spikes observable at low temperature in TDSP at high fluences (fig. 3.1a) attributed to blister bursting during TDS experiments [36]. The presence of blisters suggests that surface morphology may be strongly modified, which may affect hydrogen desorption and transport.
- the large uncertainties in modeling of surface processes [32]
- the difficulty to reproduce experimental TDSP using equations (3.1) and (3.7) when simultaneously keeping fixed values of E_b and E_{dt}, and varying only trap concentrations to fit TDSP (see section 3.4.1).

3.3.3 Modeling of hydrogen retention induced by mutating traps

Vacancies in tungsten may be responsible for a significant retention of hydrogen isotopes in tungsten [20]. Many DFT simulations have shown that a single tungsten vacancy may accommodate several hydrogen atoms, leading to a reduction of the detrapping energy as the number of trapped hydrogen increases [116, 118]. Such mutation of traps is not included in the R-D equations (3.1) but is described in

contrast in the R-D equations (3.9).

$$\alpha \frac{\partial c_{\mathrm{f}}}{\partial T} = D \frac{\partial^2 c_{\mathrm{f}}}{\partial x^2} - \frac{\partial S(1)}{\partial T} \tag{3.9a}$$

$$\alpha \frac{\partial S(1)}{\partial T} = \nu_{\mathrm{tr}} \left[c_{\mathrm{tot}} - S(1) \right] c_{\mathrm{f}} - \nu_{\mathrm{dt}}(1) c_{\mathrm{t}}(1) \tag{3.9b}$$

$$\alpha \frac{\partial S(j)}{\partial T} = \nu_{\mathrm{tr}} c_{\mathrm{t}}(j-1) c_{\mathrm{f}} - \nu_{\mathrm{dt}}(j) c_{\mathrm{t}}(j),\ 2 \leq j \leq N \tag{3.9c}$$

where $S(j) = \sum_{i=j}^{N} c_{\mathrm{t}}(i)$ with j the number of hydrogen retained in one single trap with a maximum of $N = 6$ atoms per vacancy. Trapping rate is assumed here to be the same for all traps ($\nu_{\mathrm{tr}}(j) = \nu_{\mathrm{tr}}$).

A previous numerical work [119] suggested that TDSP resulting from TDS experiments can be modeled using indifferently equations (3.1) or equations (3.9). The validity of this observation can be assessed noticing that hydrogen desorption is retrapping-limited and trapped hydrogen concentrations are in equilibrium when hydrogen outgassing is described by equations (3.1) provided that $\frac{D}{\Delta^2} \ll \nu_{\mathrm{tr}}$ (see chapter 2). This regime also takes place for hydrogen desorption described by equations (3.9) when $\frac{D}{\Delta(k)^2} \ll \nu_{\mathrm{tr}}(k)$. When trapped hydrogen concentrations are in equilibrium, *id est* $\frac{\partial c_{\mathrm{t}}(k)}{\partial T} \approx 0$, R-D equations (3.1) and (3.9) are thus equivalent providing that

$$\frac{\nu_{\mathrm{dt}}(j)}{\nu_{\mathrm{tr}}(j)} \ll \frac{\nu_{\mathrm{dt}}(j+1)}{\nu_{\mathrm{tr}}(j+1)},\ \ j = 1 \ldots N-1 \tag{3.10}$$

.

The condition (3.10) is satisfied when several hydrogen atoms are trapped in one tungsten vacancy since the detrapping activation energy decreases as the number of hydrogen atoms sitting in the vacancy increases. Thermal desorption spectra induced by the trapping of several hydrogen atoms in single tungsten vacancy can be thus modeled using independent traps and R-D equations (3.1).

3.4 Analysis of deuterium retention via experimental thermal desorption spectra

3.4.1 Fitting of experimental thermal desorption spectra

Experimental TDSP reported in figure 3.1a have been fitted using TDSP calculated with the R-D model formed by equations (3.1) and boundary conditions (3.7) in the framework described in section 3.3. Trying to use a unique distribution of detrapping energy at all fluences and to keep the number of different

types of traps N as low as possible, the fitting of experimental TDSP was performed by adjusting only the concentrations of traps and the activation energy of readsorption E_b at each fluence, according to the following procedure:

1. fitting the main (largest) desorption peak at the highest fluence with traps $k = 1$.
2. adjusting concentrations of traps $k = 1$ to fit main desorption peaks at lower fluences and adjusting E_b for each fluence if necessary.
3. fitting outgassing flux at lower temperature (left shoulder of TDSP) at the highest fluence with traps $k > 1$.
4. fitting outgassing flux at lower temperature at lower fluences with traps $k > 1$ and adjusting E_b for each fluence if necessary.

The step 3 and 4 were repeated until experimental TDSP were well reproduced (fig. 3.3a). Finally, experimental TDSP have been fitted using an unique spectrum of detrapping energy and adjusted values of E_b, which are both reported in table 3.3. The integrated concentrations of traps N_{tot} are plotted in figure 3.3b and correspond to trap concentrations $\rho_{trap} \sim \frac{N_{tot}}{\Delta}$ with $\Delta \sim 5\,\mu$m.

Desorption tails at high temperature in experimental TDSP have been also fitted for illustration with traps $k = 7-10$ corresponding to detrapping energy $1.60\,\text{eV} < E_{dt} < 2\,\text{eV}$. Fitting of tails with additional traps may be however not meaningful since tails are likely induced by the outgassing of deuterium which has diffused beyond the retention region during TDS experiments (see section 2.7.2 in chapter 2).

Table 3.1: Trapping parameters used to fit experimental TDSP plotted in figure 3.3.

k	1	2	3	4	5	6	7-10
$E_{dt}(k)$[eV]	1.35	1.25	1.17	1.07	0.96	0.85	1.57 – 2.15
Fluence ϕ[m^{-2}]	3×10^{22}	6×10^{22}	5×10^{23}	10^{24}	5×10^{25}		
E_b[eV]	0.85	0.85	0.81	0.70	0.70		

3.4.2 Trap distribution with broad spectrum of detrapping energy

Traps $k = 2-6$ reproduce left shoulders of experimental TDSP at $T < 600\,\text{K}$ with a broad spectrum of detrapping energy between $0.85\,\text{eV}$ and $1.25\,\text{eV}$. The values of E_{dt} for traps $k = 2-6$ are in agreement with values of E_{dt} between $0.85\,\text{eV}$ and $1.00\,\text{eV}$ used to model low temperature desorption

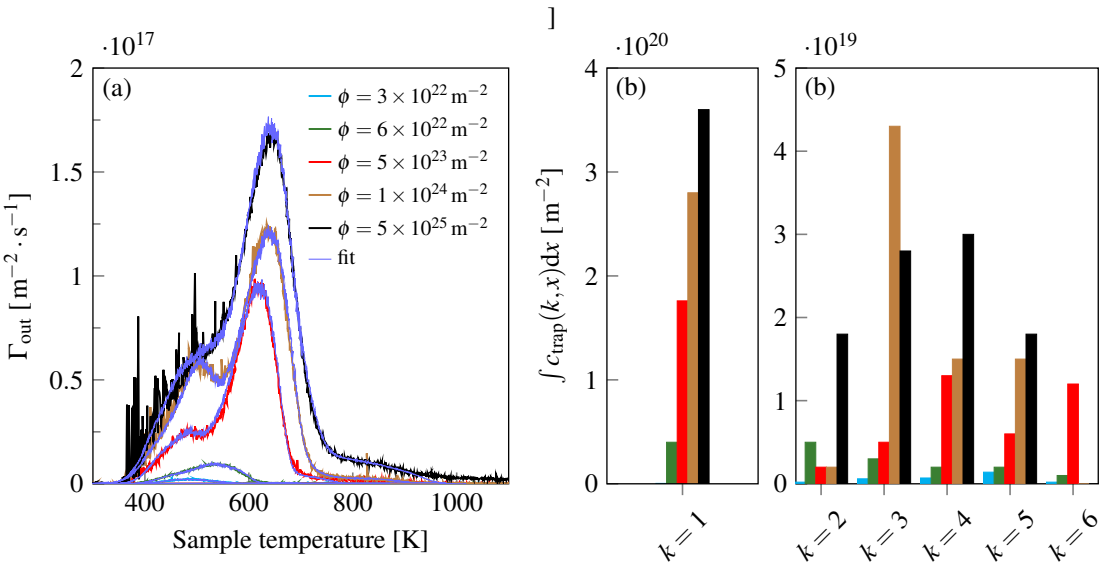

Figure 3.3: Fits of experimental TDSP (a) obtained with the R-D model using traps concentrations and trapping parameters reported in plots (b) and table 3.3.

peaks in other works [35, 77, 136]. The use of a broad spectrum of detrapping energy for traps $k = 2-6$ allows to well reproduce experimental TDSP at low temperature in contrast to previous works where the low number of traps used to fit TDSP required to adjust other trap parameters such as pre-exponential factors [36]. Traps $k = 1$ with $E_{dt} = 1.35\,\mathrm{eV}$ reproduce main desorption peaks which stand between 620 K and 680 K in TDSP. This value of E_{dt} is also in agreement with values of E_{dt} between $1.20\,\mathrm{eV}$ and $1.40\,\mathrm{eV}$ used in other works [35, 77, 136].

The amount of retained deuterium in traps $k = 1$ and in traps $k = 2-6$ increases with the fluence, suggesting that traps are created during exposure of tungsten samples to deuterium flux assuming that traps are completely filled with deuterium.

The spectrum of traps reported in table 3.1, used to reproduced experimental TDSP in figure 3.1a, is in remarkable agreement with the trap spectrum found to reproduce another TDSP reported in figure 3.4, which was obtained from a tungsten sample exposed at 300K to a deuterium flux $\Gamma_{in} = 10^{20}\,\mathrm{m^{-2}\cdot s^{-1}}$ at $200\,\mathrm{eV}$ /atom during $t_{exp} = 10^3\,\mathrm{s}$ [137]. This latter TDSP has been obtained with a heating rate about $1.3\,\mathrm{K\,s^{-1}}$ and was modeled with the R-D model and the assumptions introduced in section 3.3, considering flat profiles of trap concentration over the retention depth $\Delta = 5\times10^{-6}\,\mathrm{m}$.

The sharp desorption peak visible at $T < 400\,\mathrm{K}$ in figure 3.4a was not well reproduced by trapped hydrogen and was thus fitted by assuming that free hydrogen was present in the material at the beginning of

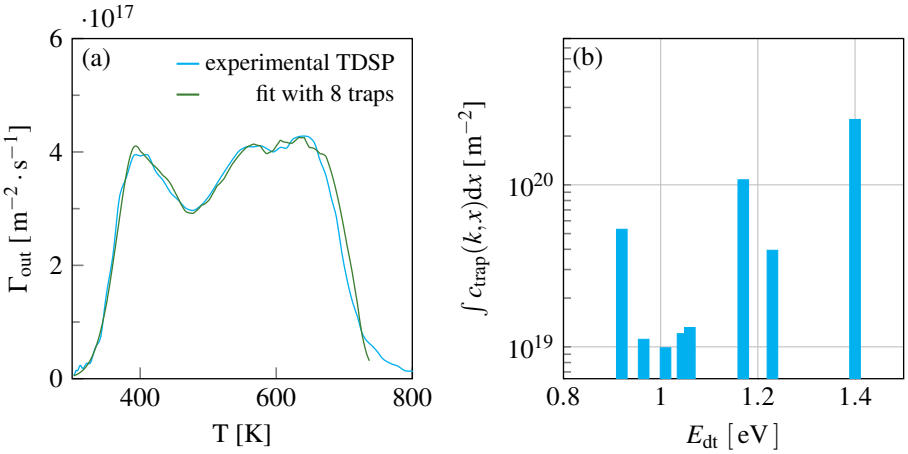

Figure 3.4: Experimental TDSP (a) obtained from tungsten sample exposed to deuterium at 300 K [137] fitted with eight traps using trap concentrations and detrapping energies reported in plot (b).

TDS experiment and by taking an activation energy of readsorption equal to $E_\mathrm{b} = 0.70\,\mathrm{eV}$. The desorption peak at $T < 400\,\mathrm{K}$ thus corresponds to the outgassing of free hydrogen in material, which is limited by surface processes. This desorption peak at $T < 400K$ is not expected in figure 3.1a since the temperature during implantation was 370 K.

3.4.3 Surface effects and temperature of desorption

The values of E_b selected to reproduce experimental TDSP decrease from $0.85\,\mathrm{eV}$ to $0.70\,\mathrm{eV}$ when the fluence increases (tab. 3.1). These values are higher than the value $E_b = 0.27\,\mathrm{eV}$ calculated with DFT simulations [134] but are in agreement with the value of $E_\mathrm{b} = 0.70\,\mathrm{eV}$ used to reproduce the desorption peak at $T < 400\,\mathrm{K}$ in figure 3.4.

Hydrogen desorption is not limited by readsorption of hydrogen on surface when $K_b\Delta/D \gg 1$. Therefore desorption peaks in TDSP are not affected by hydrogen readsorption when the temperature of desorption is above the temperature T^* which verifies $K_b(T^*)\Delta/D(T^*) = 10$. T^* strongly varies with E_b and hydrogen desorption from material is therefore affected by readsorption of hydrogen on surface when $E_\mathrm{b} > 0.80\,\mathrm{eV}$ (fig. 3.5b).

Surface effects thus alter desorption peaks at low fluences $\phi \leq 10^{23}\,\mathrm{m}^{-2}$ for which E_b was chosen above $0.80\,\mathrm{eV}$ (tab. 3.1). In contrast, surface effects are negligible at higher fluences $\phi > 10^{23}\,\mathrm{m}^{-2}$ for which $E_\mathrm{b} < 0.80\,\mathrm{eV}$, as illustrated in figure 3.5b where we have plotted the desorption temperature corresponding to desorption peaks induced by traps $k = 1$ calculated with the trap concentration corresponding to the highest fluence for several value of E_b. The temperature of desorption is indeed constant when

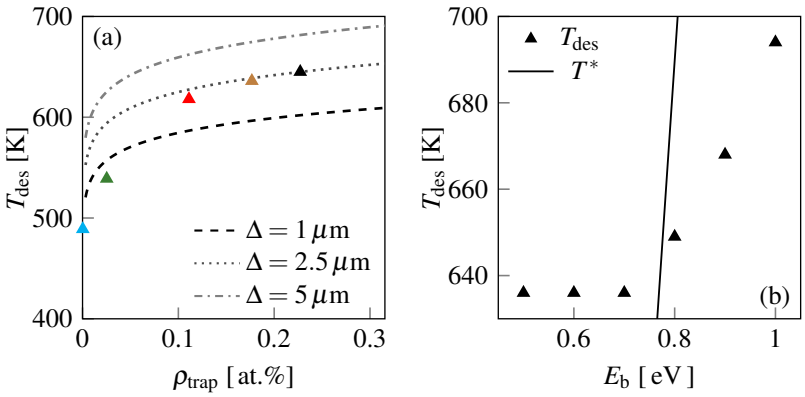

Figure 3.5: Plot (a): Temperature of desorption peaks induced by traps $k = 1$ in experimental TDSP (triangle) and desorption temperature predicted with exp. 3.11 for several values of Δ (lines).
Plot (b): Temperature of desorption peak induced by traps $k = 1$ at $\phi = 5 \times 10^{25}\,\text{m}^{-2}$ (triangle) and plot of $T^* = \frac{E_{\text{b}} - E_{\text{D}}}{\log\left(\frac{1}{10}\frac{\Delta}{\lambda_0}\right)}$.

$E_{\text{b}} < 0.80\,\text{eV}$.

The temperature of desorption of the main desorption peak increases with the fluence in exprimental TDSP (fig. 3.5a). When surface effects are negligible and when hydrogen desorption is retrapping-limited and quasi-static, which is the case in this work, the temperature of desorption increases with the trap concentration following the relationship (3.11), which has been derived in the chapter 2 in section 2.5 and is recalled below.

$$T_{\text{des}} = \frac{E_{\text{dt}}}{2} \frac{1}{\omega\left(\sqrt{\left(\frac{\lambda_0}{\Delta}\right)^2 \frac{E_{\text{dt}}}{2\alpha\rho_{\text{trap}}}}\right)} \tag{3.11}$$

The increase of the desorption temperature in experimental TDSP at high fluences is thus likely caused by the increase of trap concentration, as suggested by the comparison in figure 3.3a between the evolution of experimental desorption temperature as a function of ρ_{trap} and the evolution of desorption temperature predicted by the formula (3.11).

The temperature of desorption depends on E_{b} at low fluences, and thus the desorption temperature is expected to decrease as the fluence increases since the desorption temperature increases as E_{b} increases (fig. 3.5b). One can thus speculate that the increase of desorption temperature in experimental TDSP at low fluences is due to combined effects of the increase of trap concentrations and of the decrease of E_{b}. It may then explains differences observed in figure 3.5a at low fluences between the evolution of desorption temperature predicted with the formula (3.11) and the evolution of experimental desorption temperature.

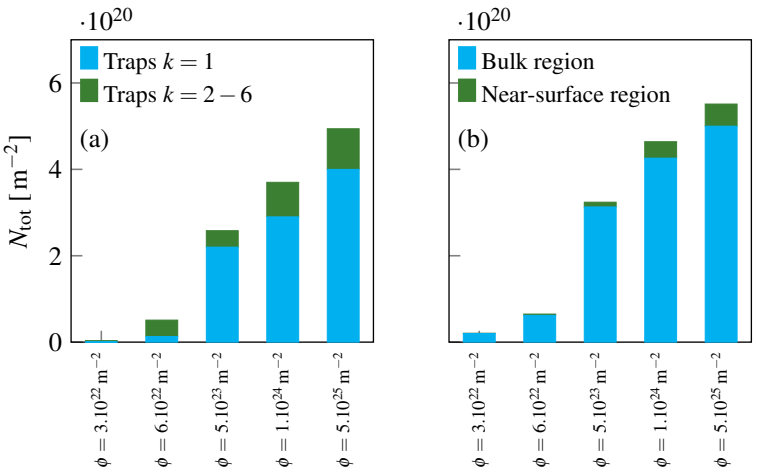

Figure 3.6: Comparison between deuterium retained in traps $k = 1$ and in traps $k = 2-6$ (a) and between deuterium retained in the near-surface region and in the bulk region (b).

3.4.4 Profiles of trap concentrations

Two retention regions can be distinguished in concentration profiles obtained with NRA (fig. 3.1b):

- the near-surface region ($0 < x < \Delta_{\text{n-s}} \approx 0.1\,\mu$m) where material is almost saturated with retained deuterium ($\rho_{\text{trap}} \gtrsim 1$ at.%)
- the bulk region ($x > \Delta_{\text{n-s}}$) where the concentration of retained deuterium is lower ($\rho_{\text{trap}} < 0.5$ at.%)

The quantity of deuterium retained in the near-surface region is compared to the quantity of deuterium retained in the bulk region in figure 3.6b. In parallel, the quantity of deuterium retained in traps $k = 2-6$, which form the left shoulders in experimental TDSP, is compared in figure 3.6a to the quantity of deuterium retained in traps $k = 1$, which form the main desorption peaks in experimental TDSP.

The ratio of deuterium retained in near-surface region versus deuterium retained in bulk region and the ratio of deuterium retained in traps $k = 2-6$ versus deuterium retained in traps $k = 1$ follow a similar trend when fluence increases, suggesting that traps $k = 2-6$ may be predominantly located in the near-surface region whereas traps $k = 1$ may be predominantly located in the bulk region.

3.4.5 Desorption tails in thermal desorption spectra

Desorption tails visible in experimental TDSP were fitted in this work with additional traps $k = 7-10$ to illustrate the interest of using a large number of different types of traps to accurately fit TDSP. However, it was shown in the chapter 2 that desorption tails are in reality induced by the diffusion of

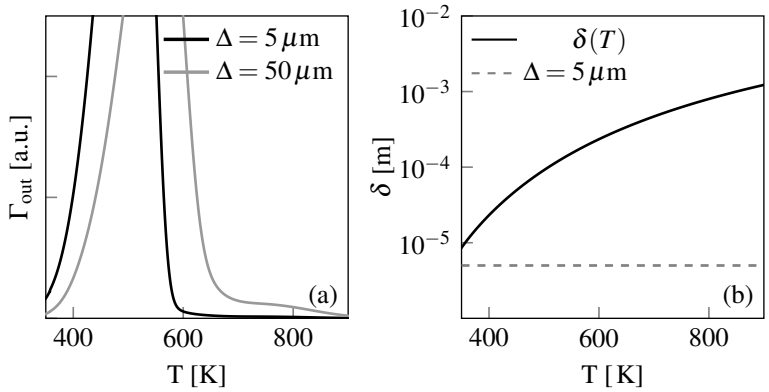

Figure 3.7: Desorption tails in TDSP. Plot (a): Desorption peaks with $E_{dt} = 1.10\,\text{eV}$ and $N_{tot} = c_{trap}\Delta = 2.5 \times 10^{20}\,\text{m}^{-2}$ calculated for $\Delta = 5\,\mu$m and $\Delta = 50\,\mu$m. Plot (b): characteristic depth of diffusion δ calculated with $\alpha = 0.05\,\text{K}\,\text{s}^{-1}$.

hydrogen beyond the retention region at $x > \Delta$ and by the desorption of this hydrogen at high temperature during TDS experiments. The magnitude of these tails can be characterized by $f = \frac{\Delta}{\delta(T_{des})}$ and tails are usually visible when $f \gtrsim 0.1$. In this work, the characteristic depth of diffusion $\delta(T) = \sqrt{\int_{T_0}^{T} D(T')\text{d}T'}$ is large compared to Δ even at low temperature due to the low heating rate $\alpha \sim 0.05\,\text{K}\,\text{s}^{-1}$ used in TDS experiments (fig. 3.7b).

Consequently, desorption tails can be induced only by traps located in retention regions which extend above $\Delta \gtrsim 50\,\mu$m considering temperature of desorption $T_{des} < 650\,\text{K}$ as illustrated in figure 3.7a. Tails visible in experimental TDSP might be thus induced by hydrogen retained in traps located far in material well beyond the NRA information depth limited at $8\,\mu$m. The concentrations of these traps cannot be higher than $\rho_{trap} \sim 10^{-3}$ at.% and the detrapping energy should not exceed $E_{dt} \sim 1.1\,\text{eV}$ to allow desorption peaks to stand below 650 K. Such traps may therefore correspond to natural defects or impurities present in tungsten samples used in experiments, for which the purity is usually around ~ 99.97 wt.% [36].

Desorption tails in experimental TDSP can be used to estimate the activation energy of diffusion E_D as demonstrated in the chapter 2, where E_D was estimated to be about $0.45\,\text{eV}$ using the desorption tail in the TDSP at $\phi = 5 \times 10^{25}\,\text{m}^{-2}$, in agreement with $E_D = 0.39\,\text{eV}$ found in previous permeation experiments [59].

3.5 Discussion

The nature of the traps which induce deuterium retention in tungsten is unclear as various crystal defects (grain boundaries, edge dislocations, impurity atoms, vacancies, interstitial atom, cavities,...) may be responsible for hydrogen retention.

For instance, main desorption peaks in TDSP stand at $T \sim 800\,\mathrm{K}$ when tungsten samples are formed by single crystal, whereas these desorption peaks stand at $T \sim 600\,\mathrm{K}$ when samples are polycrystalline [46]. These experimental observations suggest that traps forming these main desorption peaks may depend on the presence of grain boundaries. Besides, the quantity of deuterium retained in traps forming the main desorption peaks diminishes when tungsten samples are recrystallized before implantation [95]. A. Manhard has also noticed in [36] that the concentration of dislocations decreases in material due to the recrystallization process, suggesting that dislocations may also induce main desorption peaks. Traps forming main desorption peaks, *id est* traps $k = 1$ with $E_{\mathrm{dt}} = 1.35\,\mathrm{eV}$ in this work, may thus correspond to either trapping in grain boundaries or in dislocations.

Traps $k = 1$ may also correspond to voids filled with hydrogen molecules in material bulk [138]. The existence of such void-like defects in material bulk has been suggested by some authors [109, 100]. There is however no consensus about nucleation processes leading to such defects in material since hydrogen cannot be self-trapped and form clusters in tungsten, unlike helium atoms [139]. Kong et al.[140] have however recently suggested that impurity atoms may lead to a local accumulation of hydrogen and to the formation of stable impurity-hydrogen-vacancy complexes, which may nucleate to form void-like defects.

Traps $k = 1$ may also correspond to tungsten vacancy since DFT simulations have shown that detrapping energy of a single hydrogen atom in a tungsten vacancy is about $1.4\,\mathrm{eV}$ [116, 118]. Although the energy of incoming hydrogen ions, which is about $38\,\mathrm{eV}/\mathrm{ion}$ in experiments, is much lower than the atom displacement threshold in tungsten, which is about $800\,\mathrm{eV}/\mathrm{ion}$, other mechanisms may lead to the formation of vacancies such as plastic deformation caused by deuterium supersaturation in near-surface regions [96, 141].

The presence of large concentrations of vacancy in the near-surface region is supported by noticing that traps $k = 2-6$, assumed to lie in the near-surface region (sec. 3.4.4), may correspond to vacancies occupied by several hydrogen atoms. Indeed, many DFT simulations have shown that tungsten vacancy can accommodate up to six hydrogen atoms and that E_{dt} decreases as the number of trapped hydrogen atoms increases [116, 118]. Values of E_{dt} found in DFT simulations recalled in table 3.2 are surprisingly

Table 3.2: Detrapping energy when several hydrogen are trapped in a single tungsten vacancy calculated in DFT simulations [116, 118].

Number of H in W vacancy	1	2	3	4	5	6	Ref.
$E_{dt}[\,\mathrm{eV}\,]$	1.41	1.40	1.14	1.12	0.91	0.79	[116]
$E_{dt}[\,\mathrm{eV}\,]$	1.43	1.42	1.25	1.17	1.11	0.86	[118]

in very good agreement with values of E_{dt} found for traps $k = 2-6$.

Similarities in spectrum of detrapping energy reported in table 3.1 and in 3.2 thus strongly suggest that traps $k = 2-6$ correspond to trapping of several hydrogen atoms in single tungsten vacancy in the near-surface region. Trapping of several hydrogen atoms in single vacancy, which corresponds to a trap mutation mechanism, can be indeed modeled using R-D equations (3.1) as mentioned in section 3.3.3.

However, vacancies created in the near-surface region cannot diffuse into material bulk when samples are implanted with deuterium at 370 K, since diffusion activation energy of vacancies is large $E_D = 1.6\,\mathrm{eV}$ [115] and thus $\sqrt{D_{\mathrm{vacancy}}(370\,\mathrm{K})t_{\mathrm{exp}}} < 10^{-8}\,\mathrm{m}$. It is thus unlikely that traps $k = 1$, which mainly lie in material bulk, correspond only to tungsten vacancies created in the near-surface region.

The distribution of trap concentrations in figure 3.3b shows that concentrations of traps $k = 1$ are much larger than concentrations of traps $k = 2-6$. If traps $k = 1$ and $k = 2-6$ were formed by vacancies containing one or more hydrogen atoms, we may expect similar concentrations of traps $k = 1$ and $k = 2-3$ since deuterium cannot escape from traps when $E_{dt} > 1.16\,\mathrm{eV}$ during the storage period at room temperature $\left(\nu_{dt}\, t_{\mathrm{storage}} < 1 \text{ when } E_{dt} > 1.16\,\mathrm{eV} \text{ without taking into account retrapping}\right)$. It is thus possible that the trapping of single hydrogen atoms in vacancies may contribute to only a tiny portion of main desorption peaks induced by traps $k = 1$.

Differences in concentrations of traps $k = 2-6$ shown in figure 3.3b cannot be due to differences between values of E_{dt} since equilibrium concentrations of trapped deuterium vary of several orders of magnitude considering values of E_{dt} reported in table I. These differences may be however due to hydrogen detrapping from traps at low activation energy ($E_{dt} < 1.16\,\mathrm{eV}$) during storage period, as suggested by Quastel's experiments which show a decrease of the magnitude of desorption peaks at low temperature $T < 450K$ as the storage time increases [108].

The readsorption activation energy $E_b \sim 0.80\,\mathrm{eV}$ decreases as the fluence increases (tab. 3.1). It thus suggests that surface effects are stronger at low fluences, in agreement with the positive skewness of the desorption peak observed at the lowest fluence $\phi = 3\times10^{22}\,\mathrm{m}^{-2}$, which may indicate that hydrogen desorption is limited by surface processes (see chapter 2). But the nature of surface processes which could

be modeled with readsorption activation energy larger than the one predicted in DFT simulations [134] remains unclear.

The values of $E_b \sim 0.80\,\mathrm{eV}$ found in this work at low fluences are however similar to the detrapping activation energy $E_{\mathrm{dt}} \approx 0.85\,\mathrm{eV}$ attributed to the trapping of hydrogen in microstructural defects by Ogorodnikova [110]. The presence of such microstructural defects in the near-surface region may be explained by large stress fields caused by blistering observed on tungsten surfaces [36], which may also directly alter diffusion of hydrogen near material surface [109]. The desorption temperature of main desorption peaks indeed decreases from 680 K to 615 K when no blisters are observed on material surfaces [95].

3.6 Summary

TDSP resulting from TDS experiments performed by A.Manhard on tungsten samples exposed to deuterium at different fluences have been analyzed using a R-D model including a large number of types of traps. The use of several types of traps allows accurate fitting of experimental TDSP with a unique spectrum of detrapping energy at all fluences, provided that the activation energy of hydrogen readsorption, which models effects of surface processes, is adjusted at low fluences.

Main desorption peaks in experimental TDSP were reproduced using traps $k = 1$ with $E_{\mathrm{dt}} = 1.35\,\mathrm{eV}$, whereas left shoulders of TDSP were fitted with five types of traps $k = 2-6$ characterized by a broad distribution of detrapping energy $E_{\mathrm{dt}} = 0.85 - 1.25\,\mathrm{eV}$. The comparison between deuterium retained in traps $k = 1$ and in traps $k = 2-6$ and the comparison between deuterium retained in the near-surface region and in the bulk region of material suggest that traps $k = 2-6$ are predominantly located in the near-surface region, while traps $k = 1$ are predominantly located in material bulk.

Desorption tails observed in TDSP cannot be reproduced considering trap concentration profiles observed in NRA where the depth of retention is about $8\,\mu\mathrm{m}$ because of the low heating rate $\alpha \sim 0.05\,\mathrm{K\,s^{-1}}$ used in TDS experiments. Tails are thus likely induced by traps at low concentration located beyond $8\,\mu\mathrm{m}$ in material. Defects and impurities naturally present in material are thus good candidates to induce desorption tails observed in TDSP.

The readsorption activation energy, which characterizes effects of surface processes on hydrogen outgassing from material, was adjusted at each fluence to fit TDSP. At high fluences where the readsorption activation energy is about $0.70\,\mathrm{eV}$, hydrogen outgassing is limited by hydrogen diffusion in the bulk, and surface effects are thus negligible. At low fluences, the readsorption activation energy is larger than $0.80\,\mathrm{eV}$

and is similar to detrapping energy attributed by other authors to hydrogen retained in micro-structural defects, which may be induced by blisters experimentally observed on material surface.

The broad spectrum of detrapping energy found in this work to fit experimental TDSP is in very good agreement with spectra of detrapping energy predicted by DFT simulations when up to six hydrogen atoms are retained in a single tungsten vacancy. Traps $k = 2 - 6$, which may therefore correspond to tungsten vacancies, are found to be located near material surface where vacancies have been experimentally observed. Large concentrations of vacancies near material surface may be expected due to the saturation of the near-surface region with deuterium during exposure of tungsten samples to deuterium flux.

Finally, we have illustrated in this work how a large number of types of traps in R-D model can be used to accurately analyze experimental TDSP and to consistently characterize traps inducing hydrogen retention. This approach offers new insights via TDS experiments on retention mechanisms such as, for example, trapping of several hydrogen atoms in single tungsten vacancy.

Chapter 3, in full, is a reprint of the material as it appears in J. Guterl, R.D. Smirnov, S.I. Krasheninnikov, M. Zibrov and A. Pisarev, Theoretical analysis of deuterium retention in tungsten plasma-facing components induced by various traps via thermal desorption spectroscopy, accepted in *Nuclear Fusion*, 2015. The dissertation author was the primary investigator and author of this paper.

Chapter 4

Long-term hydrogen outgassing from plasma facing components during off-plasma events

4.1 Introduction

Experimental measurements of the outgassing hydrogen flux during off-plasma events from graphite PFC in ToreSupra, loaded with hydrogen during long-plasma discharges, showed that the hydrogen outgassing flux decays in time following a power-law $\sim t^{-0.7\pm0.1}$ [29, 142]. Surprisingly, experiments performed on JET in ITER-like wall configuration, with tungsten divertor and beryllium walls, indicated that the evolution in time of hydrogen outgassing flux from PFC during off-plasma events follows a similar power-law $\sim t^{-0.8}$ [27]. These similar power-law exponents suggest that mechanisms controlling hydrogen outgassing from PFC during off-plasma events may be independent from PFC material, and may actually correspond to intrinsic properties of hydrogen retention in PFC material.

Two models have been proposed to describe the power-law decay of outgassing flux during off-plasma events:

- In [29], Grisolia et al. described hydrogen outgassing from graphite wall using a R-D model with a single type of traps, where hydrogen atoms can diffuse in material, and reproduced a power-law dependency $\sim t^{-0.73}$.

- Andrew et al. [143] used a similar model with a single type of trap but applied to wall surface only, i.e. without diffusion of hydrogen in material, and found that hydrogen outgassing flux decay following a power-law $\sim t^{-2/3}$.

Power-law exponents found in [29] and [143] are thus similar, although assumptions about hydrogen diffusion in material are different. Ehrenberg et al. [144] have suggested that these power-law dependencies of the outgassing flux can be obtained only when hydrogen outgassing is limited by molecular hydrogen recombination and desorption from PFC surface.

We propose here to reconcile results obtained from Andrew's and Grisolia's models by revisiting the standard reaction-diffusion model used by Grisolia in [29] to describe hydrogen retention and outgassing in PFC. This reaction-diffusion model, which includes only a single type of traps, is formed by equations (1.9a) and (1.9b) and is shortly discussed in the framework of long-term outgassing in the first section of this chapter. It is then shown that trapping and detrapping processes are in equilibrium during hydrogen outgassing. In this regime, hydrogen outgassing from the wall can be either diffusion-limited or surface-limited, depending on hydrogen concentration in wall material. Finally, power-law exponents characterizing the decrease in time of the outgassing flux are then identified and compared to experimental observations mentioned above.

4.2 Model of hydrogen outgassing during off-plasma events

4.2.1 Reaction-diffusion equations

Hydrogen retention and outgassing is modeled here with the reaction-diffusion (R-D) equations similar to the equations 1.9 given in the introduction and used in chapters 2 and 3. In contrast with R-D equations used in the chapters 2 and 3 to model hydrogen outgassing during TDS experiments, R-D equations used in this chapter are expressed as a function of the time only and do not explicitly include effects of variable temperature, since hydrogen outgassing considered in this chapter occurs at room temperature during off-plasma events. Considering immobile traps at fixed concentration during hydrogen outgassing, the time evolution of the concentrations of free hydrogen $\hat{c}_{\mathrm{f}}$ and trapped hydrogen $\hat{c}_{\mathrm{t}}$ in an 1D

wall of thickness L is described by:

$$\frac{\partial \hat{c}_\mathrm{f}}{\partial t} = D\frac{\partial^2 \hat{c}_\mathrm{f}}{\partial x^2} - \nu_\mathrm{tr}\hat{c}_\mathrm{f}(1-\hat{c}_\mathrm{t}) + \nu_\mathrm{dt}\hat{c}_\mathrm{t} \tag{4.1a}$$

$$\frac{\partial \hat{c}_\mathrm{t}}{\partial t} = \nu_\mathrm{tr}\hat{c}_\mathrm{f}(1-\hat{c}_\mathrm{t}) - \nu_\mathrm{dt}\hat{c}_\mathrm{t} \tag{4.1b}$$

The notations used in equations (4.1a) and (4.1b) are similar to the ones used in chapters 2 and 3. The hydrogen concentrations $\hat{c}_\mathrm{f}$ and $\hat{c}_\mathrm{t}$ are normalized by the concentration of traps c_trap in material, which is assumed to be uniform in the retention region of depth Δ. x is the material depth, D is the diffusion coefficient of free hydrogen in the material and ν_tr and ν_dt are the trapping and detrapping frequencies with $\nu_\mathrm{tr} = K_\mathrm{tr}c_\mathrm{trap}$.

4.2.2 Evolution of surface hydrogen concentration

The evolution of hydrogen surface concentrations is described here using the formalism and the notations given in the section 1.4.2 based on the surface model introduced in [47]. The front material surface exposed to plasma and the rear material surface stand respectively at $x_\mathrm{s} = 0$ and $x_\mathrm{s} = L$. The rear surface of PFC material is usually in contact with the frame of the vessel, and outgassing of hydrogen from PFC into the vacuum chamber only occurs from the front surface of PFC. Diffusion of hydrogen from PFC to vessel frame material through the rear PFC surface is thus assumed to be limited and negligible in comparison with diffusion of hydrogen toward front surface ($D\left.\frac{\partial c_\mathrm{f}}{\partial x}\right|_{x=L} \approx 0$). Only the evolution of the hydrogen surface concentration c_s on front surface of PFC material exposed to plasma is thus of interest.

The evolution of c_s is described by

$$\frac{\partial c_\mathrm{s}}{\partial t} = \Gamma_\mathrm{b} - \Gamma_\mathrm{out} - \Gamma_\mathrm{a} \tag{4.2}$$

where $\Gamma_\mathrm{out} = K_\mathrm{r}c_\mathrm{s}^2$ is the hydrogen desorption flux of hydrogen atoms recombining into molecules on material surface and desorbing into vacuum, $\Gamma_\mathrm{a} = K_\mathrm{a}c_\mathrm{s}$ is the absorbtion flux of hydrogen adsorded on surface into material bulk and $\Gamma_\mathrm{b} = K_\mathrm{b}c_{\mathrm{f},0}$ is the readsorpion flux of hydrogen from bulk onto material

surface with $c_{\mathrm{f},0} = c_{\mathrm{f}}(x=0)$. The balance of particles flux at the front material surfaces imposes

$$D \left.\frac{\partial c_{\mathrm{f}}}{\partial x}\right|_{x=0} = \Gamma_{\mathrm{a}} - \Gamma_{\mathrm{b}} \tag{4.3}$$

which constitute the other boundary condition of the R-D equation (4.1a). The equation (4.2) and boundary condition (4.3) are voluntary not expressed as a function of the normalized concentration $\hat{c}_{\mathrm{f}}$ to avoid unnecessary additional notations.

It can be assumed that the hydrogen surface concentration is in equilibrium during long-term hydrogen outgassing from graphite and beryllium wall at constant temperature $\left(\frac{\partial c_{\mathrm{s}}}{\partial t} \approx 0 \text{ in eq. (4.2)}\right)$, regarding the low solubility heat of hydrogen in C and Be ($Q_{\mathrm{sol}} \lesssim 0.2\,\mathrm{eV}$ [20]). When hydrogen surface concentration is in equilibrium, hydrogen outgassing can be either limited by:

- hydrogen recombination on surface ($\Gamma_{\mathrm{out}} \ll \Gamma_{\mathrm{a}}$) and the outgassing flux is thus:

$$\Gamma_{\mathrm{out}} = K_{\mathrm{r}} \left(\frac{K_{\mathrm{b}}}{K_{\mathrm{a}}}\right)^2 c_{\mathrm{f},0}^2 \tag{4.4}$$

- hydrogen readsorption ($\Gamma_{\mathrm{out}} \gg \Gamma_{\mathrm{a}}$) and the outgassing flux is thus

$$\Gamma_{\mathrm{out}} = K_{\mathrm{b}}\, c_{\mathrm{f},0} \tag{4.5}$$

Hydrogen outgassing from graphite and beryllium walls is commonly assumed to be limited by hydrogen recombination on surface in literature [144, 29]. We however consider here both readsorption-limited and recombination-limited regimes by introducing the kinetic order q of the process controlling hydrogen outgassing. Besides values of q corresponding to recombination-limited and readsorption-limited outgassing regimes ($q=1$ and $q=2$), we consider here any positive value of $q>0$, which may model other complex processes affecting desorption on material surface, such as islands or impurities [114].

We thus consider in this work the following generic expressions of the outgassing flux and diffusion flux at the front material surface

$$\begin{cases} \Gamma_{\mathrm{out}} = K_{\mathrm{q}}\, [c_{\mathrm{f},0}]^q \\ D \left.\frac{\partial c_{\mathrm{f}}}{\partial x}\right|_{x=0} = K_{\mathrm{q}}\, [c_{\mathrm{f},0}]^q \end{cases} \tag{4.6}$$

4.2.3 Equilibrium of trapped hydrogen concentration

Trapped hydrogen concentration can be assumed to be in equilibrium $\left(\frac{\partial \hat{c}_\mathrm{t}}{\partial t} \approx 0 \text{ in eq. 4.1b}\right)$ when $\frac{D}{\Delta^2} \ll \nu_\mathrm{tr} + \nu_\mathrm{dt}$, similar to trapped hydrogen equilibrium regime during TDS experiments (see section 2.3.2 in the chapter 2). This latter condition is usually satisfied during hydrogen outgassing from graphite and beryllium PFC considering values of trapping and detrapping rates commonly admitted for hydrogen in beryllium [20] and graphite [29], and retention regions which are usually much thicker than 1 nm $\left(\Delta \gg 10^{-9}\,\mathrm{m}\right)$.

When trapped hydrogen concentration is in equilibrium, the equation (4.1b) reads

$$\hat{c}_\mathrm{f} \approx \xi_\mathrm{dt} \frac{\hat{c}_\mathrm{t}}{(1-\hat{c}_\mathrm{t})} \tag{4.7}$$

where $\xi_\mathrm{dt} = \frac{\nu_\mathrm{dt}}{\nu_\mathrm{tr}}$, as introduced in the chapter 2. Values of ξ_dt at room temperature are usually much lower than the unity for hydrogen retention in beryllium and graphite, such that the inequality $\sqrt{\xi_\mathrm{dt}} \ll 1$ also holds. The concentration of free hydrogen $\hat{c}_\mathrm{f}$ in the material can be expressed as a function of the total concentration of hydrogen in material $\hat{c}_\mathrm{H} = \hat{c}_\mathrm{f} + \hat{c}_\mathrm{t}$ using the expression (4.7).

$$\hat{c}_\mathrm{f}(\hat{c}_\mathrm{H}) = \underbrace{\frac{\hat{c}_\mathrm{H} - (1+\xi_\mathrm{dt})}{2} + \sqrt{\left(\frac{\hat{c}_\mathrm{H} - (1+\xi_\mathrm{dt})}{2}\right)^2 + \xi_\mathrm{dt}\hat{c}_\mathrm{H}}}_{F(\hat{c}_\mathrm{H})} \tag{4.8}$$

The reaction-diffusion (4.1a) and the boundary condition (4.6) can be thus recast as a function of $\hat{c}_\mathrm{H}$ into

$$\frac{\partial \hat{c}_\mathrm{H}}{\partial t} = \frac{\partial}{\partial x}\left(\hat{D}_\mathrm{eff}(\hat{c}_\mathrm{H}) \frac{\partial \hat{c}_\mathrm{H}}{\partial x}\right) \tag{4.9}$$

$$\left(\hat{D}_\mathrm{eff}(\hat{c}_\mathrm{H}) \frac{\partial \hat{c}_\mathrm{H}}{\partial x}\right)_{x=0} = \hat{K}_\mathrm{eff,q}\left(\hat{c}_\mathrm{H,0}\right) \tag{4.10}$$

where we have introduced the effective diffusion coefficient $\hat{D}_\mathrm{eff}(\hat{c}_\mathrm{H}) = D\frac{\partial F(\hat{c}_\mathrm{H})}{\partial c_\mathrm{H}}$ and the effective desorption rate $\hat{K}_\mathrm{eff,q}(\hat{c}_\mathrm{H}) = \hat{K}_\mathrm{q}\left[F\left(\hat{c}_\mathrm{H}\right)\right]^q$ using an adhoc normalization. The non-linear diffusion equation (4.9) and the associate diffusion coefficient $\hat{D}_\mathrm{eff}(\hat{c}_\mathrm{H})$ are similar to the diffusion equation (2.18) introduced in chapter 2. Both diffusion equations describe hydrogen outgassing when trapped hdyrogen concentration is in equilibrium. The normalized hydrogen outgasing flux is here given by $\hat{\Gamma}_\mathrm{out} = \hat{K}_\mathrm{eff,q}(\hat{c}_\mathrm{H})$.

Analytical solutions of the non-linear diffusion equation (4.9) with the boundary condition

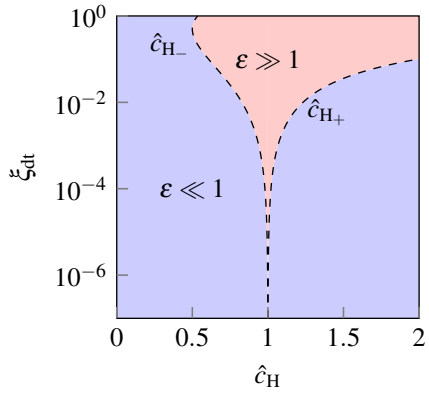

Figure 4.1: Values of $\varepsilon = \frac{4\xi_{dt}\hat{c}_H}{(\hat{c}_H-(1+\xi_{dt}))^2}$ as a function of ξ_{dt} and $\hat{c}_H$.

(4.10) can be derived when $F(\hat{c}_H)$ is expressed in the convoluted form $F(\hat{c}_H) = a(b_0 + b_1\hat{c}_H)^\mu$. The total concentration of hydrogen in material may exceed the unity when traps are saturated with hydrogen and we thus analyze the function F considering separately $0 < \hat{c}_H < 1$ and $\hat{c}_H \gtrsim 1$. The function F can be recast into

$$F(\hat{c}_H) = \frac{\hat{c}_H - 1 - \xi_{dt}}{2} + \left|\frac{\hat{c}_H - 1 - \xi_{dt}}{2}\right| \sqrt{1+\varepsilon} \tag{4.11}$$

where $\varepsilon = \frac{4\xi_{dt}\hat{c}_H}{(\hat{c}_H-(1+\xi_{dt}))^2}$ is larger than the unity when $\hat{c}_{H_-} < \hat{c}_H < \hat{c}_{H_+}$ and smaller than the unity otherwise. The interval $\hat{c}_{H_-} < \hat{c}_H < \hat{c}_{H_+}$ is very narrow when $\xi_{dt} \ll 1$, which is usually the case for hydrogen retention in PFC (fig. 4.1). Approximations of the function F can be thus found assuming that $\varepsilon \gg 1$:

- when $\hat{c}_H > 1$,

$$F(\hat{c}_H) \approx \hat{c}_H - 1 \tag{4.12}$$

- when $\hat{c}_H \approx \hat{c}_0 < 1$, $F(\hat{c}_H) \approx \xi_{dt}\frac{\hat{c}_H}{1-\hat{c}_H}$ which can be expressed in the convoluted form

$$F(\hat{c}_H) \approx \xi_{dt}\frac{\hat{c}_0}{1-\hat{c}_0}\left(1 + \frac{1-2\hat{c}_0}{\hat{c}_0(1-\hat{c}_0)}(\hat{c}_H - \hat{c}_0)\right)^{\mu_0} \tag{4.13}$$

  The exponent $\mu_0 = \frac{1}{1-2\hat{c}_0}$ depends on hydrogen concentration in material.

These approximations of F are used below to find time dependencies of the outgassing flux $\hat{\Gamma}_{out}$.

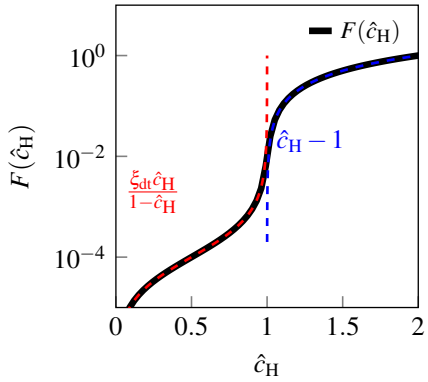

Figure 4.2: Graph of the function F and its approximations for $\xi_{dt} = 10^{-4}$.

4.3 Surface effects on hydrogen outgassing

Hydrogen outgassing from material can be limited either by surface processes characterized by $\hat{K}_{eff,q}$ or by the hydrogen diffusion characterized by $\hat{D}_{eff}$. To determine the outgassing regime, we compare the characteristic time $\tau_D = \Delta^2/\hat{D}_{eff}$, required by hydrogen to diffuse in material toward the front material surface, with the characteristic time $\tau_s = \hat{c}_H\Delta/\hat{K}_{eff,q}$, required to desorb hydrogen from material when outgassing is limited by surface processes. Introducing the dimensionless parameter σ,

$$\sigma = \frac{\tau_s}{\tau_D} = \frac{D}{K_q\Delta}\frac{\hat{c}_H F'(\hat{c}_H)}{[F(\hat{c}_H)]^q} \tag{4.14}$$

the hydrogen outgassing is thus:

- diffusion-limited when $\sigma < 1$
- surface-limited when $\sigma > 1$

The value of σ strongly depends on the temperature of the sample during hydrogen outgassing via D, K_q and ξ_{dt}. The outgassing regime may thus change when the sample temperature is modified.

For instance, values of σ, corresponding to hydrogen outgassing from graphite PFC at room temperature considering diffusion, trap parameters and second-order desorption from surface ($q = 2$) proposed in [29] (tab. 4.1), are plotted in figure 4.3 as a function of $\hat{c}_H$ for different retention depth Δ. It indicates that hydrogen outgassing is likely surface-limited when hydrogen is retained further than 10 nm.

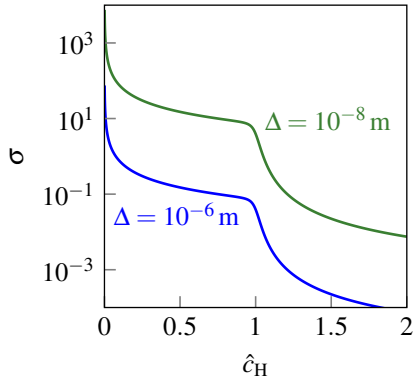

Figure 4.3: Values of σ as a function of $\hat{c}_H$ illustrated with values reported in table 4.1 for $\Delta = 10^{-8}$ m and $\Delta = 10^{-6}$ m.

4.3.1 Surface-limited hydrogen outgassing

When the hydrogen outgassing is surface-limited ($\sigma > 1$), hydrogen diffusion is fast and $\hat{c}_H$ is approximatively constant in material. The diffusion equation (4.9) can be then integrated, leading to

$$\frac{\partial \hat{c}_H}{\partial \hat{t}} = -[F(\hat{c}_H)]^q \tag{4.15}$$

where $\hat{t}$ is the normalized time $\hat{t} = \frac{K_q}{\Delta} t$.

Using the approximations (4.12) and (4.13), the function F can expressed in a convoluted form as $F(\hat{c}_H) \approx a(b_0 + b_1 \hat{c}_H)^\mu$ where $\mu = 1$ when $\hat{c}_H > 1$ and $\mu = \frac{1}{1-2\hat{c}_H}$ when $\hat{c}_H < 1$. The evolution in time of $\hat{\Gamma}_{out}$ can be obtained as a function of μ and q considering the initial concentration of trapped hydrogen in material $\hat{c}_H(\hat{t} = 0, x) = \hat{c}_i$:

- when $q\mu = 1$,

$$\hat{\Gamma}_{out} \sim e^{-a^q b_1 \hat{t}} \tag{4.16}$$

- when $q\mu \neq 1$,

$$\hat{\Gamma}_{out} \sim \hat{t}^{-\kappa} \tag{4.17}$$

with $\kappa = \frac{q\mu}{1-q\mu}$ for $\hat{t} > \left| \frac{1}{a^q b_1 (q\mu - 1)} \right|$.

Values of κ are plotted in figure 4.4 as a function of $\hat{c}_H$, showing that κ decreases from $+\infty$ to 0.5 when $q = 1$, and from 2 to $2/3$ when $q = 2$ as hydrogen concentration $\hat{c}_H$ increases up to 1. When the concentration of hydrogen exceeds 1, $\kappa = 2$ when hydrogen desorption is of second order ($q = 2$), whereas the outgassing flux decays exponentially in time when $q = 1$.

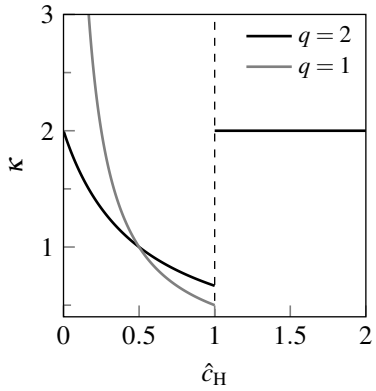

Figure 4.4: Values of $\kappa = \frac{q\mu}{1-q\mu}$ as a function of $\hat{c}_H$ with $\mu = \frac{1}{1-2\hat{c}_H}$ when $\hat{c}_H < 1$.

Numerical solutions of the diffusion equation (4.9) with the boundary conditions (4.10) have been calculated in surface-limited regime with $\xi_{dt} = 10^{-4}$, adhoc diffusion coefficient D, desorption rate K_q and retention depth Δ such that $\sigma(\hat{c}_i) \approx 10$ with $\hat{c}_i = 1.2$ considering respectively $q = 2$ and $q = 1$. Resulting outgassing flux reported in figures 4.5a and 4.5b follow time dependencies predicted by the relationships (4.16) and (4.17). $\hat{\Gamma}_{out}$ first decreases following a quadratic (resp. exponential) time dependency when $\hat{c}_H > 1$, and then following a power-law decay with an power close to $-2/3$ (resp. $-1/2$) when $\hat{c}_H \approx 1$ and close to -2 (resp. $-\infty$) when $\hat{c}_H < 1$. Power-law exponents $\kappa = 0.7$ for $q = 2$ and $\kappa = 0.6$ for $q = 1$ obtained by fitting outgassing flux are slightly lower that the values of κ expected when $\hat{c}_H \approx 1$ ($\kappa = 0.66$ for $q = 2$ and $\kappa = 0.5$ for $q = 1$) because of the decrease of $\hat{c}_H$ during outgassing, which induces smaller values for κ (fig. 4.4).

In Andrew's model [143], hydrogen outgassing is modeled as being a surface process described by an first-order reaction equation similar to the equation (4.15) considering $F(\hat{c}_H) \approx \xi_{dt} \frac{\hat{c}_H}{1-\hat{c}_H}$, and assuming that the kinetic of the surface process is of second-order ($q = 2$). Outgassing flux calculated with Andrew's model exhibits a power-law decay $\hat{\Gamma}_{out} \sim t^{-2/3}$, which is in agreement with the time dependency of $\hat{\Gamma}_{out}$ outlined in the previous paragraph when hydrogen outgassing is surface limited (fig. 4.5b). The equation (4.15) constituting the Andrew's model thus applies here to describe hydrogen outgassing when hydrogen diffusion in material is fast compared to surface processes ($\sigma > 1$) and when hydrogen diffusion is slow enough to allow equilibrium of trapping and detrapping (exp. 4.7). Andrew's model thus describe hydrogen outgassing when the following condition holds

$$K_r \xi_{dt} \Delta < D < \Delta^2 (\nu_{tr} + \nu_{dt}) \tag{4.18}$$

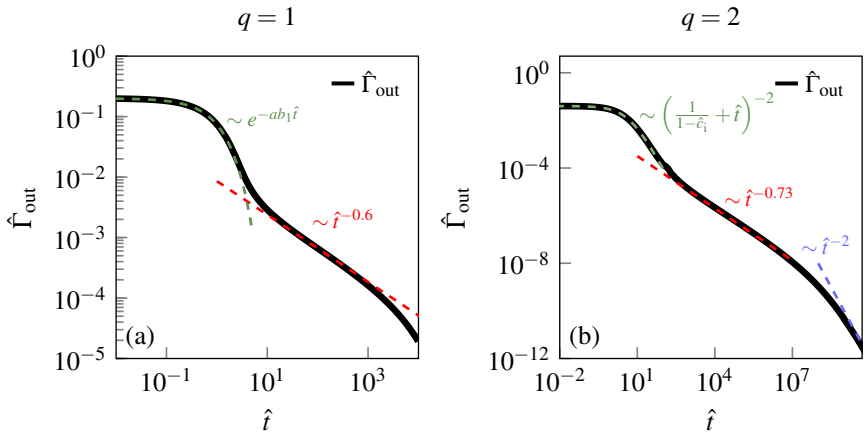

Figure 4.5: Normalized outgassing flux $\hat{\Gamma}_{out} = \frac{\Gamma_{out}}{K_q}$ as a function of $\hat{t}$ calculated with $\nu = 10^{-4}$ and $\hat{c}_i = 1.2$ in surface-limited regime ($\sigma > 1$) for $q = 1$ (a) and $q = 2$ (b).

Regarding the proximity of the values of power-law exponents in figures 4.5a and 4.5b corresponding to $q = 1$ and $q = 2$ (respectively $\kappa = 0.6$ and $\kappa = 0.73$,), one should not exclude that hydrogen outgassing flux exhibiting a power-law decay close to $\sim t^{-2/3}$ may be also caused by surface processes which do not induce second-order kinetic desorption ($q \neq 2$).

4.3.2 Diffusion-limited hydrogen outgassing

In diffusion-limited regime ($\sigma < 1$), the retention region can be treated as an semi infinite space ($\Delta \to +\infty$) when hydrogen outgassing occurs in time inferior to the characteristic time of diffusion $t < \tau_D = \Delta^2/\hat{D}_{eff}(\hat{c}_i)$. When hydrogen outgassing is diffusion-limited, surface effects are negligible and hydrogen concentration at the front material surface is thus low ($\hat{c}_H(x = 0, t) \ll \hat{c}_i$). The evolution of the total hydrogen concentration in the material can be thus described by $\frac{\partial \hat{c}_i \delta(t)}{\partial t} \approx 2D\frac{F(\hat{c}_i)}{\delta(t)}$, where $\delta(t)$ is the characteristic depth of hydrogen concentration profile. The evolutions of $\delta(t)$ and $\hat{\Gamma}_{out}$ therefore follow the classical time dependencies expected for a diffusion-limited process $\left(\delta(t) \sim t^{1/2}\right.$ and $\left.\hat{\Gamma}_{out} \sim t^{-1/2}\right)$. Numerical solutions of the diffusion equation (4.9) obtained for $\sigma = 0.01 < 1$ show indeed that δ and $\hat{\Gamma}_{out}$ always evolve following $t^{1/2}$ and $t^{-1/2}$ after depletion of hydrogen retained in near-surface region, independently of the initial concentration $\hat{c}_i$ (fig. 4.6) and of the value of q.

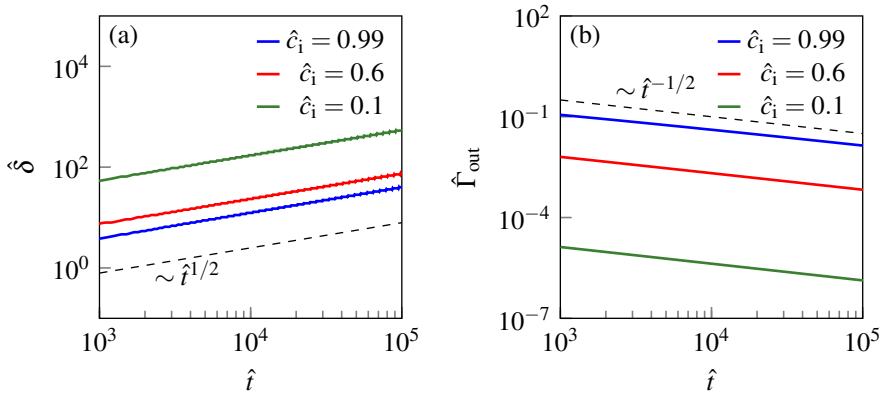

Figure 4.6: Characteristic depth $\hat{\delta}$ of hydrogen concentration profile in material (a) and normalized outgassing flux $\hat{\Gamma}_{out}$ (b) as a function of $\hat{t}$ calculated with $\nu = 10^{-4}$ and $q = 2$ in diffusion-limited regime ($\sigma < 1$) with different initial hydrogen concentrations $\hat{c}_i$.

4.4 Hydrogen desorption from material surface vs hydrogen desorption from material bulk

In Grisolia's work [29], hydrogen outgassing from graphite wall was modeled using the R-D model formed by equations 4.1a, 4.1b and 4.6 assuming no hydrogen loss at the rear surface of the PFC $\left(\left(D\frac{\partial \hat{c}_H}{\partial x}\right)_{x=L} = 0\right)$ and second-order surface process ($q = 2$). Two experimental frameworks corresponding to hydrogen outgassing from PFC material during helium glow discharges (HeGD) and hydrogen outgassing from PFC material after plasma discharges (PD) were considered.

Using parameters of hydrogen diffusion, retention and desorption reported in table 4.1, experimental observations showing that $\hat{\Gamma}_{out} \sim t^{-0.5}$ for long time during HeGD and that $\hat{\Gamma}_{out} \sim t^{-0.73}$ for long time after PD were reproduced with the R-D model in [29]. In this model, trapping and detrapping processes are in equilibrium $\left(\frac{D}{\Delta^2} \ll \nu_{dt} + \nu_{tr}\right)$, considering retention parameters reported in table 4.1. The R-D model describing hydrogen outgassing formed by equations 4.1 with boundary conditions 4.6 is thus equivalent to equations (4.9) and (4.10), and results derived in the section 4.3 apply.

As noticed by Grisolia in [29], detrapping induced by He atoms diffusing in the material is negligible compared to thermal detrapping. The difference observed in the power-law exponents ($\sim t^{-0.5}$ during HeGD and $\sim t^{-0.7}$ after PD) are thus only caused by the differences between initial hydrogen concentration profile in PFC material. The initial concentration profile considered for HeGD in [29] is constant in the PFC ($\Delta > 100\,\text{nm}$) with $\hat{c}_i = 1.04$, leading to $\sigma = \frac{DF'(\hat{c}_i)}{K_r F(\hat{c}_i)^2 \Delta} = 0.2 < 1$ during HeGD. Hydrogen outgassing is thus diffusion-limited during HeGD and $\hat{\Gamma}_{out} \sim t^{-1/2}$, in agreement with the results

Table 4.1: Parameters used in [29] to model hydrogen outgassing from graphite PFC.

D	K_r	ν_dt	ν_tr	ν	Δ
$7.5\times10^{-19}\,\mathrm{m^2 s^{-1}}$	$2\times10^{-8}\,\mathrm{m s^{-1}}$	$5\times10^{-2}\,\mathrm{s^{-1}}$	$100\,\mathrm{s^{-1}}$	5×10^{-4}	$>10^{-7}\,\mathrm{m}$

of the section 4.3.2.

Profiles of hydrogen concentration after PD and before the outgassing phase were predicted in [29] and show that trapped and free hydrogen are concentrated in a near-surface region ($\Delta\approx10^{-8}\,\mathrm{m}$) with $\hat{c}_\mathrm{H}\gtrsim1$ such that $\sigma\approx\frac{D\mathrm{F}'(\hat{c}_\mathrm{H})}{K_r\mathrm{F}(\hat{c}_\mathrm{H})^2\Delta}\approx5>1$. The outgassing of hydrogen retained in the sub-surface region ($\Delta\approx10^{-8}\,\mathrm{m}$) is thus surface-limited.

However, a background concentration profile of retained hydrogen increasing from $\hat{c}_\mathrm{t}=0.65$ at the surface to $\hat{c}_\mathrm{t}=1$ beyond $x=10^{-7}\,\mathrm{m}$ was also predicted in [29] and may affect outgassing flux and modify observed power-law exponents. Effects of retained hydrogen background concentration profiles on hydrogen outgassing is illustrated in figure 4.7, where evolutions of the hydrogen outgassing flux were calculated using equations (4.9) with different initial hydrogen concentration profiles. The hydrogen background profile calculated in [29] is shown in figure 4.7c and leads to a time dependency $\sim t^{-0.70}$. This power-law dependency is observed later ($t\sim10^3\,\mathrm{s}$) than in Grisolia's work ($t\sim10\,\mathrm{s}$) because of a volumetric recombination term introduced in equation (4.1a) in [29]. Nevertheless, power-law dependencies experimentally observed between plasma discharges occur at similar time $t\sim10^3\,\mathrm{s}$ [142].

When hydrogen background concentration is higher (fig. 4.7d), $\hat{\Gamma}_\mathrm{out}$ tends to follow a diffusion-limited power-law decay ($\hat{\Gamma}_\mathrm{out}\sim t^{-1/2}$). Without hydrogen background profile (fig. 4.7a), the power-law exponent becomes larger ($\sim t^{-0.84}$) due the faster reduction of hydrogen concentration near surface (κ increases when $\hat{c}_\mathrm{H}$ decreases as indicated by the figure 4.4). Similarly, the power-law exponent remains larger when no hydrogen diffusion is permitted beyond $\Delta=10^{-8}\,\mathrm{m}$ (fig. 4.5b). The power-law exponents may thus vary between 0.5 and 0.9 as a function of the hydrogen background, which can slow down the decrease of hydrogren concentration near the surface.

The fast decay of the calculated outgassing flux observed at short time ($\sim t^{-2}$) in figure 4.5a is due to the release of the excess of free hydrogen near the surface, and has been experimentally observed in graphite [142, 29].

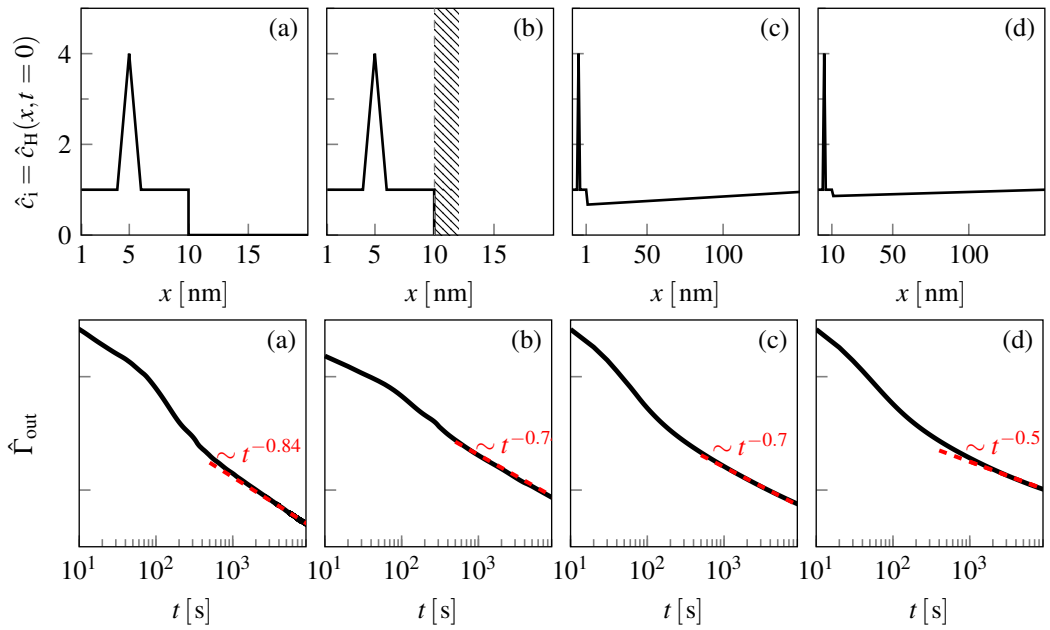

Figure 4.7: Outgassing flux calculated with equations (4.9) and (4.10) for different initial concentrations of hydrogen. The profile (c) is the one corresponding to retained hydrogen profile in ToreSupra PFC after PD calculated in [29]. Hydrogen diffusion in material is limited to $\Delta = 10^{-8}$ m for the profile (b).

4.5 Summary

When the diffusion of hydrogen in wall is slow enough to allow equilibrium between trapping and detrapping processes, and fast enough to not limit outgassing of hydrogen from material (surface-limited regime), the outgassing model taking into account the diffusion of hydrogen in wall proposed by Grisolia et al. in [29] is equivalent to the model of hydrogen outgassing from wall surfaces proposed by Andrew et al. [143]. In surface-limited regime, these two models can predict a power-law decrease of the outgassing flux with an exponent $\kappa \approx 0.7$ in agreement with experimental observations in Tore Supra and JET.

Such power-law decays of outgassing flux may also exist with a kinetic order of surface processes different from 2 (for example, when $q = 1$, power-law exponents are about $\kappa \approx 0.6$, close to experimental values of 0.7). This result suggests that complex surface processes with $q \neq 2$ may also induce power-law decay. In addition, hydrogen retained deeper in material may also affect power-law exponents and further investigations are thus required to model such effects. Additional information on outgassing regime and surface processes may be provided by investigating long-term hydrogen outgassing at higher temperature.

Chapter 4, in full, is a reprint of the material as it appears in J. Guterl, R.D. Smirnov, S.I. Krasheninnikov, Long-Term Hydrogen Outgassing from Plasma Facing Components in *Contributions to Plasma Physics* 54 (4-6), 415-420 (2013). The dissertation author was the primary investigator and author

of this paper.

Chapter 5

Atomic modeling of hydrogen desorption from tungsten surface

5.1 Motivation and outline

Large time and space scales relevant for hydrogen retention in PFC of fusion reactors impose to model hydrogen retention in PFC using the reaction-diffusion equations (1.9). The boundary conditions of these R-D equations are determined by surface processes modeled by the equations (1.10), which rely on the energy diagram reported in figure 1.11 in the introduction. Hydrogen desorption from tungsten surface is usually described as a two-steps process where hydrogen molecules are first formed by recombination of two adsorbed hydrogen atoms on surface before desorbing. The flux Γ_{out} of hydrogen desorbing from tungsten surface (and thus outgassed from material) is then described as corresponding to a second-order kinetic process (5.1), where c_{s} is the concentration of adsorbed hydrogen on surface and K_{r} is the desorption rate.

$$\Gamma_{\text{out}} = \underbrace{K_{\text{r},0}\, e^{-\frac{E_{\text{r}}}{T}}}_{K_{\text{r}}}\, [c_{\text{s}}]^2 \tag{5.1}$$

However, experimental data show large discrepancies in estimations of $K_{\text{r},0}$ and E_{r} and contradictory temperature dependencies for K_{r} [32]. In addition, several binding states for adsorbed hydrogen on tungsten surface were observed in thermodesorption experiments, and the kinetic order of the desorption

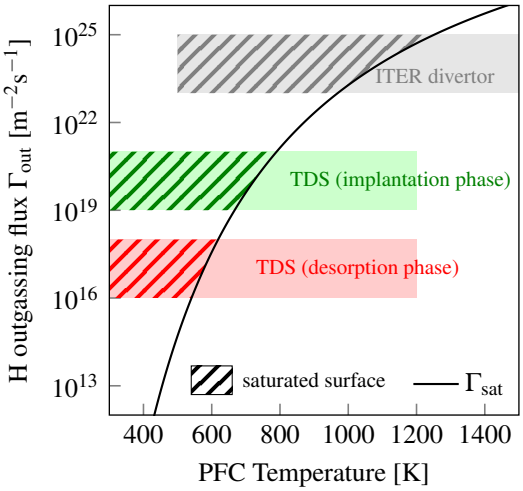

Figure 5.1: Maximum hydrogen outgassing flux from non-saturated tungsten surface as a function of the PFC temperature (black), calculated with $\theta = 1/2$ and with desorption parameters for non-saturated surface reported in [145]. Hydrogen outgassing regimes for TDS experiments and divertor in ITER are indicated assuming full recycling of particles hitting PFC or implanted in PFC.

process q may be different from two [112, 145]. The desorption parameters E_r and $K_{r,0}$ also significantly vary when the hydrogen surface coverage $\theta = c_s\lambda_0^2$ exceeds 0.5 [64] (λ_0 is the lattice cell size of tungsten. See table 2.1 in chapter 2).

These experimental results suggest that hydrogen desorption processes might be not well described by the expression (5.1). These surface processes may however play an important role in hydrogen outgassing when hydrogen coverage of tungsten surface is high, which is expected for long term exposure of tungsten components to high flux of hydrogen (e.g. in ITER or in TDS experiments, see fig. 5.1). Accurate modeling of hydrogen desorption mechanisms is thus required to predict hydrogen retention in tungsten exposed to high doses of hydrogen. Analyzing hydrogen desorption from tungsten surface using macroscopic models with reaction-diffusion equations is difficult, as indicated by the large discrepancies in experimental estimations of surface processes parameters E_r, $K_{r,0}$ and q. Atomic processes governing hydrogen desorption from tungsten surface are thus investigated here using molecular dynamics simulations (MD) and accelerated molecular dynamics simulations (AMD) [40].

MD simulations were performed using a W-H Tersoff interatomic potential proposed in [146] and revisited in [147]. Due to high computational costs induced by Tersoff interatomic potentials, only temperature accelerated dynamics (TAD) was used as AMD method [148, 149]. Hydrogen desorption is considered here to occur from clean and flat tungsten $\langle 100 \rangle$ and $\langle 110 \rangle$ surfaces. In the first section, hydrogen adsorption sites on $\langle 100 \rangle$ tungsten surfaces are characterized and TAD is used to analyze

hydrogen diffusion on surface. Hydrogen desorption from tungsten surfaces is then investigated at high temperature and analysis of interatomic potential parameters affecting desorption is provided. In the last section, we examine diffusion of hydrogen on tungsten surfaces at high coverage and low temperature, for which hydrogen clustering is observed on tungsten surfaces. Hydrogen clustering is modeled and its effects on desorption are discussed.

5.2 Hydrogen adsorption states and diffusion paths on tungsten surfaces

In MD and AMD simulations, tungsten surfaces were normal to the z-direction and the simulation box was periodic in the x and y directions. Upper surfaces at $z = 0$ were kept as free surface, while the four last layers forming the opposite surface were frozen. The time step in MD simulations was set to 0.1 fs. Hydrogen adsorption sites on tungsten surface were analyzed by sampling the potential energy of interaction $U_{\text{H-W}} < 0$ between a single hydrogen atom and tungsten surface at $z = z_0$. One hydrogen atom was slowly moved toward W surface in the z-direction for several x and y positions (fig. 5.2). Tungsten surface was maintained at temperature lower than 0.1 K by an external viscous force. The map of the binding energy $E_{\text{H-W}}(x,y) = \max_{z_0<z<+\infty}(-U_{\text{H-W}})$ of hydrogen adsorbed on $\langle 100\rangle$ W surface shows several adsorption sites with different adsorption energy $E_{\text{ads}} = E_{\text{H-W}}$ (fig. 5.2): the bridge site (B) ($E_{\text{ads}} = 2.39\,\text{eV}$), the three-fold hollow site (T) ($E_{\text{ads}} = 2.35\,\text{eV}$), the orthohedral site (O) ($E_{\text{ads}} = 2.4\,\text{eV}$) and several narrow sites (D) ($E_{\text{ads}} = 1.9\,\text{eV}$). Similar adsorption sites are also present on $\langle 110\rangle$ tungsten surface (fig. 5.2).

E_{ads} for (B) sites on $\langle 100\rangle$ surface is close to E_{ads} found with LEPS potential (2.40 eV) [150], and in relatively good agreement with experimental values of the activation energy $E_{\text{des,H}}$ of hydrogen desorption as single atom from polycrystalline tungsten ($E_{\text{des,H}} \approx 2.91\,\text{eV}$ [52]). Moreover, dissociation of H_2 molecules have been experimentally observed on tungsten surface in bridge sites [52], and is known to be exothermic, which is satisfied by adsorption energies found on $\langle 100\rangle$ surface $\left(E_{\text{ads}} < \frac{E_{\text{H}_2}}{2} \approx 2.26\,\text{eV}\right)$.

Activation energies of hydrogen transition (migration) between adsorption sites are needed to characterize hydrogen diffusion on tungsten surface. But these activation energies cannot be determined with the map of the binding energy $E_{\text{H-W}}$ in figure 5.2 because free hydrogen motion in x and y directions is necessary to characterize transition paths between adsorption sites. TAD simulations with one hydrogen atom on tungsten surface were then used to analyze hydrogen transitions between adsorption sites, and to estimate activation energy of these transitions with the nudged elastic band (NEB) method [151]. Using

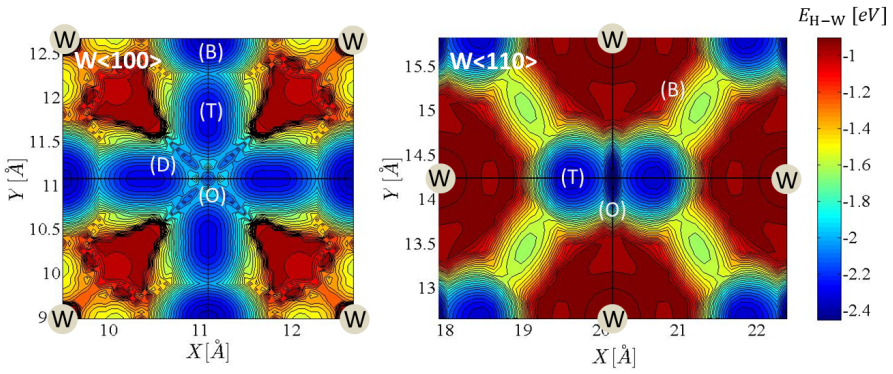

Figure 5.2: Hydrogen binding energy $E_{\text{H-W}}(x,y)$ on $\langle 100 \rangle$ and $\langle 110 \rangle$ tungsten surfaces. Several adsorption sites can be identified (B,T,O,D). Beige circles represent tungsten surface atoms at rest.

low temperature equal to 500 K and high temperature equal to 1200 K, TAD simulations were performed on $\langle 100 \rangle$ surface, revealing one additional adsorption site (T2) with $E_{\text{ads}} \approx 2.15$ eV , in addition to other adsorption sites previously found (fig. 5.3).

Activation energies of hydrogen transition between adsorption sites estimated with NEB method are plotted in figure 5.3. The transition $\text{(T)} \rightarrow \text{(B)}$ has the highest activation energy ($E_{\text{(T)}\rightarrow\text{(B)}} \approx 0.55$ eV), whereas the reciprocal transition shows $E_{\text{(B)}\rightarrow\text{(T)}} \approx 0.35$ eV . Activation energies for other transitions do not exceed 0.35 eV and are weak for $\text{(D)} \rightarrow \text{(T2)}$ ($E_{\text{(D)}\rightarrow\text{(T2)}} < 0.1$ eV). Transitions between adsorption sites occur only between spatially adjacent states, and hydrogen atoms can thus only migrate from one lattice cell to an adjacent one through (B) sites. It suggests that the diffusion of hydrogen on $\langle 100 \rangle$ surface is limited by hydrogen migration from (T) to (B) sites, and that the activation energy for diffusion E_{D} is determined by $E_{\text{D}} = E_{\text{(T)}\rightarrow\text{(B)}} \approx 0.55 eV$.

However, transition barriers between adsorption sites other than (B) sites are lower than barriers for transitions toward (B) sites. Hydrogen atoms therefore mostly explore the adsorption sites (T), (T2) ,(O) and (D) before exploring the (B) site. Since transition barriers toward (D) sites are low, hydrogen easily migrates from (T) to (D), which tends to complicate effective adsorption potential structure in lattice cells, and eventually affect hydrogen migration between lattice cells. The quantitative estimation of the residency time of hydrogen atom in each adsorption site during TAD simulations is plotted in figure 5.4 and shows that hydrogen atoms mostly occupy the sites (T), (T2) and (D) $\left(t_{\text{residency}}^{\text{(T),(T2),(D)}} \sim 10^{-7}\,\text{s}\right)$, and rarely visits the site (B) $\left(t_{\text{residency}}^{\text{(B)}} \sim 10^{-9}\,\text{s}\right)$.

These observations suggest that the diffusion of hydrogen atoms on $\langle 100 \rangle$ tungsten surface might be more complex than diffusion modeled as single hops of hydrogen from one lattice cell to

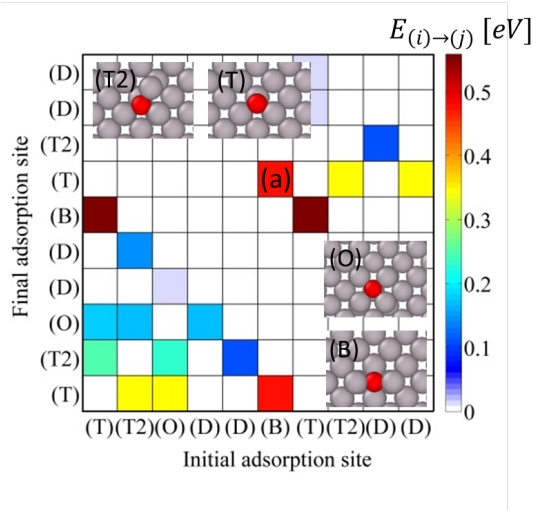

Figure 5.3: Activation energy $E_{(\mathrm{i})\to(\mathrm{j})}$ of transition between adsorption states (i) and (j) on $\langle 100\rangle$ tungsten surface estimated with NEB method. E.g. transition (a) corresponds to the transition $E_{(\mathrm{B})\to(\mathrm{T})}$ with $E_{(\mathrm{B})\to(\mathrm{T})} = 0.48\,\mathrm{eV}$.

another one. In particular, the dependency of hydrogen diffusion coefficient on temperature may be more complex than predicted by an Arrhenius law with pre-exponential factor and activation energy independent of the temperature. Statistical estimations of the diffusion coefficient of hydrogen on $\langle 100\rangle$ surface $\left(D = \lim_{t\to+\infty} \frac{\langle r^2\rangle}{2t}\right)$ performed with MD simulations in the range of temperature $1000\,\mathrm{K} < T < 1500\,\mathrm{K}$ show that E_D strongly depends on temperature.

Experimental measurements of hydrogen diffusion coefficient on $\langle 100\rangle$ tungsten surface for $T > 220\,\mathrm{K}$ indicate that $E_\mathrm{D} \approx 0.30\,\mathrm{eV}$ [152]. This experimental value of E_D is in reasonable agreement with transition barriers found for (B) and (T) sites $\left(E_{\mathrm{site}\to(\mathrm{T})} \approx 0.35\,\mathrm{eV}, E_{(\mathrm{T})\to(\mathrm{B})} \approx 0.55\,\mathrm{eV}\right)$, and is lower than $E_{(\mathrm{T})\to(\mathrm{B})}$, which is expected if hydrogen diffusion is not limited by the transition $(\mathrm{T})\to(\mathrm{B})$. No further quantitative analysis of adsorption sites and diffusion process can however be reasonably performed without better validation of the W-H interatomic potential. For instance, the existence of the (D) sites is questionable regarding their narrowness, and may be due to cut-off effects in the interatomic potential. Despite uncertainties in the interatomic potential, the relative good agreement between adsorption energies found in MD simulations and adsorption energies measured in experiments suggests that the W-H interatomic potential given in [146, 147] and used in MD simulation may still well describe main features of hydrogen adsorption on W surfaces, in particular effects of multiple neighboring adsorption sites on hydrogen diffusion.

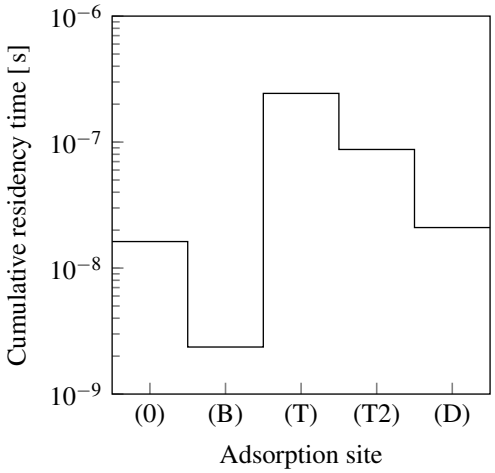

Figure 5.4: Cumulative residency time of hydrogen in the different adsorption sites of $\langle 100 \rangle$ tungsten surface calculated in TAD simulations.

5.3 Hydrogen molecular desorption from tungsten surfaces

The desorption of molecular hydrogen from tungsten surface is the result of the recombination of hydrogen atoms into H_2 molecules on tungsten surface followed by the desorption of H_2 molecules from tungsten surface. Experimental observations of H_2 dissociation on tungsten surface suggest that hydrogen recombination into H_2 is the process governing hydrogen molecular desorption [52]. In this section, we analyze hydrogen recombination and desorption on tungsten surface by performing MD simulations at high temperature ($T > 2000\,\mathrm{K}$) on $\langle 100 \rangle$ surfaces. High temperatures in MD simulations are required due to the large activation energy $E_\mathrm{r} \approx 1.4 - 1.6\,\mathrm{eV}$ experimentally measured for hydrogen molecular desorption [112, 145], which leads to a low frequency of desorption events $f_\mathrm{des} \approx 10^{13} e^{-\frac{E_\mathrm{r}}{T}}\,\mathrm{s}^{-1}$. TAD simulations cannot be used to investigate hydrogen recombination because of the dramatic decrease of TAD efficiency with more than one hydrogen atom on tungsten surface.

High hydrogen surface coverage is required to induce a large desorption rate. Therefore, hydrogen atoms were injected during MD simulations at the constant volumetric rate $S_\mathrm{H} = 10^{-3}\,\mathrm{atoms.\mathring{A}^{-3}.ps^{-1}}$ into bottom layers of tungsten samples to balance hydrogen atoms lost by desorption, and thus maintain high hydrogen surface coverage $\theta > 0.1$. Results of MD simulations at $T = 2500\,\mathrm{K}$ performed with the W-H interatomic potential given in [146] and [147] show that no molecular desorption occurs during 5 ns simulations, which is unexpected since $f_\mathrm{des}(T = 2500\,\mathrm{K}) \approx 100\,\mathrm{ps}$, leading to the saturation of tungsten sample with hydrogen. Similar observations were made for $\langle 110 \rangle$ surfaces.

To determine why no hydrogen molecular desorption occurs at high temperature during long MD

simulations, we forced recombination of hydrogen atoms on a frozen $\langle 100 \rangle$ tungsten surface by moving the two hydrogen atoms toward each other along the same axis in the plan of the surface layer ($z = 0$) as sketched in the figure 5.5a. The potential energy of this W-H-H system is plotted as a function of the distance between the two hydrogen atoms in the figure 5.5, showing a large and sharp energy barrier $\sim 7\,\mathrm{eV}$ for hydrogen recombination when hydrogen distance is about 1.6Å. To examine the origin of this barrier, all three-body interactions (TBI) involving hydrogen in the W-H Tersoff potential were turned off by setting their amplitude γ to zero, leading to the disappearance of the large energy barrier (fig. 5.5). Among TBI involving hydrogen, the magnitude of H-H-H and H-W-H interactions reported in [146] and [147] ($\gamma = 12.33$) is much larger than the magnitude of other TBI ($\gamma < 0.1$). Since H-H-H interactions is not relevant for the recombination of two hydrogen, only the amplitude $\gamma_{\text{H-W-H}}$ of the H-W-H interactions was tuned. The sharp recombination barrier diminishes as $\gamma_{\text{H-W-H}}$ decreases (fig. 5.5), suggesting that the activation energy E_r of hydrogen recombination into H_2 strongly depends on $\gamma_{\text{H-W-H}}$.

Estimating E_r as a function of $\gamma_{\text{H-W-H}}$ for realistic recombination process is difficult due to numerous paths available for recombination of two hydrogen on tungsten surface. MD simulations were then performed at $T = 2500\,\mathrm{K}$ using the setup described above to estimate the rate of molecular desorption as a function of $\gamma_{\text{H-W-H}}$. When $\gamma_{\text{H-W-H}}$ vanishes, the rate of molecular desorption decreases due to the binding of hydrogen molecules on surface, which should be rather weak since H_2 dissociates on tungsten surface. A non-zero H-W-H TBI is thus required to avoid strong binding of hydrogen molecules onto tungsten surface, and thus $\gamma_{\text{H-W-H}}$ cannot vanish. On the other hand, the desorption rate is very low when $\gamma_{\text{H-W-H}} > 1$ due to high values of $E_\mathrm{r} > 2\,\mathrm{eV}$. To estimate values of E_r corresponding to $0 < \gamma_{\text{H-W-H}} < 1$, MD simulations were performed at several temperature ($2300\,\mathrm{K} < T < 2800\,\mathrm{K}$) for several values of $\gamma_{\text{H-W-H}}$. Arrhenius plots giving estimations of E_r was obtained for each value of $\gamma_{\text{H-W-H}}$, showing that $E_\mathrm{r} \approx 1.5\,\mathrm{eV}$ when $\gamma_{\text{H-W-H}} = 0.55$, in good agreement with experimental values of $E_\mathrm{r} \approx 1.4 - 1.6\,\mathrm{eV}$ [112, 145]. The value of $\gamma_{\text{H-W-H}} = 0.55$ reported above does not take into account effects of high hydrogen coverage in MD simulations, which may strongly affect molecular recombination [64].

We therefore conclude that the W-H interatomic potential proposed in [146] and revisited in [147] does not qualitatively describe hydrogen recombination into H_2 on tungsten surface. The parameterization of the H-W-H TBI given in [146, 147] does not well model short range hydrogen-hydrogen interactions in tungsten environment, which are essential in the recombination of hydrogen atoms into molecules on tungsten surface. The amplitude $\gamma_{\text{H-W-H}}$ of these TBI should be adjust to $\gamma_{\text{H-W-H}} \sim 0.55$ in the W-H interatomic potential to simulate processes involving molecular recombination or short range hydrogen-

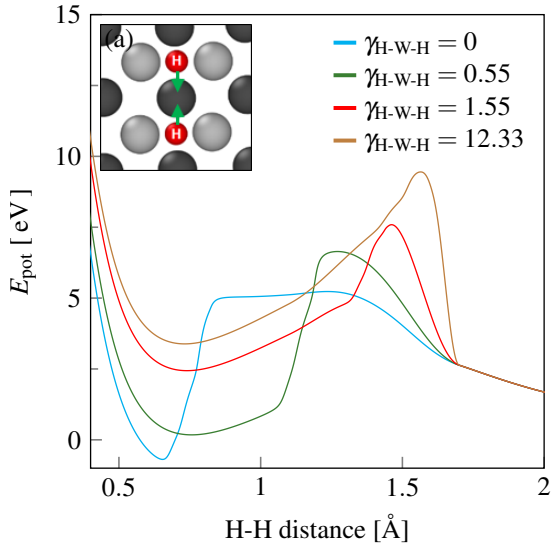

Figure 5.5: Potential energy E_{pot} as a function of the distance between hydrogen atoms when hydrogen atoms (red) are moving toward each other in the plan $z = 0$ of a frozen $\langle 100 \rangle$ tungsten surface (grey and black atoms in picture (a)) . E_{pot} is calculated for different magnitudes $\gamma_{\text{H-W-H}}$ of the three body interaction H-W-H in the Tersoff W-H interatomic potential given in [146]. The red curve corresponds to $\gamma_{\text{H-W-H}} = 12.33$, which is the original value given in [146].

hydrogen interactions in MD simulations.

5.4 Hydrogen clustering on tungsten surface

In this section, we investigate effects of high hydrogen surface coverage on hydrogen recombination process, neglected for the sake of simplicity in the previous section, but which may be important as suggested by experimental data [64]. To explore collective effects of hydrogen clustering on hydrogen desorption, MD simulations were performed with hydrogen atoms deposited on $\langle 110 \rangle$ and $\langle 100 \rangle$ tungsten surfaces with a coverage $\theta \sim 0.1$ during 10 ns at $T = 1500$ K, such that hydrogen atoms remain on tungsten surface. Indeed, characteristic times of absorption of adsorbed atom from surface into bulk and of molecular hydrogen desorption are larger than 10 ns when $T \leq 1500$ K. MD simulations show that hydrogen atoms form stable elongated surface clusters after ~ 10 ps on $\langle 100 \rangle$ and $\langle 110 \rangle$ surfaces (fig. 5.6). Because interatomic distances between hydrogen atoms forming clusters are larger than 1.5Å, hydrogen-hydrogen interactions in clusters are weak (< 0.05 eV) and hydrogen clustering does not depend on $\gamma_{\text{H-W-H}}$.

Introducing the average binding energy $\overline{E_{\text{kH-W}}} = \frac{E_{\text{kH-W}}}{k}$, where $E_{\text{kH-W}}$ is the binding energy of a k-atoms cluster to tungsten surface ($E_{\text{kH-W}} > 0$), MD simulations show that $\overline{E_{\text{kH-W}}} \approx 3.1$ eV for large clusters ($k > 3$) and $\overline{E_{\text{kH-W}}} < 0.1$ eV for small clusters ($k \leq 3$). Moreover, $E_{\text{kH-W}}$ weakly depends on the

cluster size for large clusters. According to results in section 5.2, $E_{\text{ads}} \approx 2.4\,\text{eV}$, and thus the binding energy of hydrogen atom to tungsten surface in large clusters increases of $\Delta E_{\text{H-W}} = \overline{E_{\text{kH-W}}} - E_{\text{ads}} \approx 0.7\,\text{eV}$. This increase is due to the trapping of hydrogen atoms into sub-surface sites, which can be reached by hydrogen atoms nearby other hydrogen, which induce slight reorganization of tungsten surface lattices (fig. 5.6b). Sub-surface trapping sites induce stronger binding of hydrogen atoms to tungsten surface due to the presence of rows of tungsten atoms above hydrogen atoms. However, such reorganization only occurs when $k > 3$, justifying that $\Delta E_{\text{H-W}} \approx 0$ for small clusters ($k \leq 3$).

The effects of hydrogen clustering on hydrogen desorption cannot be observed during MD simulations due to the low simulation temperature $T = 1500\,\text{K}$, which implies that $f_{\text{des}} \approx 10^{-7}\,\text{s}^{-1}$. Nevertheless, we can speculate that hydrogen clustering may affect hydrogen desorption by:

- increasing the residency time of hydrogen in the vicinity of other hydrogen atoms
- reducing the amount of isolated hydrogen atoms which can recombine in small clusters (two or three atoms)
- affecting the recombination path for two adjacent hydrogen atoms in clusters.

The formation and the dissolution of k-atoms clusters on tungsten surface can be modeled as trapping/de-trapping processes defined by:

- the trapping rate $\tilde{K}_{\text{tr}}(k) = \tilde{K}_{\text{tr},0}\, f_c(k)\, e^{-\tilde{E}_{\text{tr}}(k)/T}$
- the detrapping rate $\tilde{K}_{\text{dt}}(k) = \tilde{K}_{\text{dt},0}\, f_c(k)\, e^{-\tilde{E}_{\text{dt}}(k)/T}$
- the desorption rate $\tilde{K}_{\text{r}}(k) = \tilde{K}_{\text{r},0}\, f_c(k)\, e^{-}\tilde{E}_{\text{r}}(k)/T$ where $f_c(k) \sim k$ (elongated cluster).

Since $\Delta E_{\text{H-W}}$ weakly varies with the size of large clusters, we can assume for large clusters that $\tilde{E}_{\text{r}}(k) \approx E_{\text{r}} + \Delta\tilde{E}_{\text{r}}(k)$ and $\tilde{E}_{\text{dt}}(k) \approx E_{\text{D}} + \Delta\tilde{E}_{\text{dt}}(k)$, where E_{D} is the activation energy of diffusion of isolated hydrogen on tungsten surface and E_{r} is the activation energy of recombination and desorption of two isolated hydrogen atoms into H_2 (see energy diagram in figure 1.11). $\Delta\tilde{E}_{\text{r}} = 0\,\text{eV}$ by definition for clusters of two atoms and we assume that $\Delta\tilde{E}_{\text{r}} \approx 0\,\text{eV}$ for clusters of three atoms.

Using the NEB method, the binding energy $\Delta\tilde{E}_{\text{dt}}$ of hydrogen atom to cluster can be estimated to be $\Delta\tilde{E}_{\text{dt}}(k > 3) \leq \Delta E_{\text{H-W}} = 0.7\,\text{eV}$ for large clusters and $\Delta\tilde{E}_{\text{dt}}(k \leq 3) < 0.1\,\text{eV}$ for small clusters. Although effects of clustering on recombination are unclear ($\Delta\tilde{E}_{\text{r}}$ may be positive or negative), we can assume that $\tilde{K}_{\text{r}} \ll \tilde{K}_{\text{dt}}$ regarding experimental values of E_{r} ($E_{\text{r}} \approx 1.6\,\text{eV}$ [112, 145]). When the total surface concentration of hydrogen $c_{\text{s,tot}}$ is small enough to avoid cluster percolation $\left(L_c(k)\sqrt{c_{\text{s,tot}}} \ll 1\right.$ where

$L_c(k)$ is the characteristic size of k-atoms clusters$\big)$ and when the diffusion is fast compared to cluster dissolution ($c_{\mathrm{s,tot}}D \gg \tilde{K}_{\mathrm{dt}}$), cluster formation can be supposed to be limited by diffusion of hydrogen atoms ($E_{\mathrm{tr}}(k) \approx E_D$), assuming that there is no significant activation energy for trapping of hydrogen in clusters. Assuming that neither small nor large clusters diffuse on surface and recalling that $\tilde{K}_{\mathrm{r}} \gg \tilde{K}_{\mathrm{dt}}$, the equilibrium of cluster surface concentrations $c_{\mathrm{s}}(k)$ is determined by the balance between the formation and the dissolution of clusters on tungsten surface. Within these assumptions, the coexistence of large and small clusters is only possible in a very narrow range of temperature and hydrogen concentration. Hydrogen surface coverage is thus dominated either by small clusters $\big($small clusters regime where $c_{\mathrm{s}}(1,2,3) \gg c_{\mathrm{s}}(k>3)\big)$ or by large clusters $\big($large clusters regime where $c_{\mathrm{s}}(k_{\max}) \gg c_{\mathrm{s}}(k<k_{\max})\big)$. Cluster growth is limited by hydrogen desorption and thus $k_{\max}$ may vary during hydrogen outgassing.

The regime of surface coverage is determined by the nucleation process of small clusters. Large clusters dominate when the nucleation process of small clusters is fast $\left(P_{\mathrm{cluster}} = \frac{\tilde{K}_{\mathrm{tr}}(2,3)\theta}{\tilde{K}_{\mathrm{dt}}(2,3)} > 1\right)$. In contrast, small clusters dominate when the nucleation process is slow ($P_{\mathrm{cluster}} < 1$). Since $\Delta\tilde{E}_{\mathrm{dt}} < 0.1\,\mathrm{eV}$ for small clusters, $P_{\mathrm{cluster}} \approx C_0\theta$ with $C_0 \sim O(1)$. Formation of large clusters is thus expected to weakly depend on the surface temperature and to occur only at high coverage ($\theta > 0.1$).

To evaluate effects of clustering on hydrogen desorption, we introduce the ratio R_{des} defined as the rate of desorption from k-atoms clusters over the rate of desorption from small clusters (3-atoms clusters are neglected):

$$\begin{aligned} R_{\mathrm{des}} &= \left(\frac{\tilde{K}_{\mathrm{tr}}(k-1)\theta(k-1)\theta(1)\times\tilde{K}_{\mathrm{r}}(k)\theta(k)}{\tilde{K}_{\mathrm{dt}}(k)\theta(k)}\right) \Big/ \left(\frac{\tilde{K}_{\mathrm{tr}}(2)\theta(1)^2\times\tilde{K}_{\mathrm{r}}(2)\theta(2)}{\tilde{K}_{\mathrm{dt}}(2)\theta(2)}\right) \\ &\approx C_{R_{\mathrm{des}}} k \frac{\theta(k-1)}{\theta(1)} e^{-\frac{\Delta\tilde{E}_{\mathrm{r}}-\Delta\tilde{E}_{\mathrm{dt}}}{T}} \end{aligned} \tag{5.2}$$

where $C_{R_{\mathrm{des}}} \sim O(1)$ and $\theta(k) = c_{\mathrm{s}}(k)\lambda_0^2$. The time evolution of $\theta = c_{\mathrm{s}}\lambda_0^2 = \sum_{i=1}^{k_{\max}}\theta(i)$ is then described by the equation (5.3), where Γ_{out} is the desorption (outgassing) flux.

$$\frac{\partial\theta}{\partial t} = -\Gamma_{\mathrm{out}} \approx -2\tilde{K}_{\mathrm{r},0}e^{-\frac{E_{\mathrm{r}}}{T}}\theta(1)^2\left(1+\underbrace{C_{R_{\mathrm{des}}}k_{\max}\frac{\theta(k_{\max})}{\theta(1)}e^{-\frac{\Delta\tilde{E}_{\mathrm{r}}-\Delta\tilde{E}_{\mathrm{dt}}}{T}}}_{R_{\mathrm{des}}}\right) \tag{5.3}$$

In large cluster regime ($P_{\mathrm{cluster}} > 1$), $\theta \approx k_{\max}\theta(k_{\max})$ with $\theta(k_{\max}) \gg \theta(k<k_{\max})$ and we can show that $\theta(k_{\max}) \sim \theta(1)^m$ with $m \sim k_{\max}^{-1} \ll 1$. Consequently, if $R_{\mathrm{des}} \gg 1$, hydrogen desorption is

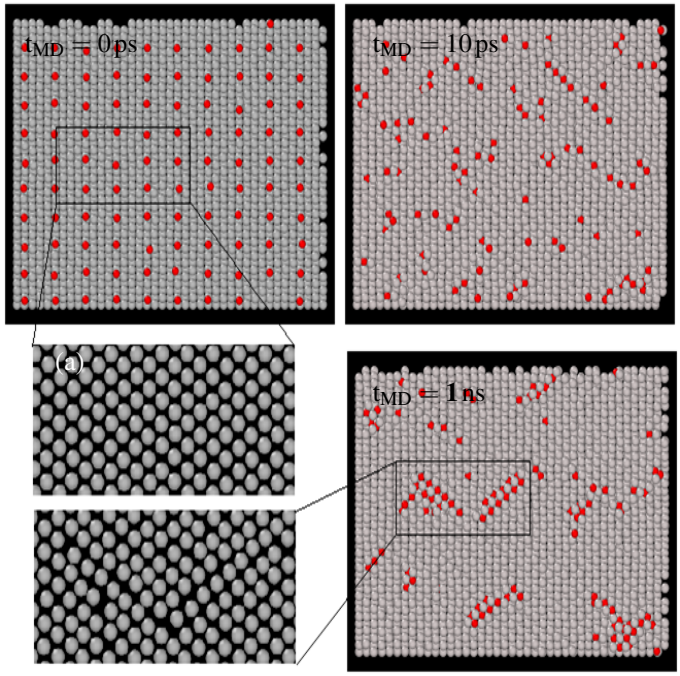

Figure 5.6: Top view of tungsten surface with hydrogen coverage $\theta = 0.1$ during MD simulations at $T = 1500\,\mathrm{K}$. Hydrogen atoms (red) form elongated clusters on tungsten surface (gray).

dominated by recombination occurring in large clusters and $\Gamma_{out} \sim \theta$. In this cluster-controlled desorption regime, the effective desorption energy is $\overline{E_r} = E_r + \Delta\tilde{E}_r - \Delta\tilde{E}_{dt}$. If $R_{des} \ll 1$, hydrogen desorption is dominated by hydrogen recombination occurring in small clusters and $\Gamma_{out} \sim \theta^2$ in small clusters regime.

Experimental measurements have shown that $\overline{E_r}$ sharply decreases from $1.6\,\mathrm{eV}$ to $1\,\mathrm{eV}$, and that the effective pre-exponential factor $\overline{K}_{r,0}$ diminishes of eight orders of magnitude when $\theta > 0.5$ [64]. Sudden variations of desorption parameters when hydrogen surface coverage increases might be qualitatively described with the cluster model introduced above, since the transition from the small clusters regime to the large clusters regime is sharp and occur at large coverage. In large clusters regime, desorption is cluster-controlled $\left(R_{des} \gg 1 \text{ due to } \frac{\theta(k_{max})}{\theta(1)} \gg 1\right)$. Assuming that large clusters are indeed formed in experiments at $\theta \approx 0.5$ and induce cluster-controlled desorption, it can be estimated that $\Delta\tilde{E}_r - \Delta\tilde{E}_{dt} \approx -0.6\,\mathrm{eV}$ and thus $\Delta\tilde{E}_r \approx 0.1\,\mathrm{eV}$. This latter value suggests that direct effects of clustering on recombination of hydrogen are weak. The sudden strong decrease of $\bar{K}_{tr,0}$ when the surface coverage increases above 0.5 may also be qualitatively explained within the cluster model considering that in cluster-controlled desorption regime, $\frac{\bar{K}_{tr,0}}{\bar{K}_{tr,0}} \sim \frac{\theta(1)}{\theta} \ll 1$.

5.5 Summary

Using MD simulations, several hydrogen adsorption sites were found on tungsten surface and main features of bridge sites and activation energies for migration of hydrogen through adsorption sites are in qualitative agreement with experimental observations. The existence of several adsorption sites may lead to complex diffusion process for hydrogen on tungsten surface. Hydrogen molecular desorption is not well described by the W-H Tersoff interatomic potential proposed in [146], and three-body interactions parameters of this potential, which describe effects of tungsten environment on hydrogen recombination, should be adjusted to qualitatively reproduce main features of hydrogen recombination into H_2. When tungsten surface coverage is high, hydrogen clustering is observed on surface and a kinetic model was proposed to qualitatively describe effects of clustering on molecular desorption. This model shows the existence of a large clusters regime, where surface coverage is dominated by large hydrogen clusters. In this regime, sudden variations of desorption parameters as a function of the hydrogen surface coverage, experimentally reported in [64], can be qualitatively described by the clustering model, suggesting that the kinetic of hydrogen desorption from tungsten surface may be not always second-order. Quantitative descriptions of adsorption, diffusion and clustering of hydrogen on tungsten surface however strongly depend on W-H interatomic potential. Therefore, a better assessment of W-H interatomic potential is required for studying W-H interactions on W surface, e.g. with DFT.

Chapter 5, in part, is a reprint of the material as it appears in J. Guterl, R.D. Smirnov, S.I. Krasheninnikov, B. Uberuaga, A.F. Voter, D. Perez, Modeling of hydrogen desorption from tungsten surface published in *Journal of Nuclear Materials*, 2014. The dissertation author was the primary investigator and author of this paper.

Conclusions

Plasma-material interactions may strongly influence plasma performance and life-time of future magnetic fusion devices. Retention and recycling of hydrogen isotopes in plasma-facing components may lead to dynamics plasma-material interactions and significant accumulation of tritium in material. Understanding the multifaceted physics of hydrogen retention in PFC is thus crucial, but remains challenging due to the wide spectrum of retention processes on PFC surface (erosion, co-deposition, etc.) and in PFC bulk (trap sites, bubbles, etc.) induced by long-time exposure of PFC to high flux of energy and particles.

In this context, we revisited in this work some aspects of the reaction-diffusion models used to describe hydrogen retention in metallic PFC as well as some aspects of the atomic modeling of hydrogen desorption from PFC surface, focusing on tungsten PFC which has been chosen as divertor material in ITER and in future fusion reactors (DEMO). We first focused on analysis of thermal desorption spectroscopy considering only one type of traps in material and neglecting surface effects. We showed that solute hydrogen concentration in retention region usually remains in equilibrium during TDS experiments. In this regime, analytic description of thermal desorption spectra indicates that trapping of solute hydrogen during TDS experiments cannot be ignored. Main features of thermal desorption spectra were then analytically described and a refined interpretation of Arrhenius plots was proposed. We also highlighted the use of tails and skewness of thermal desorption spectra to estimate activation energy of diffusion and to determine whether surface effects affect hydrogen release or not during TDS.

Hydrogen retention induced by large number of traps was addressed next. Modeling of TDS experiments with a large number of different traps was presented for the first time, and was illustrated with several experimental thermal desorption spectra, which were consistently reproduced using several traps with a fixed broad spectrum of detrapping energies. Values of detrapping energies were shown to be in agreement with values predicted by DFT models when several hydrogen atoms are trapped in one material vacancy.

Long-term outgassing of hydrogen from PFC during off-plasma events was then examined, focusing on the superdiffusive power-law decay in time of the hydrogen outgassing flux . Hydrogen outgassing was modeled with a revisited single trap model, showing the existence of different regimes of hydrogen outgassing as a function of the characteristics of processes governing hydrogen retention (surface conditions, material depth, trapping/detrapping rates). We identified two regimes of hydrogen outgassing, depending on whether the hydrogen release is surface-limited or diffusion-limited. We also analyzed the influence of the thickness of the material on the power-law exponents. Finally, our results reconciled different models proposed in the literature to describe power law decays of the outgassing flux experimentally observed.

Hydrogen desorption from tungsten surface was investigated in the last part using molecular dynamics simulations, motivated by the large discrepancy in experimental measurements of hydrogen desorption parameters from tungsten surface in fusion-related conditions. Using MD simulations, several hydrogen adsorptions sites were found on tungsten surface. Main features of bridge sites and activation energies for migration of hydrogen through adsorptions sites are in qualitative agreement with experimental observations. The existence of several adsorptions sites may lead to complex diffusion process for hydrogen on tungsten surface. MD simulations indicated that molecular hydrogen desorption is not well described by the W-H Tersoff interatomic potential proposed in the literature. Three-body interactions parameters of this potential, which describe effects of tungsten environment on hydrogen recombination, should be adjusted to qualitatively reproduce main features of molecular hydrogen recombination. When tungsten surface coverage is high, hydrogen clustering was observed on surface and a kinetic model was proposed to qualitatively describe effects of clustering on molecular desorption. This model shows the existence of a large clusters regime where surface coverage is dominated by large hydrogen clusters. In this regime, experimentally observed sudden variations of desorption characteristics as a function of the hydrogen surface coverage can be qualitatively described by the model, suggesting that the kinetic of hydrogen desorption from tungsten surface may be not always of second-order.

R-D models of hydrogen retention were examined in this work assuming that surface processes do not affect hydrogen retention and outgassing and that traps are immobile and do not recombine or mutate in the bulk of PFC material. These latter assumptions may however not always hold in fusion related conditions. For example, effects of surface processes might be expected when PFC are repetitively exposed to high flux of hydrogen as shown by the analysis of long-term hydrogen outgassing from PFC during off-plasma events. Including effects of these processes on hydrogen retention and outgassing thus requires

additional work to extend current R-D models and to characterize these processes. Atomic description of these processes may be thus necessary, as illustrated in this work with the modeling of hydrogen desorption from PFC surface with MD simulations. In this context, quantum modeling of hydrogen retention processes in tungsten is necessary because of existing limitations in interatomic potentials available to describe hydrogen tungsten interactions, especially on tungsten surface.

Appendices

A The Lambert function

The Lambert function ω is implicitly defined by $\omega(\zeta)e^{\omega(\zeta)} = \zeta$ for $\zeta \geq -e^{-1}$ (fig. 5.7). The first-order derivative of ω is

$$\frac{\partial \omega(\zeta)}{\partial \zeta} = \frac{\omega}{\zeta(1+\omega(\zeta))} \tag{5.4}$$

and the second-order derivative is

$$\frac{\partial^2 \omega(\zeta)}{\partial \zeta^2} = -\frac{\partial \omega(\zeta)}{\partial \zeta}\frac{\omega(\zeta)^2 + 2\omega(\zeta)}{\zeta(1+\omega(\zeta))^2} \tag{5.5}$$

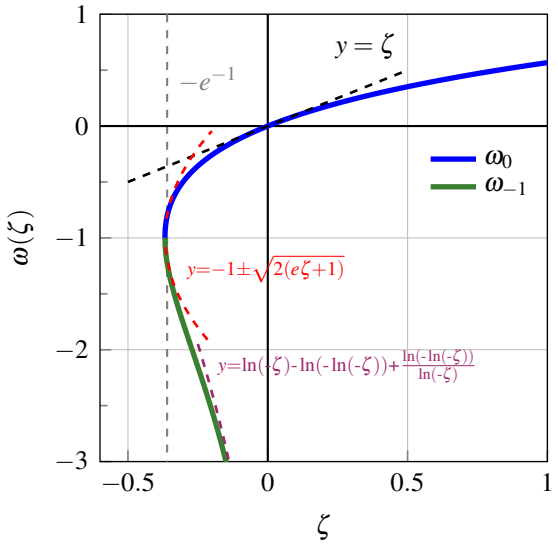

Figure 5.7: Graph of branches 0 and -1 of the Lambert function.

B Analytic solution of quasi-static reaction-diffusion equations

When free hydrogen concentration is in equilibrium $\left(\frac{\partial \bar{c}_\mathrm{f}}{\partial t} \approx 0\right)$, the equation (2.13a) reads $\frac{\partial \bar{c}_\mathrm{t}}{\partial T} = -\nu_\mathrm{D}\bar{c}_\mathrm{f}$. The combination of equations (2.13a) and (2.13b) thus gives

$$\frac{\partial \bar{c}_\mathrm{t}}{\partial T}\left[\frac{\nu_\mathrm{tr}+\nu_D}{\nu_\mathrm{tr}\bar{c}_\mathrm{t}} - 1\right] = -\nu_\mathrm{dt}\nu_D \tag{5.6}$$

Assuming that variations of $\frac{\nu_\mathrm{tr}}{\nu_D}$ with temperature are negligible, the differential equation (5.6) can be integrated to give

$$\left(1+\frac{\nu_D(T)}{\nu_\mathrm{tr}(T)}\right)\ln\left(\bar{c}_\mathrm{t}(T)/\hat{c}_0\right) - \left(\bar{c}_\mathrm{t}(T)-\hat{c}_0\right) = -\underbrace{\int_{T_0}^{T}\nu_\mathrm{dt}(T')\nu_D(T')\mathrm{d}T'}_{\Omega_\mathrm{eff}(T)} \tag{5.7}$$

A formal expression of $\bar{c}_\mathrm{t}$ can be deduced from equation (5.7) by introducing the Lambert function ω

$$\bar{c}_\mathrm{t}(T) = \Omega_0^{-1}(T)\,\omega\left(\Omega_0(T)e^{\Omega_0(T)-\Omega_\mathrm{eff}(T)}\right) \tag{5.8}$$

where $\Omega_0 = -\dfrac{\nu_\mathrm{tr}\hat{c}_0}{D/\Delta^2+\nu_\mathrm{tr}}$.

C Derivation of the expression of desorption temperature

T_des is defined by $\left.\frac{\partial \hat{\Gamma}_\mathrm{out}}{\partial T}\right|_{T_\mathrm{des}} = 0$ and using expressions of the outgassing flux (2.26) and (2.27):

- in detrapping-limited regime, the outgassing flux is given by (2.26) and the equation $\frac{\partial \hat{\Gamma}_\mathrm{out}(T_\mathrm{des})}{\partial T} = 0$ becomes

$$\left(\frac{\partial\,\Omega_\mathrm{dt}(T_\mathrm{des})}{\partial T}\right)^2 = \frac{\partial^2\,\Omega_\mathrm{dt}(T_\mathrm{des})}{\partial T^2} \tag{5.9}$$

  which can be recast into $\Omega_\mathrm{dt}(T_\mathrm{des}) = 1$. Using the Lambert function ω, T_des is then given by

$$T_\mathrm{des} = \frac{E_\mathrm{dt}}{2}\frac{1}{\omega\left(\sqrt{\frac{E_\mathrm{dt}\nu_{dt,0}}{4\alpha}}\right)} \tag{5.10}$$

- in retrapping-limited regime, the outgassing flux is given by (2.27) and the equation $\frac{\partial \hat{\Gamma}_\mathrm{out}(T_\mathrm{des})}{\partial T} = 0$

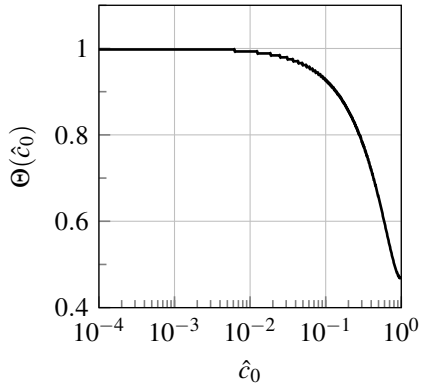

Figure 5.8: Graph of Θ as a function of $\hat{c}_0$

becomes after some algebra

$$\frac{\omega^2(\varphi)+2\omega(\varphi)}{(1+\omega(\varphi))^2} = -1 + \frac{\frac{\partial^2 \Omega_{\text{eff}}}{\partial T^2}}{\left(\frac{\partial \Omega_{\text{eff}}}{\partial T}\right)^2} \tag{5.11}$$

where $\varphi = \Omega_0 e^{\Omega_0 - \Omega_{\text{eff}}}$. The expression (5.11) can be then recast into

$$\left(\frac{\partial \Omega_{\text{eff}}(T_{\text{des}})}{\partial T}\right)^2 = (1+\omega(\varphi(T_{\text{des}})))^2 \frac{\partial^2 \Omega_{\text{eff}}(T_{\text{des}})}{\partial T^2} \tag{5.12}$$

Since $\Omega_{\text{eff}}(T) \approx \frac{D_{\text{eff}}(T)}{\Delta^2}\frac{T^2}{E_{\text{eff}}}$ and usually $\frac{E_{\text{eff}}}{T} \gg 1$, the previous equation (5.12) can be simplified into

$$\Omega_{\text{eff}}(T_{\text{des}}) \approx \underbrace{\left[1+\omega\left(\Omega_0 e^{\Omega_0 - \Omega_{\text{eff}}(T_{\text{des}})}\right)\right]^2}_{\Theta(\hat{c}_0)} \tag{5.13}$$

The implicit function $\Theta(\hat{c}_0)$ defined by $\Theta(\hat{c}_0) = \left[1+\omega\left(-\hat{c}_0 e^{-\hat{c}_0} e^{-\Theta(\hat{c}_0)}\right)\right]^2$ decreases as function of $\hat{c}_0$ in the interval $0.46 < \Theta < 1$ (fig. 5.8).

The temperature T_{des} is then finally given by

$$T_{\text{des}} = \frac{E_{\text{eff}}}{2} \frac{1}{\omega\left(\sqrt{\frac{\frac{\nu_{dt,0}D_0}{\nu_{tr,0}\Delta^2}E_{\text{eff}}}{2\alpha\Theta(\hat{c}_0)}}\right)} \tag{5.14}$$

D Analytical estimation of skewness of desorption peak

The temperatures $T_+ > T_p$ and $T_- < T_p$ are formally defined by $\frac{\Gamma_{out}(T_\pm(\beta))}{\Gamma_{out}(T_p)} = \beta$ with $0 < \beta \leq 1$.

The skewness estimator $\hat{S} = \frac{T_+ + T_-}{2T_{\text{des}}} - 1$ can be analytically expressed using expressions of outgassing flux (2.26) and (2.27):

$$\hat{S}(\beta) = \frac{\omega(u)}{2}\left[\omega^{-1}\left(\frac{u}{\sqrt{s_0(\beta)}}\right) + \omega^{-1}\left(\frac{u}{\sqrt{s_{-1}(\beta)}}\right)\right] - 1 \tag{5.15}$$

where $u = \sqrt{\frac{E_{\text{dt}}\nu_{\text{dt},0}}{4\alpha}}$ in detrapping-limited regime and $u = \sqrt{\frac{E_{\text{eff}}\nu_{\text{eff},0}}{4\alpha\Theta(\hat{c}_0)}}$.

The functions s_0 and s_{-1} follow the dependencies $s_0(\beta) \sim \omega_0(\beta e^{-1})$ and $s_{-1}(\beta) \sim -\omega_{-1}(-\beta e^{-1})$ in both regimes. ω_0 and ω_{-1} are respectively here the 0 and -1 branches for the Lambert function. Noticing that $u \gg 1$, it can be shown after some algebra with a good approximation that

$$\hat{S}(\beta) \sim \frac{e^{-1}}{2}\frac{\ln\beta}{\ln u} \tag{5.16}$$

The magnitude of the estimator $\hat{A} = \frac{\partial\hat{S}}{\partial\ln\beta} \sim \frac{e^{-1}}{2\ln u}$ thus depends on the value of u which varies of several orders of magnitude between detrapping-limited regime and retrapping-limited regime since $\nu_{\text{eff},0} \ll \nu_{\text{dt},0}$.

There is therefore a clear difference between lower values of $\hat{A}$ in detrapping-limited regime and higher values of $\hat{A}$ in retrapping-limited regime. Considering typical retention and desorption parameters, $\hat{A} < 0.01$ in detrapping-limited regime and $\hat{A} > 0.01$ in retrapping-limited regime.

Bibliography

[1] R. Reagan. Joint Soviet-United States Statement on the Summit Meeting in Geneva. November 21, 1985.

[2] ITER project website. http://www.iter.org.

[3] F. Chen. *An indispensable truth: how fusion power can save the planet*. Springer Science & Business Media, 2011.

[4] H.A. Bethe. Energy Production in Stars. *Physical Review*, 55:434–456, Mar 1939.

[5] J. Wesson and D.J. Campbell. *Tokamaks*. International Series of Monographs on Physics. OUP Oxford, 2011.

[6] Tokamak and ITER. http://www.euro-fusion.org/2005/12/50-years-of-lawson-criteria/.

[7] M. Greenwald. Density limits in toroidal plasmas. *Plasma Physics and Controlled Fusion*, 44(8):R27, 2002.

[8] X. Garbet, P. Mantica, C. Angioni, E. Asp, Y. Baranov, C. Bourdelle, R. Budny, F. Crisanti, G. Cordey, L. Garzotti, N. Kirneva, D. Hogeweij, T. Hoang, F. Imbeaux, E. Joffrin, X. Litaudon, A. Manini, D.C. McDonald, H. Nordman, V. Parail, A. Peeters, F. Ryter, C. Sozzi, M. Valovic, T. Tala, A. Thyagaraja, I. Voitsekhovitch, J. Weiland, H. Weisen, A. Zabolotsky, and the JET EFDA Contributors. Physics of transport in tokamaks. *Plasma Physics and Controlled Fusion*, 46(12B):B557, 2004.

[9] ITER Physics Basis Editors, ITER Physics Expert Group Chairs, Co-Chairs and ITER Joint Central Team, and Physics Integration Unit. Chapter 1: Overview and summary. *Nuclear Fusion*, 39(12):2137, 1999.

[10] D.J. Ward. The physics of DEMO. *Plasma Physics and Controlled Fusion*, 52(12):124033, 2010.

[11] H. Bolt, V. Barabash, G. Federici, J. Linke, A. Loarte, J. Roth, and K. Sato. Plasma facing and high heat flux materials–needs for iter and beyond. *Journal of Nuclear Materials*, 307:43–52, 2002.

[12] R.A. Pitts, S. Carpentier, F. Escourbiac, T. Hirai, V. Komarov, A.S. Kukushkin, S. Lisgo, A. Loarte, M. Merola, and R. Mitteau. Physics basis and design of the ITER plasma-facing components. *Journal of Nuclear Materials*, 415(1):S957–S964, 2011.

[13] S. Kajita, W. Sakaguchi, N. Ohno, N. Yoshida, and T. Saeki. Formation process of tungsten nanostructure by the exposure to helium plasma under fusion relevant plasma conditions. *Nuclear Fusion*, 49(9):095005, 2009.

[14] G. Federici, C.H. Skinner, J.N. Brooks, J.P. Coad, C. Grisolia, A.A. Haasz, A. Hassanein, V. Philipps, C.S. Pitcher, and J. Roth. Plasma-material interactions in current tokamaks and their implications for next step fusion reactors. *Nuclear Fusion*, 41(12):1967, 2001.

[15] J. Roth, E. Tsitrone, A. Loarte, T. Loarer, G. Counsell, R. Neu, V. Philipps, S. Brezinsek, M. Lehnen, P. Coad, Ch. Grisolia, K. Schmid, K. Krieger, A. Kallenbach, B. Lipschultz, R. Doerner, R. Causey, V. Alimov, W. Shu, O. Ogorodnikova, A. Kirschner, G. Federici, and A. Kukushkin. Recent analysis of key plasma wall interactions issues for ITER. *Journal of Nuclear Materials*, 390-391(0):1–9, 2009.

[16] R.A. Pitts. Key plasma-wall interaction physics issues for ITER. *Proceedings of the 3th ITER International Summer School*, page 1294, 2009.

[17] J.W. Coenen, G. Arnoux, B. Bazylev, G.F. Matthews, S. Jachmich, I. Balboa, M. Clever, R. Dejarnac, I. Coffey, Y. Corre, S. Devaux, L. Frassinetti, E. Gauthier, J. Horacek, M. Knaup, M. Komm, K. Krieger, S. Marsen, A. Meigs, Ph. Mertens, R.A. Pitts, T. Puetterich, M. Rack, M. Stamp, G. Sergienko, P. Tamain, and V. Thompson. ELM induced tungsten melting and its impact on tokamak operation . *Journal of Nuclear Materials*, (0), 2014.

[18] S. Balibar, Y. Pomeau, and J. Treiner. La France et l'énergie des étoiles. Le Monde, 24 October 2004.

[19] C. Kittel. *Introduction to Solid State Physics*. Hoboken, NJ, 8th edition edition, 2005.

[20] R.A. Causey. Hydrogen isotope retention and recycling in fusion reactor plasma-facing components. *Journal of Nuclear Materials*, 300(2):91–117, 2002.

[21] C.H. Skinner, A.A. Haasz, N. Bekris, R.A. Causey, R.E.H. Clark, J.P. Coad, J.W. Davis, R.P. Doerner, M. Mayer, A. Pisarev, J. Roth, and T. Tanabe. Recent advances on hydrogen retention in ITER's plasma-facing material : beryllium, carbon, and tungsten. *Fusion Science and Technology*, 54:891, 2008.

[22] T. Loewenhoff, J. Linke, G. Pintsuk, R.A. Pitts, and B. Riccardi. ITER-W monoblocks under high pulse number transient heat loads at high temperature. *Journal of Nuclear Materials*, (0):–, 2014.

[23] M. Shimada, Y. Hatano, Y. Oya, T. Oda, M. Hara, G. Cao, M. Kobayashi, M. Sokolov, H. Watanabe, and B. Tyburska-Püschel. Overview of the us–japan collaborative investigation on hydrogen isotope retention in neutron-irradiated and ion-damaged tungsten. *Fusion Engineering and Design*, 87(7):1166–1170, 2012.

[24] A. Takayama, A.M. Ito, Y. Oda, and H. Nakamura. First principles investigation of cluster consisting of hydrogen-helium atoms interstitially-trapped in tungsten. *Journal of Nuclear Materials*, (0), 2014.

[25] Y. Ueda, J.W. Coenen, G. De Temmerman, R.P. Doerner, J. Linke, V. Philipps, and E. Tsitrone. Research status and issues of tungsten plasma facing materials for ITER and beyond. *Fusion Engineering and Design*, 89(7):901–906, 2014. Proceedings of the 11th International Symposium on Fusion Nuclear Technology-11 (ISFNT-11) Barcelona, Spain, 15-20 September, 2013.

[26] G. Federici and C.H. Skinner. Tritium Inventory in the materials of the ITER plasma-facing components. In *Nuclear Fusion Research*, pages 287–317. Springer, 2005.

[27] S. Brezinsek, T. Loarer, V. Philipps, H.G. Esser, S. Grünhagen, R. Smith, R. Felton, J. Banks, P. Belo, A. Boboc, J. Bucalossi, M. Clever, J.W. Coenen, I. Coffey, S. Devaux, D. Douai, M. Freisinger, D. Frigione, M. Groth, A. Huber, J. Hobirk, S. Jachmich, S. Knipe, K. Krieger, U. Kruezi, S. Marsen, G.F. Matthews, A.G. Meigs, F. Nave, I. Nunes, R. Neu, J. Roth, M.F. Stamp, S. Vartanian, and U. Samm. Fuel retention studies with the ITER-Like Wall in JET. *Nuclear Fusion*, 53(8):083023, August 2013.

[28] V. Rohde, M. Mayer, V. Mertens, R. Neu, and K. Sugiyama. Dynamic and static deuterium inventory in asdex upgrade with tungsten first wall. *Nuclear Fusion*, 49(8):085031, 2009.

[29] C. Grisolia, L.D. Horton, and J.K. Ehrenberg. Modelling of hydrogen conditioning, retention and release in Tore Supra. *Journal of Nuclear Materials*, 220–222(0):516–520, 1995.

[30] H. Takenaga, N. Asakura, S. Higashijima, T. Nakano, H. Kubo, S. Konoshima, N. Oyama, a. Isayama, S. Ide, T. Fujita, and Y. Miura. Study of plasma wall interactions in the long-pulse NB-heated discharges of JT-60U towards steady-state operation. *Journal of Nuclear Materials*, 337-339:802–807, 2005.

[31] T. Tanabe. Review of hydrogen retention in tungsten. *Physica Scripta*, 2014(T159):014044, 2014.

[32] J. Roth and K. Schmid. Hydrogen in tungsten as plasma-facing material. *Physica Scripta*, 2011(T145):014031, 2011.

[33] W.A. Lanford. Analysis for hydrogen by nuclear reaction and energy recoil detection. *Nuclear Instruments and Methods in Physics Research Section B: Beam Interactions with Materials and Atoms*, 66(1):65–82, 1992.

[34] P.A. Redhead. Thermal desorption of gases. *Vacuum*, 12(4):203–211, 1962.

[35] O.V. Ogorodnikova, J. Roth, and M. Mayer. Pre-implantation and pre-annealing effects on deuterium retention in tungsten. *Journal of Nuclear Materials*, 373(1):254–258, 2008.

[36] A. Manhard. *Deuterium inventory in tungsten after plasma exposure: a microstructural survey*. PhD thesis, University of Augsburg, 2012.

[37] L. Buzi, G. de Temmerman, B. Unterberg, M. Reinhart, T. Dittmar, D. Matveev, Ch. Linsmeier, U. Breuer, A. Kreter, and G. Van Oost. Influence of tungsten microstructure and ion flux on deuterium plasma-induced surface modifications and deuterium retention. *Journal of Nuclear Materials*, (0):–, 2014.

[38] B.J. Braams and H.-K. Chung. Atomic and Plasma-Material Interaction Data for Fusion. V. 16. 2014.

[39] W. Kohn. Nobel Lecture: Electronic structure of matter—wave functions and density functionals. *Rev. Mod. Phys.*, 71:1253–1266, Oct 1999.

[40] D. Perez, B.P. Uberuaga, Y. Shim, J.G. Amar, and A.F. Voter. Accelerated molecular dynamics methods: introduction and recent developments. *Annual Reports in Computational Chemistry*, 5:79–98, 2009.

[41] A.F. Voter. Introduction to the kinetic monte carlo method. In *Radiation Effects in Solids*, pages 1–23. Springer, 2007.

[42] A.H.M. Krom and A.D. Bakker. Hydrogen Trapping Models in Steel. *Metallurgical and Materials Transactions B*, 31(December):1475–1482, 2000.

[43] M. Oberkofler, M. Reinelt, and Ch. Linsmeier. Retention and release mechanisms of deuterium implanted into beryllium. *Nuclear Instruments and Methods in Physics Research Section B: Beam Interactions with Materials and Atoms*, 269(11):1266–1270, 2011.

[44] P. Andrew, J.P. Coad, J. Ehrenberg, D.H.J. Goodall, L.D. Horton, O.N. Jarvis, P.J. Lomas, M.J. Loughlin, G.M. McCracken, A.T. Peacock, M.A. Pick, G. Saibene, R. Sartori, and P.R. Thomas. Experiments on the release of tritium from the first wall of JET. *Nuclear Fusion*, 33(9):1389–1404, sep 1993.

[45] O.V. Ogorodnikova. Trapping effect in hydrogen retention in metals. In A. Hassanein, editor, *Hydrogen and helium recycling at plasma facing materials : proceedings of the NATO Advanced Research Workshop on Hydrogen Isotope Recycling at Plasma Facing Materials in Fusion Reactors, Argonne, Illinois, U.S.A., 22-24 August 2001*, NATO Science Series, pages 7–15. Kluwer Academic, 2002.

[46] J.P. Roszell, J.W. Davis, and A.A. Haasz. Temperature dependence of deuterium retention mechanisms in tungsten. *Journal of Nuclear Materials*, 429(1-3):48–54, 2012.

[47] M.A. Pick and K. Sonnenberg. A model for atomic hydrogen-metal interactions: application to recycling, recombination and permeation. *Journal of Nuclear Materials*, 131:208–220, 1985.

[48] I. Langmuir. Tungsten Lamps of High Efficiency-I. *American Institute of Electrical Engineers, Transactions of the*, 32(2), 1913.

[49] D.D. Eley. The interchange of hydrogen in the adsorbed film on tungsten. *Proceedings of the Royal Society of London. Series A. Mathematical and Physical Sciences*, 178(975):452–464, 1941.

[50] J.K. Roberts. The adsorption of hydrogen on tungsten. *Proceedings of the Royal Society of London. Series A-Mathematical and Physical Sciences*, 152(876):445–463, 1935.

[51] G. Bryce. The dissociation of hydrogen by tungsten. *Mathematical Proceedings of the Cambridge Philosophical Society*, 32:648–652, 12 1936.

[52] T. W. Hickmott. Interaction of Hydrogen with Tungsten. *The Journal of Chemical Physics*, 32(3):810–823, 1960.

[53] J. Eisinger. Properties of Hydrogen Chemisorbed on Tungsten. *The Journal of Chemical Physics*, 29(5):1154–1160, 1958.

[54] G. Halsey and H.S. Taylor. The adsorption of hydrogen on tungsten powders. *The Journal of Chemical Physics*, 15(9):624–630, 1947.

[55] R. Gomer, R. Wortman, and R. Lundy. Mobility and adsorption of hydrogen on tungsten. *The Journal of Chemical Physics*, 26(5):1147–1164, 1957.

[56] D. Brennan and P.C. Fletcher. The atomization of hydrogen on tungsten. *Proceedings of the Royal Society of London. Series A. Mathematical and Physical Sciences*, 250(1262):389–408, 1959.

[57] V.J. Mimeault and R.S. Hansen. Flash desorption and isotopic mixing of hydrogen and deuterium adsorbed on tungsten, iridium, and rhodium. *The Journal of Chemical Physics*, 45(6):2240–2250, 1966.

[58] P.J. Estrup and J. Anderson. Chemisorption of hydrogen on tungsten (100). *The Journal of Chemical Physics*, 45(6):2254–2260, 1966.

[59] R. Frauenfelder. Solution and diffusion of hydrogen in tungsten. *Journal of Vacuum Science and Technology*, 6(3):388–397, 1969.

[60] J.H. McCreery and G. Wolken Jr. Recombination dynamics of hydrogen on a tungsten surface. *The Journal of Chemical Physics*, 63(9):4072–4073, 1975.

[61] R. DiFoggio and R. Gomer. Diffusion of hydrogen and deuterium on the (110) plane of tungsten. *Physical Review B*, 25(6):3490, 1982.

[62] M. Tringides and R. Gomer. Anisotropy in surface diffusion: Oxygen, hydrogen, and deuterium on the (110) plane of tungsten. *Surface Science*, 155(1):254–278, 1985.

[63] E.A. Daniels, J.C. Lin, and R. Gomer. Diffusion anisotropy of hydrogen and deuterium on the tungsten (211) plane. *Surface Science*, 204(1):129–146, 1988.

[64] P. Alnot, A. Cassuto, and D.A. King. Adsorption and desorption kinetics with no precursor trapping: hydrogen and deuterium on W $\{100\}$. *Surface Science*, 215(1):29–46, 1989.

[65] M. Poon, R.G. Macaulay-Newcombe, J.W. Davis, and A.A. Haasz. Flux dependence of deuterium retention in single crystal tungsten. *Journal of Nuclear Materials*, 307:723–728, 2002.

[66] V.Kh. Alimov, W.M. Shu, J. Roth, D.A. Komarov, S. Lindig, K. Isobe, H. Nakamura, and T. Yamanishi. Surface Modification and Deuterium Retention in Tungsten and Molybdenum Exposed to Low-Energy, High Flux Deuterium Plasmas. In *Advanced Materials Research*, volume 59, pages 42–45. Trans Tech Publ, 2009.

[67] V.Kh. Alimov, B. Tyburska-Püschel, Y. Hatano, J. Roth, K. Isobe, M. Matsuyama, and T. Yamanishi. The effect of displacement damage on deuterium retention in ITER-grade tungsten exposed to low-energy, high-flux pure and helium-seeded deuterium plasmas. *Journal of Nuclear Materials*, 420(1):370–373, 2012.

[68] R.A. Causey, K. Wilson, T. Venhaus, and W.R. Wampler. Tritium retention in tungsten exposed to intense fluxes of 100 eV tritons. *Journal of Nuclear Materials*, 266:467–471, 1999.

[69] H. Xu, G. Luo, H. Schut, Y. Yuan, B. Fu, A. Godfrey, W. Liu, and G. de Temmerman. Enhanced modification of tungsten surface by nanostructure formation during high flux deuterium plasma exposure. *Journal of Nuclear Materials*, 447(1):22–27, 2014.

[70] G.-N. Luo, W.M. Shu, and M. Nishi. Incident energy dependence of blistering at tungsten irradiated by low energy high flux deuterium plasma beams. *Journal of Nuclear Materials*, 347(1):111–117, 2005.

[71] S. Lindig, M. Balden, V.Kh. Alimov, T. Yamanishi, W.M. Shu, and J. Roth. Subsurface morphology changes due to deuterium bombardment of tungsten. *Physica Scripta*, 2009(T138):014040, 2009.

[72] V.Kh. Alimov, J. Roth, W.M. Shu, D.A. Komarov, K. Isobe, and T. Yamanishi. Deuterium trapping in tungsten deposition layers formed by deuterium plasma sputtering. *Journal of Nuclear Materials*, 399(2):225–230, 2010.

[73] A.A. Haasz and J.W. Davis. Deuterium retention in beryllium, molybdenum and tungsten at high fluences. *Journal of Nuclear Materials*, 241:1076–1081, 1997.

[74] J.P. Sharpe, R.D. Kolasinski, M. Shimada, P. Calderoni, and R.A. Causey. Retention behavior in tungsten and molybdenum exposed to high fluences of deuterium ions in TPE. *Journal of Nuclear Materials*, 390:709–712, 2009.

[75] W.M. Shu, M. Nakamichi, V.K. Alimov, G.-N. Luo, K. Isobe, and T. Yamanishi. Deuterium retention, blistering and local melting at tungsten exposed to high-fluence deuterium plasma. *Journal of Nuclear Materials*, 390:1017–1021, 2009.

[76] Z. Tian, J.W. Davis, and A.A. Haasz. Deuterium retention in tungsten at fluences of up to 10 26 D+/m 2 using D+ ion beams. *Journal of Nuclear Materials*, 399(1):101–107, 2010.

[77] T. Venhaus, R. Causey, R. Doerner, and T. Abeln. Behavior of tungsten exposed to high fluences of low energy hydrogen isotopes. *Journal of Nuclear Materials*, 290-293:505–508, 2001.

[78] W.M. Shu, K. Isobe, and T. Yamanishi. Temperature dependence of blistering and deuterium retention in tungsten exposed to high-flux and low-energy deuterium plasma. *Fusion Engineering and Design*, 83(7):1044–1048, 2008.

[79] K.R. Umstadter, R. Doerner, and G. Tynan. Enhanced erosion of tungsten plasma-facing components subject to simultaneous heat pulses and deuterium plasma. *Journal of Nuclear Materials*, 386:751–755, 2009.

[80] W. Wang, M. Kobayashi, R. Kurata, S. Suzuki, N. Ashikawa, A. Sagara, N. Yoshida, Y. Hatano, G.-N. Luo, and Y. Oya. Temperature dependence of retention of energetic deuterium and carbon simultaneously implanted into tungsten. *Journal of Nuclear Materials*, 417(1):555–558, 2011.

[81] V.Kh. Alimov, W.M. Shu, J. Roth, S. Lindig, M. Balden, K. Isobe, and T. Yamanishi. Temperature dependence of surface topography and deuterium retention in tungsten exposed to low-energy, high-flux D plasma. *Journal of Nuclear Materials*, 417(1):572–575, 2011.

[82] A.A. Haasz, M. Poon, and J.W. Davis. The effect of ion damage on deuterium trapping in tungsten. *Journal of Nuclear Materials*, 266:520–525, 1999.

[83] M. Kobayashi, M. Shimada, Y. Hatano, T. Oda, B. Merrill, Y. Oya, and K. Okuno. Deuterium trapping by irradiation damage in tungsten induced by different displacement processes. *Fusion Engineering and Design*, 88(9):1749–1752, 2013.

[84] O.V. Ogorodnikova, B. Tyburska, V.Kh. Alimov, and K. Ertl. The influence of radiation damage on the plasma-induced deuterium retention in self-implanted tungsten. *Journal of Nuclear Materials*, 415(1):S661–S666, 2011.

[85] W.R. Wampler and R.P. Doerner. Deuterium retention in tungsten from exposure to plasma. *Physica Scripta*, 2009(T138):014037, 2009.

[86] I.I. Arkhipov, S.L. Kanashenko, V.M. Sharapov, R.Kh. Zalavutdinov, and A.E. Gorodetsky. Deuterium trapping in ion-damaged tungsten single crystal. *Journal of Nuclear Materials*, 363:1168–1172, 2007.

[87] M. Fukumoto, H. Kashiwagi, Y. Ohtsuka, Y. Ueda, M. Taniguchi, T. Inoue, K. Sakamoto, J. Yagyu, T. Arai, and I. Takagi. Deuterium trapping in tungsten damaged by high-energy hydrogen ion irradiation. *Journal of Nuclear Materials*, 390:572–575, 2009.

[88] B.I. Khripunov, A.N. Brukhanov, V.M. Gureev, V.S. Koidan, S.N. Kornienko, S.T. Latushkin, V.B. Petrov, A.I. Ryazanov, E.V. Semenov, and V.G. Stolyarova. Plasma effect on tungsten damaged by high-energy alpha particles: Erosion and deuterium trapping. *Journal of Nuclear Materials*, 415(1):S649–S652, 2011.

[89] M.H.J. 't Hoen, M. Mayer, A. W. Kleyn, and P. A. Zeijlmans van Emmichoven. Strongly reduced penetration of atomic deuterium in radiation-damaged tungsten. *Phys. Rev. Lett.*, 111:225001, Nov 2013.

[90] M.H.J. 't Hoen, B. Tyburska-Püschel, K. Ertl, M. Mayer, J. Rapp, A.W. Kleyn, and P.A. Zeijlmans van Emmichoven. Saturation of deuterium retention in self-damaged tungsten exposed to high-flux plasmas. *Nuclear Fusion*, 52(2):023008, 2012.

[91] B. Tyburska-Püschel, K. Ertl, M. Mayer, J. Rapp, A.W. Kleyn, P.A. Zeijlmans van Emmichoven, et al. Saturation of deuterium retention in self-damaged tungsten exposed to high-flux plasmas. *Nuclear Fusion*, 52(2):023008, 2012.

[92] H. Nakamura, T. Hayashi, Y. Iwai, and M. Nishi. The effect of annealing on the transient deuterium permeation characteristics of tungsten. *Fusion technology*, 39(2):894–898, 2001.

[93] B.M. Oliver, R.A. Causey, and S.A. Maloy. Deuterium retention and release from highly irradiated annealed tungsten after exposure to a deuterium DC glow discharge. *Journal of Nuclear Materials*, 329:977–981, 2004.

[94] H.T. Lee, E. Markina, Y. Otsuka, and Y. Ueda. Deuterium ion-driven permeation in tungsten with different microstructures. *Physica Scripta*, 2011(T145):014045, 2011.

[95] A. Manhard, K. Schmid, M. Balden, and W. Jacob. Influence of the microstructure on the deuterium retention in tungsten. *Journal of Nuclear Materials*, 415:S632–S635, 2011.

[96] V.Kh. Alimov, J. Roth, and M. Mayer. Depth distribution of deuterium in single-and polycrystalline tungsten up to depths of several micrometers. *Journal of Nuclear Materials*, 337:619–623, 2005.

[97] O.V. Ogorodnikova, T. Schwarz-Selinger, K. Sugiyama, T. Dürbeck, and W. Jacob. Deuterium retention in different tungsten grades. *Physica Scripta*, 2009(T138):014053, 2009.

[98] M. Oya, H.T. Lee, Y. Ohtsuka, Y. Ueda, H. Kurishita, M. Oyaidzu, and T. Yamanishi. Deuterium retention in various toughened, fine-grained recrystallized tungsten materials under different irradiation conditions. *Physica Scripta*, 2014(T159):014048, 2014.

[99] A. Rusinov, M. Sakamato, H. Zushi, R. Ohyama, K. Honda, I. Takagi, T. Tanabe, and N. Yoshida. Deuterium Trapping in Rolled Polycrystalline Tungsten Exposed to Low Energy Plasma. *Plasma and Fusion Research*, 7(0):1405105–1405105, 2012.

[100] J.P. Roszell, J.W. Davis, V.Kh. Alimov, K. Sugiyama, and A.A. Haasz. Deuterium retention in single-crystal tungsten irradiated with 10-500 eV/D+. *Journal of Nuclear Materials*, 438:1084–1087, 2013.

[101] R.A. Anderl, D.F. Holland, G.R. Longhurst, R.J. Pawelko, C.L. Trybus, and C.H. Sellers. Deuterium Transport and Trapping in Polycrystalline Tungsten . *Fusion Science and Technology*, 21(2P2):745–752, 1992.

[102] A.A. Haasz, M. Poon, R.G. Macaulay-Newcombe, and J.W. Davis. Deuterium retention in single crystal tungsten. *Journal of Nuclear Materials*, 290:85–88, 2001.

[103] H. Eleveld and A. van Veen. Deuterium interaction with impurities in tungsten studied with TDS. *Journal of Nuclear Materials*, 191:433–438, 1992.

[104] Y. Zayachuk, P.A. Zeijlmans van Emmichoven, D. Terentyev, I. Uytdenhouwen, and G. Van Oost. Surface modification of tungsten and tungsten-tantalum alloys exposed to high-flux deuterium plasma and its impact on deuterium retention. *Nuclear Fusion*, 53(1):013013, 2013.

[105] D.A. Komarov, A.V. Markin, S.Y. Rybakov, and A.P. Zakharov. Role of grain boundaries and carbon deposition in deuterium retention behavior of deuterium plasma exposed tungsten. *Journal of Nuclear Materials*, 290:433–436, 2001.

[106] M. Balden, A. Manhard, and S. Elgeti. Deuterium retention and morphological modifications of the surface in five grades of tungsten after deuterium plasma exposure. *Journal of Nuclear Materials*, 452(1):248–256, 2014.

[107] K.A. Moshkunov, K. Schmid, M. Mayer, V.A. Kurnaev, and Y.M. Gasparyan. Air exposure and sample storage time influence on hydrogen release from tungsten. *Journal of Nuclear Materials*, 404(3):174–177, 2010.

[108] A.D. Quastel, J.W. Davis, A.A. Haasz, and R.G. Macaulay-Newcombe. Effect of post-D+-irradiation time delay and pre-TDS heating on D retention in single crystal tungsten. *Journal of Nuclear Materials*, 359(1-2):8–16, 2006.

[109] R.A. Causey, R. Doerner, H. Fraser, R.D. Kolasinski, J. Smugeresky, K. Umstadter, and R. Williams. Defects in tungsten responsible for molecular hydrogen isotope retention after exposure to low energy plasmas. *Journal of Nuclear Materials*, 390-391(null):717–720, 2009.

[110] O.V. Ogorodnikova, J. Roth, and M. Mayer. Deuterium retention in tungsten in dependence of the surface conditions. *Journal of Nuclear Materials*, 313:469–477, 2003.

[111] G.R. Longhurst. *TMAP7: Tritium Migration Analysis Program*. Idaho National Laboratory, user manual edition, 2004. INEEL/EXT-04-02352.

[112] P. W. Tamm and L. D. Schmidt. Binding States of Hydrogen on Tungsten. *The Journal of Chemical Physics*, 54(11):4775–4787, 1971.

[113] D.A. King. Thermal desorption from metal surfaces: A review. *Surface Science*, 47(1):384–402, 1975. Proceedings of the Third Symposium on Surface Physics University of Utrecht, The Netherlands 26-28 June 1974.

[114] A.A. Pisarev. Hydrogen adsorption on the surface of metals. volume 2, page 1. Elsevier, 2012.

[115] L. Bukonte, T. Ahlgren, and K. Heinola. Modelling of monovacancy diffusion in W over wide temperature range. *Journal of Applied Physics*, 115(12):123504, 2014.

[116] D.F. Johnson and E.A. Carter. Hydrogen in tungsten: Absorption, diffusion, vacancy trapping, and decohesion. *Journal of Materials Research*, 25(02):315–327, January 2011.

[117] K. Heinola and T. Ahlgren. First-principles study of H on the reconstructed W(100) surface. *Physical Review B*, 81:073409, 2010.

[118] N. Fernandez, Y. Ferro, and D. Kato. Hydrogen diffusion and vacancies formation in tungsten: Density functional theory calculations and statistical models. *Acta Materialia*, 94:307–318, 2015.

[119] K. Schmid, U. von Toussaint, and T. Schwarz-Selinger. Transport of hydrogen in metals with occupancy dependent trap energies. *Journal of Applied Physics*, 116(13), 2014.

[120] T. Ahlgren, K. Heinola, K. Vortler, and J. Keinonen. Simulation of irradiation induced deuterium trapping in tungsten. *Journal of Nuclear Materials*, 427(1-3):152–161, 2012.

[121] M.H.J. 't Hoen, M. Balden, A. Manhard, M. Mayer, S. Elgeti, A.W. Kleyn, and P.A. Zeijlmans Zeijlmans van Emmichoven. Surface morphology and deuterium retention of tungsten after low- and high-flux deuterium plasma exposure. *Nuclear Fusion*, 54(8):083014, 2014.

[122] J.L. Barton, Y.Q. Wang, T. Dittmar, R.P. Doerner, and G.R. Tynan. Deuterium retention in tungsten after heavy ion damage and hydrogen isotope exchange in PISCES. *Nuclear Instruments and Methods in Physics Research Section B: Beam Interactions with Materials and Atoms*, 332:275–279, 2014.

[123] C.-M. Chan, R. Aris, and W.H. Weinberg. An analysis of thermal desorption mass spectra. I. *Applications of Surface Science*, 1(3):360–376, May 1978.

[124] M. Poon, A.A. Haasz, and J.W. Davis. Modelling deuterium release during thermal desorption of D+-irradiated tungsten. *Journal of Nuclear Materials*, 374:390–402, 2008.

[125] R. D. Smirnov, S. I. Krasheninnikov, J. Guterl, M. J. Baldwin, and R. P. Doerner. Modeling of Hydrogen Retention and Outgassing from Co-Deposits with Distributed Energy States. *Contributions to Plasma Physics*, 54(4-6):610–614, 2014.

[126] S.I. Krasheninnikov, E.D. Marenkov, R.D. Smirnov, and A.A. Pisarev. Hydrogen transport in solids with traps in the case of continuum distribution of detrapping energies. *Physica Scripta*, 2014(T159):014060, 2014.

[127] B.J. Merrill, M. Shimada, and P.W. Humrickhouse. Simulating Tritium Retention in Tungsten with a Multiple Trap Model in the TMAP Code. *Journal of Plasma and Fusion Research Series*, 10:71–75, 2013.

[128] A. Manhard, T. Schwarz-Selinger, and W. Jacob. Quantification of the deuterium ion fluxes from a plasma source. *Plasma Sources Science and Technology*, 20:015010, 2011.

[129] E Salançon, T Dürbeck, T Schwarz-Selinger, F Genoese, and W Jacob. Redeposition of amorphous hydrogenated carbon films during thermal decomposition. *Journal of Nuclear Materials*, 376:160ÂŰ168, 2008.

[130] M. Mayer, E. Gauthier, K. Sugiyama, and U. von Toussaint. Quantitative depth profiling of deuterium up to very large depths. *Nuclear Instruments and Methods in Physics Research Section B: Beam Interactions with Materials and Atoms*, 267(3):506–512, 2009.

[131] M. Mayer. SIMNRA, a simulation program for the analysis of NRA, RBS and ERDA. *AIP Conference Proceedings*, 475:541–544, 1999.

[132] K. Schmid and U. von Toussaint. Statistically sound evaluation of trace element depth profiles by ion beam analysis. *Nuclear Instruments and Methods in Physics Research Section B: Beam Interactions with Materials and Atoms*, 281:64–71, 2012.

[133] O.V. Ogorodnikova. Comparison of hydrogen gas–, atom–and ion–metal interactions. *Journal of Nuclear Materials*, 277(2):130–142, 2000.

[134] K. Heinola, T. Ahlgren, K. Nordlund, and J. Keinonen. Hydrogen interaction with point defects in tungsten. *Physical Review B*, 82:094102, 2010.

[135] K. Christmann. Interaction of hydrogen with solid surfaces. *Surface Science Reports*, 9(1-3):1–163, 1988.

[136] K. Schmid, V. Rieger, and A. Manhard. Comparison of hydrogen retention in W and W/Ta alloys. *Journal of Nuclear Materials*, 426:247–253, 2012.

[137] A.A. Pisarev and M. Zibrov. private communication.

[138] A. Van Veen, H.A. Filius, J. De Vries, K.R. Bijkerk, G.J. Rozing, and D. Segers. Hydrogen exchange with voids in tungsten observed with TDS and PA. *Journal of Nuclear Materials*, 155-157:1113–1117, 1988.

[139] K.O.E. Henriksson. The depths of hydrogen and helium bubbles in tungsten: a comparison. *Fusion Science and Technology*, 50(July):43–57, 2006.

[140] X.-S. Kong, Y.-W. You, Q.F. Fang, C.S. Liu, J.-L. Chen, G.-N. Luo, B.C. Pan, and Z. Wang. The role of impurity oxygen in hydrogen bubble nucleation in tungsten. *Journal of Nuclear Materials*, 433(1-3):357–363, February 2013.

[141] W.M. Shu, G.-N. Luo, and T. Yamanishi. Mechanisms of retention and blistering in near-surface region of tungsten exposed to high flux deuterium plasmas of tens of eV. *Journal of Nuclear Materials*, 367-370:1463–1467, 2007.

[142] S. Panayotis, B. Pégourié, E. Caprin, D. Douai, J.-C. Hatchressian, V. Negrier, J.-Y. Pascal, S. Vartanian, J. Bucalossi, and P. Monier-Garbet. Deuterium inventory in Tore Supra: Contribution of carbon deposits outgassing. *Journal of Nuclear Materials*, 438, Supplement(0):S1059–S1062, 2013.

[143] P. Andrew and M. Pick. Hydrogen retention in the first wall. *Journal of Nuclear Materials*, 220–222(0):601–605, 1995.

[144] J. Ehrenberg, V. Philipps, L. De Kock, R.A. Causey, and W.L. Hsu. Analysis of deuterium recycling in JET under beryllium first wall conditions. *Journal of Nuclear Materials*, 176-177(0):226–230, 1990.

[145] S. Markelj, O.V. Ogorodnikova, P. Pelicon, T. Schwarz-Selinger, and I. Čadež. Temperature dependence of D atom adsorption on polycrystalline tungsten. *Applied Surface Science*, 282:478–486, 2013.

[146] N. Juslin, P. Erhart, P. Träskelin, J. Nord, K.O.E. Henriksson, K. Nordlund, E. Salonen, and K. Albe. Analytical interatomic potential for modeling nonequilibrium processes in the w–c–h system. *Journal of Applied Physics*, 98(12):123520, 2005.

[147] X.-C. Li, X. Shu, Y.-N. Liu, F. Gao, and G.-H. Lu. Modified analytical interatomic potential for a W–H system with defects. *Journal of Nuclear Materials*, 408(1):12–17, 2011.

[148] M.R. Sorensen and A.F. Voter. Temperature-accelerated dynamics for simulation of infrequent events. *The Journal of Chemical Physics*, 112(21):9599–9606, 2000.

[149] D. Perez, B.P. Uberuaga, Y. Shim, J.G. Amar, and A.F. Voter. Accelerated Molecular Dynamics Methods: Introduction and Recent Developments. volume 5 of *Annual Reports in Computational Chemistry*, chapter 4, pages 79–98. Elsevier, 2009.

[150] M. Rutigliano and M. Cacciatore. Eley–Rideal recombination of hydrogen atoms on a tungsten surface. *Physical Chemistry Chemical Physics*, 13(16):7475–7484, 2011.

[151] G. Mills and H. Jónsson. Quantum and thermal effects in H_2 dissociative adsorption: Evaluation of free energy barriers in multidimensional quantum systems. *Physical Review Letters*, 72:1124–1127, Feb 1994.

[152] E.A. Daniels and R. Gomer. Diffusion of 1H and 2H on W(001). *Surface Science*, 336(3):245–261, 1995.